Contents

Preface

This PhD thesis describes the work that I have carried out during my PhD studies at the Lundbeck Foundation Center for Theoretical Chemistry, Department of Chemistry, Aarhus University, under supervision of Poul Jørgensen from 2007 to 2011.

Publications

During the PhD program a number of scientific papers have been produced:

- Paper [1]:
  "Efficient elimination of response parameters in molecular property calculations for variational and nonvariational energies"
  Kasper Kristensen, Poul Jørgensen, Andreas J. Thorvaldsen, and Trygve Helgaker, *J. Chem. Phys.* **129**, 214103 (2008)

- Paper [2]:
  "A density matrix-based quasi-energy formulation of the Kohn–Sham density functional response theory using perturbation- and time-dependent basis sets"
  Andreas J. Thorvaldsen, Kenneth Ruud, Kasper Kristensen, Poul Jørgensen, and Sonia Coriani, *J. Chem. Phys.* **129**, 214108 (2008)

- Paper [3]:
  "Variational response-function formulation of vibrational circular dichroism"
  Sonia Coriani, Andreas J. Thorvaldsen, Kasper Kristensen and Poul Jørgensen, *Phys. Chem. Chem. Phys.* **13**, 4224 (2011)

- Paper [4]:
  "Quasi-energy formulation of damped response theory"
  Kasper Kristensen, Joanna Kauczor, Thomas Kjærgaard, and Poul Jørgensen, *J. Chem. Phys.* **131**, 044112 (2009)

- Paper [5]:
  "Comparison of standard and damped response formulations of Magnetic Circular Dichroism"
  Thomas Kjærgaard, Kasper Kristensen, Joanna Kauczor, Poul Jørgensen, Sonia Coriani, and Andreas J. Thorvaldsen *J. Chem. Phys.* **135**, 024112 (2011)

- Paper [6]:
  "Damped response theory description of two-photon absorption"
  Kasper Kristensen, Joanna Kauczor, Andreas J. Thorvaldsen, Poul Jørgensen, Thomas Kjærgaard, and Antonio Rizzo, *J. Chem. Phys.* **134**, 214104 (2011)

- Paper [7]:
  "A Locality Analysis of the Divide-Expand-Consolidate Coupled Cluster Amplitude Equations"
  Kasper Kristensen, Marcin Ziółkowski, Branislav Jansík, Thomas Kjærgaard, and Poul Jørgensen, *J. Chem. Theory Comput.* **7**, 1677 (2011)

- Paper [8]:
  "On the theoretical foundation of the divide-expand-consolidate (DEC) coupled cluster method. Numerical illustrations using second order Møller-Plesset perturbation theory"
  Ida-Marie Høyvik, Kasper Kristensen, Branislav Jansík, and Poul Jørgensen (in preparation)

- Paper [9]:
  "MP2 molecular gradient using the Divide-Expand-Consolidate approach"
  Kasper Kristensen, Simen Reine, Thomas Kjærgaard, Branislav Jansík, Ida-Marie Høyvik, and Poul Jørgensen (submitted)

- Paper [10]:
  "Local orbitals by minimizing powers of the orbital variance"
  Branislav Jansík, Stinne Høst, Kasper Kristensen, and Poul Jørgensen, *J. Chem. Phys.* **134**, 194104 (2011)

- Paper [11]:
  "Recent advances in wave-function-based methods of molecular-property calculations"
  Trygve Helgaker, Sonia Coriani, Poul Jørgensen, Kasper Kristensen, Jeppe Olsen, and Kenneth Ruud (submitted)

The original papers are attached at the end of the thesis. The first ten chapters of this thesis describe papers [1]-[10] in that order. Since paper [11] is a review paper containing no new developments as such, it is not treated in detail in this thesis. However, it should be noted that the introduction to response theory in Chapter 1, the description of density-matrix based response theory in Chapter 2, and the description to damped response theory in Chapter 4 have been inspired by the treatments of these subjects in paper [11].

As is evident from the titles given above, several different topics have been investigated during my PhD studies. One common aspect is the goal of reformulating standard quantum chemical models to make these applicable to large molecular systems – optimally to obtain implementations where the computational time scales only linearly with system size. Nevertheless,

quite different subjects have been covered, and for clarity the thesis is divided into two main areas of research:

- **Part A** describes developments in response theory – with focus on Hartree-Fock (HF) theory and density functional theory (DFT) – where the aim has been to reformulate the conventional response theory expressions to be able to perform calculations on large molecular systems. Chapter 1 contains a general introduction to response theory, Chapters 2-3 describe density-matrix based HF/DFT response theory in the atomic orbital basis, and damped response theory is treated in Chapters 4–6.

- **Part B** is devoted to the Divide-Expand-Consolidate (DEC) coupled-cluster method, which is an attempt to reformulate and implement standard coupled-cluster theory in a linear-scaling and embarrassingly parallel fashion, with control of the errors introduced compared to a conventional coupled-cluster calculation. In particular, Chapters 7 and 8 describe the DEC method for evaluating the coupled-cluster energy, and the molecular gradient is considered in Chapter 9. The existence of a set of local HF orbitals is crucial for the validity of the DEC approach, and Chapter 10 describes such local HF orbitals may be obtained.

Using the division of articles into separate chapters it has been my intention to give future PhD students easy access to summarized descriptions of each of the various topics – i.e., each chapter in this thesis can be read relatively independently of the other chapters.

My work has been focused mainly on the – somewhat lengthy and tedious – theoretical formulations aiming at linear-scaling implementations, rather than on performing actual applications on large molecular systems.

Miscellaneous

Atomic units are used throughout this thesis unless stated otherwise.

The theory developments presented in this thesis have been implemented in the LSDalton (Linear-Scaling Dalton) program [12]. The response theory developments presented in part A are publicly available, while, at this stage, the DEC method described in part B has only been implemented in a local version of the LSDalton program.

Acknowledgements

First of all I would like to thank my supervisor Poul Jørgensen for giving me the opportunity to pursue a PhD in the field of theoretical chemistry. Despite his forty years in the field he is still going strong, and his genuine dedication to science has been an invaluable source of motivation during the past four years. He has always been extremely helpful for discussing theoretical derivation details for hours on the blackboard (only interrupted by some Poul-induced cake sessions), for implementation issues, and for coming up with new ideas to be tested.

With respect to financial support I acknowledge the Lundbeck Foundation. I also acknowledge The Danish Center for Scientific Computing, in particular the Aarhus branch (CSCAA), for providing computational resources.

I thank my coauthors for their collaboration and for interesting discussions. I acknowledge Andreas Thorvaldsen for useful discussions in the context of density-matrix based response theory. Marcin Ziółkowski was very helpful when I was introduced to the DEC project. Branislav Jansík has been a very important go-to-guy for technical issues and has been involved in many interesting discussions regarding the DEC project. I am grateful to Thomas Kjærgaard and Joanna Kauczor (who are unfortunately no longer in Aarhus) for many great scientific – and equally many nonscientific – discussions.

I thank the entire theoretical chemistry group in Aarhus for providing a stimulating and friendly environment, and I thank family and friends for moral support. In particular, I would like to thank my office mates (Mikkel Hansen, Kristian Sneskov, and Stinne Høst) for an infinite number of delightful discussions, competitions, and laughs in the office – scientific as well as nonscientific. You really made the difference on an everyday basis. A special thanks goes to Mikkel who has been an inexhaustible source of technical support, which I have heavily exploited. He is also my running mate (sorry that I am always so slow), co-singer (the most intense and heartfelt version of *All out of love* ever performed), gambling buddy, and much more.

Above all I thank Ida-Marie. You have been an invaluable support, both with respect to discussing technical issues for the DEC program, but mainly for cheering me up when I am down, and for keeping up with me in good times and bad times. My life would indeed be empty without you!

Finally, I would like to thank Mikkel, Kristian, and Ida-Marie for proof-reading this thesis, and Rasmus Bertelsen for making the front page of this thesis.

PART A: Self-Consistent Field Response Theory and Damped Response Theory

Chapter 1

Response theory

Section 1.7 describes the work presented in **paper [1]**.

1.1 Introduction

Molecular properties represent the link between observable quantities that can be determined in experimental investigations and quantum chemical calculations [13]. For this reason, the calculation of molecular properties has been an essential target since the development of modern electronic-structure methods was initiated. Nowadays, electronic-structure calculations provide invaluable help in the interpretation of experimental measurements of a broad range of molecular properties, including rotational and vibrational spectroscopies [14], ultraviolet–visible spectroscopies [15, 16], magnetic-resonance spectroscopies [17–19], linear and nonlinear optics [20–22], and optical activity [23].

Response theory, as developed in the eighties [13], has been used successfully to calculate a large variety of molecular properties for ground and excited states and for transitions between these states. In the nineties, the quasi-energy approach [24, 25] tied response function theory closely to the energy-derivative techniques in time-independent theory. Using the quasi-energy approach, response functions may straightforwardly be derived for both variational and nonvariational wave functions [25].

In this chapter we consider response theory using the quasi-energy formulation. Although the focus is on exact theory, the working equations for determining response functions and response parameters are also valid for approximate variational wave function models. In Section 1.2 we consider the time-evolution of an exact state, and in Section 1.3 we discuss the variation principle for the quasi-energy. Sections 1.4 and 1.5 are devoted to response functions and their residues, respectively, whereas response equations are discussed in Section 1.6. Section 1.7 describes how to obtain the computationally simplest expressions for response functions.

1.2 The time-development of an exact state

Consider a time-dependent electronic wave function $|\bar{0}\rangle$ for a molecular system. The time development of $|\bar{0}\rangle$ is governed by the *time-dependent Schrödinger equation*

$$H\,|\bar{0}\rangle = \mathrm{i}\,\partial_\mathrm{t}\,|\bar{0}\rangle \tag{1.1}$$

where $\partial_\mathrm{t} = \frac{\partial}{\partial t}$ represents the derivative with respect to time, and the Hamiltonian consists of a time-independent part H_0 and a time-dependent perturbation $V(t)$

$$H = H_0 + V(t) \tag{1.2}$$

In electronic structure theory H_0 may be written as,

$$H_0 = T + V_\mathrm{Ne} + V_\mathrm{ee} + h_\mathrm{nuc} \tag{1.3}$$

where T is the kinetic energy, V_Ne is the nuclear-electron attraction, V_ee is the electron-electron repulsion, and h_nuc is the nuclear-nuclear repulsion,

$$T = -\sum_i \tfrac{1}{2}\nabla_i^2 \tag{1.4a}$$

$$V_\mathrm{Ne} = -\sum_{iK} Z_K r_{iK}^{-1} \tag{1.4b}$$

$$V_\mathrm{ee} = \frac{1}{2}\sum_{i\neq j}\frac{1}{r_{ij}} \tag{1.4c}$$

$$h_\mathrm{nuc} = \frac{1}{2}\sum_{I\neq J}\frac{Z_I Z_J}{R_{IJ}} \tag{1.4d}$$

In Eq. (1.4) Z_K is the charge of nucleus K, r_{iK} is the distance between electron i and nucleus K, r_{ij} is the distance between electrons i and j, and R_{IJ} is the inter-nuclear distance between nuclei I and J. The form of $V(t)$ will be specified in Section 1.3.

Both components of the Hamiltonian in Eq. (1.2) are Hermitian, i.e., $H_0 = H_0^\dagger$ and $V(t) = V(t)^\dagger$. From Eq. (1.1) it then follows that the norm $\langle\bar{0}|\bar{0}\rangle$ is independent of time:

$$\partial_\mathrm{t}\langle\bar{0}|\bar{0}\rangle = \langle\dot{\bar{0}}|\bar{0}\rangle + \langle\bar{0}|\dot{\bar{0}}\rangle = i\,\langle\bar{0}\,|H|\,\bar{0}\rangle - i\,\langle\bar{0}\,|H|\,\bar{0}\rangle = 0 \tag{1.5}$$

Thus, assuming that $|\bar{0}\rangle$ is normalized at $t = 0$,

$$\langle\bar{0}(t=0)|\bar{0}(t=0)\rangle = 1 \tag{1.6}$$

it is also normalized at all subsequent times t.

It is convenient to separate a phase factor out from the wave function, by writing $|\bar{0}\rangle$ as a product of a *real* phase factor $F(t)$ and a *regular wave function* $|\tilde{0}\rangle$:

$$|\bar{0}\rangle = \mathrm{e}^{-\mathrm{i}F(t)}\,|\tilde{0}\rangle \tag{1.7}$$

Note that by construction $|\tilde{0}\rangle$ is a normalized wave function because $|\bar{0}\rangle$ is normalized.

By substituting the representation of $|\bar{0}\rangle$ of Eq. (1.7) into Eq. (1.1), we obtain the time-dependent Schrödinger equation in terms of $|\tilde{0}\rangle$ and $F(t)$:

$$\left(H - \mathrm{i}\,\partial_\mathrm{t} - \dot{F}(t)\right)|\tilde{0}\rangle = 0 \tag{1.8}$$

Projecting this equation onto the orthogonal complement to $|\tilde{0}\rangle$ by the projection operator

$$P = 1 - |\,\tilde{0}\rangle\langle\tilde{0}\,| \tag{1.9}$$

we arrive at the following projected time-dependent Schrödinger equation for the regular wave function:

$$P\,(H - \mathrm{i}\,\partial_\mathrm{t})\,|\tilde{0}\rangle = 0 \tag{1.10}$$

On the other hand, projection onto $|\,\tilde{0}\rangle$ yields an equation for the phase factor:

$$\dot{F}(t) = \langle\tilde{0}\,|H - \mathrm{i}\,\partial_\mathrm{t}|\,\tilde{0}\rangle \tag{1.11}$$

By first solving Eq. (1.10) for the regular wave function and subsequently determining the phase factor by integrating Eq. (1.11), we obtain the full solution to the Schrödinger equation. It is instructive to consider the special case, where $V(t) = 0$ and $|\tilde{0}\rangle$ is chosen as the time-independent eigenfunction $|\,\mathrm{o}\rangle$ for the ground state of H_0,

$$H_0|\,\mathrm{o}\rangle = E_0|\,\mathrm{o}\rangle \tag{1.12}$$

In this case Eq. (1.11) yields

$$\dot{F}(t) = \langle\mathrm{o}\,|H_0|\,\mathrm{o}\rangle = E_0 \tag{1.13}$$

and the total wave function $|\bar{0}\rangle = e^{-iE_0t}|\,\mathrm{o}\rangle$ trivially satisfies the time-dependent Schrödinger equation in Eq. (1.1). Due to the equivalence of $\dot{F}(t)$ and E_0 for the unperturbed system, the differentiated phase factor is known as the *time-dependent quasi-energy* $Q(t)$ in the presence of a general perturbation $V(t)$:

$$Q(t) = \dot{F}(t) = \langle\tilde{0}\,|H - \mathrm{i}\,\partial_\mathrm{t}|\,\tilde{0}\rangle \tag{1.14}$$

We note that $Q(t)$ is a real quantity because $F(t)$ is real.

1.3 The time-dependent variation principle

It is possible to formulate a variation principle for the time-dependent quasi-energy. From Eq. (1.8), we obtain for an arbitrary variation $|\delta\tilde{0}\rangle$ in the regular wave function

$$\langle\delta\tilde{0}\,|H - \mathrm{i}\,\partial_\mathrm{t} - Q|\,\tilde{0}\rangle = 0 \tag{1.15}$$

Taking the complex conjugate of Eq. (1.15) and adding this term to the same equation, it follows that

$$\delta\,\langle\tilde{0}\,|H - \mathrm{i}\,\partial_\mathrm{t}|\,\tilde{0}\rangle + \mathrm{i}\frac{\mathrm{d}}{\mathrm{d}t}\langle\tilde{0}|\delta\tilde{0}\rangle = 0 \tag{1.16}$$

where we have used that $\delta \left\langle \tilde{0} \left| Q \right| \tilde{0} \right\rangle = Q\delta\langle\tilde{0}|\tilde{0}\rangle = 0$, which follows from the normalization of the wave function. This equation, which determines the time-dependent wave function at a given time t, constitutes the time-dependent variation principle of Langhoff, Epstein, and Karplus [26]. Eq. (1.16) is not a variation principle in the usual sense of the term, where the variation in the function determined vanishes at the solution.

To establish a standard variation principle for the regular wave function, we assume a *periodic time-dependent perturbation* of period T and frequency $\omega = 2\pi/T$:

$$V(t+T) = V(t) \tag{1.17}$$

In particular, we choose to the following Fourier expansion for $V(t)$,

$$V(t) = \sum_B \varepsilon_B V_B e^{-\mathrm{i}\omega_B t} \tag{1.18}$$

where ε_B is a perturbation strength parameter associated with the operator V_B. For example, ε_B may refer to the electric field strength component associated with the electric dipole operator component μ_B. The summation in Eq. (1.18) runs over both positive and negative indices, and the periodicity of $V(t)$ dictates that the frequencies ω_B may all be written as $n\omega$, where n is an integer (negative, zero, or positive). From the requirement of Hermiticity, $V(t) = V(t)^\dagger$, we obtain the following relations connecting the frequencies, perturbation strengths, and operators for indices (B) and $(-B)$:

$$\omega_{-B} = -\omega_B; \qquad V_B^\dagger = V_{-B}; \qquad \varepsilon_B^* = \varepsilon_{-B} \tag{1.19}$$

In general we allow for complex perturbation strengths. Instead of using the real and imaginary parts of ε_B as the independent parameters, it will be convenient to consider ε_B and ε_B^* as the independent parameters.

It may be shown [25] that the regular wave function oscillates with the same period T as $V(t)$:

$$|\tilde{0}(t+T)\rangle = |\tilde{0}(t)\rangle \tag{1.20}$$

The time-dependent quasi-energy $Q(t)$ in Eq. (1.14) is therefore also periodic. We now introduce the *time-average* of a periodic function $g(t)$ as

$$\{g\}_T = \frac{1}{T}\int_0^T g(t)\,\mathrm{d}t \tag{1.21}$$

and define the time-averaged quasi-energy $\mathcal{Q}$ as the time-average of the time-dependent quasi-energy:

$$\mathcal{Q} = \{Q(t)\}_T = \left\{\left\langle \tilde{0} \left| H - \mathrm{i}\,\partial_\mathrm{t} \right| \tilde{0} \right\rangle\right\}_T \tag{1.22}$$

In the following we denote the time-averaged quasi-energy $\mathcal{Q}$ simply as the *quasi-energy* since it is the analogue of the energy in time-independent theory, whereas $Q(t)$ is referred to as the time-dependent quasi-energy.

By taking the time-average of the variation principle in Eq. (1.16) and invoking the periodicity of $|\tilde{0}\rangle$ and $|\delta\tilde{0}\rangle$ the second term vanishes, and we obtain the *variation principle for the quasi-energy*:

$$\delta\mathcal{Q} = 0 \tag{1.23}$$

which is analogous to the variation principle for the energy in time-independent theory. This is the form that we will use in the following.

Let us now differentiate the quasi-energy with respect to one particular perturbation strength ε_A entering $V(t)$ and invoke the stationary condition in Eq. (1.23),

$$\begin{aligned}\frac{d\mathcal{Q}}{d\varepsilon_A} &= \left\{\left\langle\tilde{0}\left|\partial_{\varepsilon_A}H\right|\tilde{0}\right\rangle\right\}_T + \left\{\left\langle\partial_{\varepsilon_A}\tilde{0}\left|H - i\,\partial_{\mathrm{t}}\right|\tilde{0}\right\rangle\right\}_T + \left\{\left\langle\tilde{0}\left|H - i\,\partial_{\mathrm{t}}\right|\partial_{\varepsilon_A}\tilde{0}\right\rangle\right\}_T \\ &= \left\{\left\langle\tilde{0}\left|\partial_{\varepsilon_A}H\right|\tilde{0}\right\rangle\right\}_T + \delta\mathcal{Q}|_{\delta\tilde{0}=\partial_{\varepsilon_A}\tilde{0}} \\ &= \left\{\left\langle\tilde{0}\left|\partial_{\varepsilon_A}H\right|\tilde{0}\right\rangle\right\}_T \end{aligned} \tag{1.24}$$

where we have used that $\delta\mathcal{Q} = 0$ for *any* variation of the regular wave function, including the variation $\partial_{\varepsilon_A}\tilde{0}$. Eq. (1.24) constitutes a generalization of the *Hellmann–Feynman theorem* [27, 28] to the time-dependent regime. Insertion of Eq. (1.2) into Eq. (1.24) and use of Eq. (1.18) yields an expression, which is useful for identifying response functions in the following section,

$$\frac{d\mathcal{Q}}{d\varepsilon_A} = \left\{\left\langle\tilde{0}\left|V_A\mathrm{e}^{-i\omega_A t}\right|\tilde{0}\right\rangle\right\}_T = \left\{\left\langle\tilde{0}\left|V_A\right|\tilde{0}\right\rangle\mathrm{e}^{-i\omega_A t}\right\}_T \tag{1.25}$$

1.4 Response functions

We now demonstrate how response functions are determined within the quasi-energy formalism. Response functions are defined in terms of the time-dependent expectation value of an operator V_A [13]:

$$\begin{aligned}\langle V_A\rangle(t) &= \left\langle\tilde{0}\left|V_A\right|\tilde{0}\right\rangle \\ &= \langle\mathrm{o}\left|V_A\right|\mathrm{o}\rangle + \sum_B{}' \varepsilon_B\langle\langle V_A; V_B\rangle\rangle_{\omega_B}e^{-\mathrm{i}\omega_B t} \\ &+ \frac{1}{2!}\sum_{B,C}{}' \varepsilon_B\varepsilon_C\langle\langle V_A; V_B, V_C\rangle\rangle_{\omega_B,\omega_C}e^{-\mathrm{i}(\omega_B+\omega_C)t} \\ &+ \frac{1}{3!}\sum_{B,C,D}{}' \varepsilon_B\varepsilon_C\varepsilon_D\langle\langle V_A; V_B, V_C, V_D\rangle\rangle_{\omega_B,\omega_C,\omega_D}e^{-\mathrm{i}(\omega_B+\omega_C+\omega_D)t} + \cdots \end{aligned} \tag{1.26}$$

where $\langle\langle V_A; V_B\rangle\rangle_{\omega_B}$, $\langle\langle V_A; V_B, V_C\rangle\rangle_{\omega_B,\omega_C}$, and $\langle\langle V_A; V_B, V_C, V_D\rangle\rangle_{\omega_B,\omega_C,\omega_D}$ are the linear, quadratic and cubic response functions, respectively, and where the prime in the summation indicates that perturbation indices A and $-A$ are excluded from the summation. Response functions contain a wealth of information about the response of a molecular system to one or more external fields (such as the electromagnetic field of a laser). If, for example, the operators in question are electric dipole operators, then the linear, quadratic, and cubic response functions represent the polarizability, and the first and second hyperpolarizabilities, respectively. In many cases

response functions may be directly related to observables measured using various experimental techniques; some examples are given in Ref. [13].

Before connecting response functions to the quasi-energy we note that the quadratic response functions involving V_A, V_B, and V_C enter Eq. (1.26) as

$$\frac{1}{2!}\varepsilon_B\varepsilon_C\Big(\langle\langle V_A;V_B,V_C\rangle\rangle_{\omega_B,\omega_C}+\langle\langle V_A;V_C,V_B\rangle\rangle_{\omega_C,\omega_B}\Big)e^{-\mathrm{i}(\omega_B+\omega_C)t} \tag{1.27}$$

Since $\langle\langle V_A;V_B,V_C\rangle\rangle_{\omega_B,\omega_C}$ and $\langle\langle V_A;V_C,V_B\rangle\rangle_{\omega_C,\omega_B}$ multiply the same factors we may – without loss of generality – impose the symmetry requirement that

$$\langle\langle V_A;V_B,V_C\rangle\rangle_{\omega_B,\omega_C}=\langle\langle V_A;V_C,V_B\rangle\rangle_{\omega_C,\omega_B} \tag{1.28}$$

Similarly we require the following identities between cubic response functions:

$$\begin{aligned}\langle\langle V_A;V_B,V_C,V_D\rangle\rangle_{\omega_B,\omega_C,\omega_D}&=\langle\langle V_A;V_B,V_D,V_C\rangle\rangle_{\omega_B,\omega_D,\omega_C}\\&=\langle\langle V_A;V_C,V_B,V_D\rangle\rangle_{\omega_C,\omega_B,\omega_D}\\&=\langle\langle V_A;V_C,V_D,V_B\rangle\rangle_{\omega_C,\omega_D,\omega_B}\\&=\langle\langle V_A;V_D,V_B,V_C\rangle\rangle_{\omega_D,\omega_B,\omega_C}\\&=\langle\langle V_A;V_D,V_C,V_B\rangle\rangle_{\omega_D,\omega_C,\omega_B}\end{aligned} \tag{1.29}$$

To make a connection between the response functions in Eq. (1.26) and the quasi-energy entering the time-dependent Hellmann-Feynman theorem in Eq. (1.25), we multiply Eq. (1.26) by $\mathrm{e}^{-i\omega_A t}$ and take the time-average:

$$\begin{aligned}\big\{\langle\tilde{0}\,|V_A|\,\tilde{0}\rangle\,\mathrm{e}^{-i\omega_A t}\big\}_T=\langle \mathrm{o}\,|V_A|\,\mathrm{o}\rangle\,\delta_{\omega_A,0}&+\sum_B{}'\,\varepsilon_B\langle\langle V_A;V_B\rangle\rangle_{\omega_B}\delta_{\omega_A+\omega_B,0}\\&+\frac{1}{2!}\sum_{B,C}{}'\,\varepsilon_B\varepsilon_C\langle\langle V_A;V_B,V_C\rangle\rangle_{\omega_B,\omega_C}\delta_{\omega_A+\omega_B+\omega_C,0}\\&+\frac{1}{3!}\sum_{B,C,D}{}'\,\varepsilon_B\varepsilon_C\varepsilon_D\langle\langle V_A;V_B,V_C,V_D\rangle\rangle_{\omega_B,\omega_C,\omega_D}\delta_{\omega_A+\omega_B+\omega_C+\omega_D,0}+\cdots\end{aligned} \tag{1.30}$$

where we have used that

$$\frac{1}{T}\int_0^T\mathrm{e}^{\mathrm{i}\omega t}\mathrm{d}t=\delta_{\omega,0} \tag{1.31}$$

In Eqs. (1.30) and (1.31) we have generalized the Kroneker delta to encompass real numbers to obtain a compact notation,

$$\delta_{\omega,0}=\begin{cases}1 & \text{if}\quad \omega=0\\ 0 & \text{if}\quad \omega\neq 0\end{cases} \tag{1.32}$$

Combining Eqs. (1.25) and (1.30) we obtain a connection between the quasi-energy and the response functions:

$$\begin{aligned}\frac{d\mathcal{Q}}{d\varepsilon_A}=\langle \mathrm{o}\,|V_A|\,\mathrm{o}\rangle\,\delta_{\omega_A,0}&+\sum_B{}'\,\varepsilon_B\langle\langle V_A;V_B\rangle\rangle_{\omega_B}\delta_{\omega_A+\omega_B,0}\\&+\frac{1}{2!}\sum_{B,C}{}'\,\varepsilon_B\varepsilon_C\langle\langle V_A;V_B,V_C\rangle\rangle_{\omega_B,\omega_C}\delta_{\omega_A+\omega_B+\omega_C,0}\\&+\frac{1}{3!}\sum_{B,C,D}{}'\,\varepsilon_B\varepsilon_C\varepsilon_D\langle\langle V_A;V_B,V_C,V_D\rangle\rangle_{\omega_B,\omega_C,\omega_D}\delta_{\omega_A+\omega_B+\omega_C+\omega_D,0}+\cdots\end{aligned} \tag{1.33}$$

To adapt to standard notation in the following we now rename the operators $V_A = A$, $V_B = B$, etc. Using the symmetry relations in Eqs. (1.28) and (1.29) it follows from Eq. (1.33) that response functions may be identified as perturbation strength derivatives of the quasi-energy evaluated at zero perturbation strengths:

$$\langle\langle A;B\rangle\rangle_{\omega_B} = \left.\frac{d^2\mathcal{Q}}{d\varepsilon_A d\varepsilon_B}\right|_{\{\varepsilon\}=0} \equiv \mathcal{Q}^{AB} \; ; \qquad \omega_A = -\omega_B \quad (1.34a)$$

$$\langle\langle A;B,C\rangle\rangle_{\omega_B,\omega_C} = \left.\frac{d^3\mathcal{Q}}{d\varepsilon_A d\varepsilon_B d\varepsilon_C}\right|_{\{\varepsilon\}=0} \equiv \mathcal{Q}^{ABC} \; ; \qquad \omega_A = -\omega_B - \omega_C \quad (1.34b)$$

$$\langle\langle A;B,C,D\rangle\rangle_{\omega_B,\omega_C,\omega_D} = \left.\frac{d^4\mathcal{Q}}{d\varepsilon_A d\varepsilon_B d\varepsilon_C d\varepsilon_D}\right|_{\{\varepsilon\}=0} \equiv \mathcal{Q}^{ABCD} \; ; \quad \omega_A = -\omega_B - \omega_C - \omega_D \quad (1.34c)$$

where $\{\varepsilon\}$ refers to the complete set of perturbation strengths, and where we have introduced a compact notation for perturbation strength derivatives evaluated a zero perturbation strengths. Since only the time-dependent Hellmann-Feynman theorem in Eq. (1.25) and the response function definition in Eq. (1.26) have been used to derive the response function identifications in Eq. (1.34), these relations are valid in any variational wave function model and not only in exact theory.

The response functions may be written in the so-called sum-over-states expressions as [11, 13]:

$$\langle\langle A;B\rangle\rangle_{\omega_B} = P(A,B)\sum_i \frac{A^{oi}B^{io}}{\omega_B - \omega_i} = \sum_i \left(\frac{A^{oi}B^{io}}{\omega_B - \omega_i} - \frac{B^{oi}A^{io}}{\omega_B + \omega_i}\right) \quad (1.35a)$$

$$\langle\langle A;B,C\rangle\rangle_{\omega_B,\omega_C} = -P(A,B,C)\sum_{ij} \frac{A^{oi}\tilde{B}^{ij}C^{jo}}{(\omega_A + \omega_i)(\omega_C - \omega_j)} \quad (1.35b)$$

$$\begin{aligned}\langle\langle A;B,C,D\rangle\rangle_{\omega_B,\omega_C,\omega_D} = P(A,B,C,D)\Bigg[&-\sum_{ijk} \frac{A^{oi}\tilde{B}^{ij}\tilde{C}^{jk}D^{ko}}{(\omega_A + \omega_i)(\omega_C + \omega_D - \omega_j)(\omega_D - \omega_k)} \\ &+ \sum_{ij} \frac{A^{oi}B^{io}}{\omega_B - \omega_i}\frac{C^{oj}D^{jo}}{(\omega_C + \omega_j)(\omega_D - \omega_j)}\Bigg]\end{aligned} \quad (1.35c)$$

where the summations i, j, k run over all excited states (not the ground state $|\,\mathrm{o}\rangle$) in the system, and where we have introduced a compact notation for matrix transition elements,

$$B^{oi} = \langle \mathrm{o}\,|B|i\rangle; \qquad \tilde{B}^{ij} = \langle i|B|j\rangle - \langle \mathrm{o}\,|B|\,\mathrm{o}\rangle\delta_{ij} \quad (1.36)$$

The permutation operators in Eq. (1.35) create all possible permutations of the operator-frequency indices – e.g., if $f(A,B)$ and $g(A,B,C)$ are functions of the operators and corresponding frequencies then:

$$P(A,B)f(A,B) = f(A,B) + f(B,A) \quad (1.37a)$$

$$\begin{aligned}P(A,B,C)g(A,B,C) = {}& g(A,B,C) + g(A,C,B) + g(B,A,C) \\ &+ g(B,C,A) + g(C,A,B) + g(C,B,A)\end{aligned} \quad (1.37b)$$

For the linear response function in Eq. (1.35a) we have inserted $\omega_B{=}{-}\omega_A$ in the second equality for future reference.

1.5 Residues of response functions

From the spectral representations of the linear, quadratic, and cubic response functions given in Eq. (1.35), it is seen that the response functions have first-order poles when one of the external frequencies is identical to an excitation energy ω_n of the unperturbed system. The corresponding residues provide information about various transition matrix elements of the system. From Eq. (1.35a) we obtain the single residue of the linear response function

$$\lim_{\omega_B \to \omega_n} (\omega_B - \omega_n) \langle\langle A; B \rangle\rangle_{\omega_B} = A^{on} B^{no} \tag{1.38}$$

which thus contains information about the transition matrix elements $\langle \mathrm{o} | A | n \rangle$ and $\langle n | B | \mathrm{o} \rangle$. For example, if A and B are electric dipole operators, the residue in Eq. (1.38) yields a component of the one-photon absorption strength tensor for the $|\mathrm{o}\rangle \rightarrow |n\rangle$ transition.

For future reference let us also consider the residue of the quadratic response function in Eq. (1.35b) at $\omega_C = \omega_n$:

$$\lim_{\omega_C \to \omega_n} (\omega_C - \omega_n) \langle\langle A; B, C \rangle\rangle_{\omega_B, \omega_C} = -\left[P(A,B) \sum_j \frac{A^{oj} \tilde{B}^{jn}}{\omega_A + \omega_j} \right] C^{no} \tag{1.39}$$

When A, B, and C are components of the electric dipole operator, the expression inside $[\ldots]$ of Eq. (1.39) equals a component of the two-photon transition amplitude tensor [13], as will be detailed in Chapter 6.

1.6 Response equations

Let us now discuss the structure of the response equations that need to be solved in order to determine the response functions. We assume that the variation principle in Eq. (1.23) holds, but we make no assumptions about the parameterization of the $|\tilde{0}\rangle$ state. The perturbed molecular system is described in terms of a set of response parameters $x(t)$, which are expanded in orders of the perturbation,

$$x(t) = x^{(0)} + x^{(1)}(t) + x^{(2)}(t) + \ldots \tag{1.40}$$

where $x^{(0)}$ are the optimized wave function parameters for the unperturbed system.

The response parameters may be expanded in terms of the different frequency components and operators [analogously to the Fourier expansion of $V(t)$ in Eq. (1.18)],

$$x^{(1)}(t) = \sum_B \varepsilon_B x^B e^{-i\omega_B t} \tag{1.41a}$$

$$x^{(2)}(t) = \frac{1}{2} \sum_{B,C} \varepsilon_B \varepsilon_C x^{BC} e^{-i\omega_{BC} t} \tag{1.41b}$$

$$\ldots$$

$$x^{(n)}(t) = \frac{1}{n!} \sum_{B_1 B_2 \ldots B_n} \varepsilon_{B_1} \varepsilon_{B_2} \ldots \varepsilon_{B_n} x^{B_1 B_2 \ldots B_n} e^{-i\omega_{B_1 B_2 \ldots B_n} t} \tag{1.41c}$$

where $\omega_{BC} = \omega_B + \omega_C$ and $\omega_{B_1 B_2 \ldots B_n} = \omega_{B_1} + \omega_{B_2} + \ldots + \omega_{B_n}$. The response parameters are assumed to be symmetric, for example, $x^{BC} = x^{CB}$.

To determine equations for the response parameters we consider the stationary condition in Eq. (1.23) for a specific variation in $x(t)$:

$$\frac{\partial \mathcal{Q}}{\partial x} = 0 \tag{1.42}$$

Differentiating Eq. (1.42) with respect to the perturbation strengths $\varepsilon_{B_1}, \varepsilon_{B_2}, \ldots, \varepsilon_{B_n}$ and evaluating the resulting expression at $\{\varepsilon\} = 0$, we obtain an equation for the n'th order response parameter $x^{B_1 B_2 \ldots B_n}$:

$$\frac{\mathrm{d}^n}{\mathrm{d}\varepsilon_{B_1}\mathrm{d}\varepsilon_{B_2}\ldots\mathrm{d}\varepsilon_{B_n}}\left(\frac{\partial \mathcal{Q}}{\partial x}\right)\bigg|_{\{\varepsilon=0\}} = 0 \tag{1.43}$$

Using Eq. (1.43) and introducing the short-hand notations

$$\mathcal{Q}^{k,0} = \frac{\partial^k \mathcal{Q}}{\partial x^k}\bigg|_{\{\varepsilon=0\}} \tag{1.44a}$$

$$\mathcal{Q}^{k,B_1 B_2 \ldots B_n} = \frac{\partial^{k+n} \mathcal{Q}}{\partial x^k \partial\varepsilon_{B_1}\partial\varepsilon_{B_2}\ldots\partial\varepsilon_{B_n}}\bigg|_{\{\varepsilon=0\}} \tag{1.44b}$$

the response equations up to second order may be written as

$$\mathcal{Q}^{1,0} = 0 \tag{1.45a}$$

$$\mathcal{Q}^{2,0}x^B + \mathcal{Q}^{1,B} = 0 \tag{1.45b}$$

$$\mathcal{Q}^{2,0}x^{BC} + \mathcal{Q}^{2,B}x^C + \mathcal{Q}^{2,C}x^B + \mathcal{Q}^{3,0}x^B x^C + \mathcal{Q}^{1,BC} = 0 \tag{1.45c}$$

Eq. (1.45a) is simply the variation principle for the energy of the unperturbed system, $\delta E = 0$, and Eqs. (1.45b) and (1.45c) determine the first and second order response parameters, respectively. We note that the highest-order response parameter always enters in combination with the quasi-energy Hessian $\mathcal{Q}^{2,0}$, and therefore the n'th order response equation for $x^{B_1 B_2 \ldots B_n}$ may be written in the form:

$$\mathcal{Q}^{2,0}x^{B_1 B_2 \ldots B_n} = g^{B_1 B_2 \ldots B_n} \tag{1.46}$$

where the right-hand side vector $g^{B_1 B_2 \ldots B_n}$ only contains response parameters of order $n-1$ and below. Hence, by solving for the x^{B_1}, $x^{B_1 B_2}$, ..., $x^{B_1 B_2 \ldots B_n}$ parameters successively, substituting the lower-order parameters into the right-hand sides of higher-order equations, the full set of response parameters may be generated.

1.7 Elimination rules for response functions

The time-consuming step in molecular property calculations is the iterative solution of response equations. Thus, to evaluate molecular properties in an efficient manner, the underlying structure of the quasi-energy derivatives must be exploited to minimize the number of response equations that needs to be solved. For a variational quasi-energy, Wigner's $2n+1$ rule [29] may in general be applied, according to which the $(2n+1)$th quasi-energy derivative can be evaluated from response parameters up to order n – i.e., all response parameters of order $n+1$ and above

may simply be omitted from the expression for the $(2n+1)$th order quasi-energy derivative since they multiply zero.

When molecular properties are evaluated, the number of components in the different classes of perturbations may differ significantly. In particular, for certain classes of perturbations, the number of perturbations is independent of the size of the molecule (e.g., homogeneous electric or magnetic fields); for other classes, the number of perturbations is proportional to the size of the molecule (e.g., nuclear displacements or nuclear magnetic moments). These perturbations are denoted *intensive* and *extensive*, respectively. In general the extensive perturbations have many more components than the intensive perturbations. For reasons of efficiency, it is therefore better to reduce the order of the responses equations that must be solved for the extensive perturbations, rather than to treat the extensive and intensive perturbations on an equal footing by using the standard $2n+1$ rule [29]. We now describe how this can be accomplished for variational (Section 1.7.1) and nonvariational (Section 1.7.2) quasi-energies.

1.7.1 Variational quasi-energies

Before discussing a general mth order quasi-energy derivative (response function), let us consider as a special case the second quasi-energy derivative in Eq. (1.34a) (the linear response function):

$$\mathcal{Q}^{AB} = \mathcal{Q}^{0,AB} + \mathcal{Q}^{1,A}x^B + (\mathcal{Q}^{2,0}x^B + \mathcal{Q}^{1,B})x^A + \mathcal{Q}^{1,0}x^{AB} \tag{1.47}$$

where we have used the short-hand notations in Eq. (1.44) and the response parameter expansions in Eq. (1.41). From this expression, we may eliminate the term involving x^{AB} since it multiplies the zero-order stationary condition in Eq. (1.45a). Furthermore, x^A may be eliminated since it multiplies the first-order response equation for x^B in Eq. (1.45b). The second-order quasi-energy derivative may therefore be written in the simplified form

$$\mathcal{Q}^{AB} = \mathcal{Q}^{0,AB} + \mathcal{Q}^{1,A}x^B \tag{1.48}$$

Note that x^B cannot be eliminated from this expression since – by eliminating the terms in Eq. (1.47) involving x^A – we have also removed the term $\mathcal{Q}^{2,0}x^Ax^B$, such that x^B no longer multiplies a stationary condition $(\mathcal{Q}^{2,0}x^A + \mathcal{Q}^{1,A})$. Alternatively, we could have eliminated x^B while retaining x^A in Eq. (1.47).

The above discussion illustrates how we may eliminate certain response parameters from the quasi-energy derivatives but not all independently. The removal of x^A precludes the removal of x^B and vice versa. This is an example of a much more general elimination result described in paper [1], which we now summarize.

Consider a general mth order quasi-energy derivative $\mathcal{Q}^{B_1\ldots B_m}$. The expression for $\mathcal{Q}^{B_1\ldots B_m}$ – obtained by straightforward differentiation of the quasi-energy $\mathcal{Q}$ with respect to the perturbation strengths ε_{B_1}, …, ε_{B_m} – will contain a plethora of different terms containing first to mth order response parameters. We now focus on a response parameter $x^{B_1\ldots B_p}$ of order p $(1\leq p\leq m)$ entering $\mathcal{Q}^{B_1\ldots B_m}$. In paper [1] the underlying structure of the terms involving $x^{B_1\ldots B_p}$ is investigated and the following result is obtained:

- Any response parameter $x^{B_1 \ldots B_p}$ $(1 \leq p \leq m)$ may be eliminated from the expression for $\mathcal{Q}^{B_1 \ldots B_p \ldots B_m}$, but this precludes the further elimination of all response parameters involving indices $p+1, \ldots, m$.

This result follows from the variation condition in Eq. (1.42) and is the crux for identifying different elimination schemes.

To be more specific with respect to the nature of the perturbations let us now consider the particular mth order quasi-energy derivative $\mathcal{Q}^{A_1 \ldots A_k B_1 \ldots B_{m-k}}$, where $A_1 \ldots A_k$ label k extensive perturbations, while $B_1 \ldots B_{m-k}$ label $m-k$ intensive perturbations. In this case it is advantageous to eliminate as many response parameters referencing the computationally expensive extensive response parameters as possible. Using this strategy in combination with the general elimination statement for a response parameter $x^{B_1 \ldots B_p}$ given above, it is possible to derive the so-called k_{2n+1} *rule for a variational energy* [1]:

- When evaluating $\mathcal{Q}^{A_1 \ldots A_k B_1 \ldots B_{m-k}}$, all x parameters of orders above $n = \lfloor k/2 \rfloor$ in the $A_1 \ldots A_k$ indices may be omitted from the expression for $\mathcal{Q}^{A_1 \ldots A_k B_1 \ldots B_{m-k}}$, where $\lfloor k/2 \rfloor$ is the largest integer less than or equal to $k/2$. In other words, wave-function parameters to order n in the $A_1 \ldots A_k$ indices determine energy derivatives to order $2n+1$ within these indices.

The k_{2n+1} rule gives the computationally simplest expression for an mth order molecular property containing $k \leq m$ extensive perturbations and $m-k$ intensive perturbations. By treating all perturbations on an equal footing and letting $k=m$, the k_{2n+1} rule reduces to the standard $2n+1$ rule [29], which states that, for a variational quasi-energy, the $(2n+1)$th order quasi-energy derivative can be determined from response parameters up to order n.

When k is even, direct application of the k_{2n+1} rule dictates that parameters of order $k/2+1$ and above in the extensive indices may be eliminated from the expression for the quasi-energy derivative. A closer inspection [1] shows, however, that some parameters of order $k/2$ may also be eliminated. For example, for the quasi-energy derivative $\mathcal{Q}^{AB}$ with $k=m=2$, straightforward application of the 2_{2n+1} rule (equivalent to the standard $2n+1$ rule in this case) only dictates that the term involving the second order parameters x^{AB} can be eliminated. However, either x^A *or* x^B may also be eliminated as discussed in connection with Eq. (1.47) above. More generally, when k is even it is possible to eliminate half the parameters of order $k/2$. We use this freedom to eliminate as many response parameters as possible referencing the first $k/2$ perturbations in the set of extensive perturbations when defining the k_{2n+1} rule for an even number of perturbations. For a linear response function with $k=2$ we thus eliminate x^A rather than x^B.

In Table 1.1 we have collected the response parameters needed to determine up to fourth order quasi-energy derivatives using different elimination schemes. We note that for a variational quasi-energy the 1_{2n+1} and 2_{2n+1} rules are equivalent. In general, Table 1.1 gives the computationally most tractable expressions for linear, quadratic, and cubic response functions with k extensive perturbations and $m-k$ intensive perturbations. The cases with $m=k$ are equivalent to the

Table 1.1: Variational quasi-energies. Response parameters needed to determine up to fourth order quasi-energy derivatives $\mathcal{Q}^A$ ($m = 1$), $\mathcal{Q}^{AB}$ ($m = 2$), $\mathcal{Q}^{ABC}$ ($m = 3$), and $\mathcal{Q}^{ABCD}$ ($m = 4$) using the k_{2n+1} elimination rules.

	$k = 1$	$k = 2$	$k = 3$	$k = 4$
$m = 1$	No responses	—	—	—
$m = 2$	x^B	x^B	—	—
$m = 3$	x^B, x^C, x^{BC}	x^B, x^C, x^{BC}	x^A, x^B, x^C	—
$m = 4$	x^B, x^C, x^D x^{BC}, x^{BD}, x^{CD}, x^{BCD}	x^B, x^C, x^D x^{BC}, x^{BD}, x^{CD}, x^{BCD}	x^A, x^B, x^C, x^D x^{AD}, x^{BD}, x^{CD}	x^A, x^B, x^C, x^D x^{BC}, x^{BD}, x^{CD}

standard $2n+1$ rule [29] with the modification that for even m values half of the $(m/2)$th order parameters have also been eliminated. The 1_{2n+1} rule corresponds to eliminating all response parameters referencing perturbation A. For example, for m=4 the x^A parameters enter when the 4_{2n+1} rule is applied, whereas these parameters are effectively replaced by the x^{BCD} parameters when the 1_{2n+1} rule is used. We note that the k_{2n+1} rules for the same m and different k's in Table 1.1 – where a given response parameters is eliminated at the expense of determining another response parameter – may be viewed as different realizations of the Handy-Schaefer turn-over-rule [30].

1.7.2 Nonvariational quasi-energies

The elimination rules discussed in Section 1.7.1 may be generalized to nonvariational quasi-energies, where the response parameters x do not satisfy the stationary condition in Eq. (1.42), but rather some subsidiary relation

$$e(\varepsilon, x) = 0, \qquad \text{for all } \varepsilon \tag{1.49}$$

This relation may, for example, represent the amplitude equations in coupled cluster theory.

To retain the variational formulation also in such cases, it is convenient to construct a *quasi-energy Lagrangian* [31]

$$\mathcal{L}(\varepsilon, x, \bar{x}) = \mathcal{Q}(\varepsilon, x) + \bar{x}e(\varepsilon, x) \tag{1.50}$$

where $\bar{x}$ is the collection of Lagrange multipliers associated with the constraints. To simplify the notation we omit the explicit dependencies on ε, x, and $\bar{x}$ in the following equations. The Lagrangian $\mathcal{L}$ is by construction variational in the multipliers as well as in the original response parameters:

$$\frac{\partial \mathcal{L}}{\partial \bar{x}} = e = 0 \tag{1.51a}$$

$$\frac{\partial \mathcal{L}}{\partial x} = \frac{\partial \mathcal{Q}}{\partial x} + \bar{x}\frac{\partial e}{\partial x} = 0 \tag{1.51b}$$

The variation with respect to $\bar{x}$ in Eq. (1.51a) gives the equation for x in Eq. (1.49) and is trivially satisfied, whereas the variation in x in Eq. (1.51b) yields a set of linear equations

Table 1.2: Nonvariational quasi-energies. Response parameters and multipliers needed to determine up to fourth order Lagrangian quasi-energy derivatives $\mathcal{L}^{A}$ ($m = 1$) $\mathcal{L}^{AB}$ ($m = 2$), $\mathcal{L}^{ABC}$ ($m = 3$), and $\mathcal{L}^{ABCD}$ ($m = 4$) using the $k_{2n+1,2n+2}$ elimination rules.

	$k=1$	$k=2$	$k=3$	$k=4$
$m=1$	$\bar{x}$	—	—	—
$m=2$	x^B, $\bar{x}$, $\bar{x}^B$	x^A, x^B, $\bar{x}$	—	—
$m=3$	x^B, x^C, x^{BC} $\bar{x}$, $\bar{x}^B$, $\bar{x}^C$, $\bar{x}^{BC}$	x^A, x^B, x^C x^{AC}, x^{BC}, $\bar{x}$, $\bar{x}^C$	x^A, x^B, x^C $\bar{x}$, $\bar{x}^A$, $\bar{x}^B$, $\bar{x}^C$	—
$m=4$	x^B, x^C, x^D x^{BC}, x^{BD}, x^{CD}, x^{BCD} $\bar{x}$, $\bar{x}^B$, $\bar{x}^C$, $\bar{x}^D$ $\bar{x}^{BC}$, $\bar{x}^{BD}$, $\bar{x}^{CD}$, $\bar{x}^{BCD}$	x^A, x^B, x^C, x^D x^{AC}, x^{AD}, x^{BC}, x^{BD} x^{CD}, x^{ACD}, x^{BCD} $\bar{x}$, $\bar{x}^C$, $\bar{x}^D$	x^A, x^B, x^C, x^D x^{AD}, x^{BD}, x^{CD} $\bar{x}$, $\bar{x}^A$, $\bar{x}^B$, $\bar{x}^C$, $\bar{x}^D$ $\bar{x}^{AD}$, $\bar{x}^{BD}$, $\bar{x}^{CD}$	x^A, x^B, x^C, x^D x^{AB}, x^{AC}, x^{AD} x^{BC}, x^{BD}, x^{CD} $\bar{x}$, $\bar{x}^A$, $\bar{x}^B$, $\bar{x}^C$, $\bar{x}^D$

that determine the multipliers. From this Lagrangian, response functions may be determined as perturbation-strength derivatives evaluated at $\{\varepsilon\}$=0, equivalent to the variational case in Eq. (1.34):

$$\langle\langle A;B\rangle\rangle_{\omega_B} = \left.\frac{d^2\mathcal{L}}{d\varepsilon_A d\varepsilon_B}\right|_{\{\varepsilon\}=0} \equiv \mathcal{L}^{AB} \; ; \qquad \omega_A = -\omega_B \quad (1.52a)$$

$$\langle\langle A;B,C\rangle\rangle_{\omega_B,\omega_C} = \left.\frac{d^3\mathcal{L}}{d\varepsilon_A d\varepsilon_B d\varepsilon_C}\right|_{\{\varepsilon\}=0} \equiv \mathcal{L}^{ABC} \; ; \qquad \omega_A = -\omega_B - \omega_C \quad (1.52b)$$

$$\langle\langle A;B,C,D\rangle\rangle_{\omega_B,\omega_C,\omega_D} = \left.\frac{d^4\mathcal{L}}{d\varepsilon_A d\varepsilon_B d\varepsilon_C d\varepsilon_D}\right|_{\{\varepsilon\}=0} \equiv \mathcal{L}^{ABCD} \; ; \quad \omega_A = -\omega_B - \omega_C - \omega_D \quad (1.52c)$$

Similar to the treatments of the variational quasi-energy in Section 1.7.1, we may differentiate the quasi-energy Lagrangian in Eq. (1.50) and subsequently apply the variational criteria in Eq. (1.51) to eliminate response parameters and Lagrange multipliers to minimize the total number of response and multiplier equations to be solved. This is done in paper [1], and here we only provide the main result:

- *The $k_{2n+1,2n+2}$ rule*: When evaluating $\mathcal{L}^{A_1\ldots A_k B_1\ldots B_{m-k}}$ the x and $\bar{x}$ parameters may be eliminated in accordance with the $2n$+1 and $2n$+2 rules, respectively, within the $A_1\ldots A_k$ indices. In other words, response parameters (Lagrange multipliers) to order n in the $ab\ldots k$ indices determine quasi-energy derivatives to order $2n$+1 ($2n$+2) within these indices.

When k=m, the $k_{2n+1,2n+2}$ rule reduces to Wigner's $2n$+1 rule [29] for the response parameters and the $2n$+2 rule for the Lagrange multipliers [32]. The elimination rule for the multipliers ($2n$+2) is somewhat stronger than the one for the response parameters ($2n$+1) because the multipliers occur only linearly in the Lagrangian in Eq. (1.50).

Table 1.2 gives an overview of the response parameters and multipliers required to determine up to fourth order Lagrangian derivatives using the $k_{2n+1,2n+2}$ rules for different k's. In general,

Table 1.2 gives the computationally simplest expressions for Lagrangian derivatives involving k extensive and $m-k$ intensive response parameters.

1.7.3 Concluding remarks for elimination rules

Considering the quasi-energy derivative (response function) $\mathcal{Q}^{A_1 \ldots A_k B_1 \ldots B_{k-m}}$ for a variational quasi-energy – where $A_1 \ldots A_k$ and $B_1 \ldots B_{k-m}$ denote extensive and intensive perturbations, respectively – the k_{2n+1} rule gives the computationally simplest expression by minimizing the number of response equations to be solved involving the extensive parameters. Similarly, for a nonvariational quasi-energy, the $k_{2n+1,2n+2}$ gives the computationally most tractable expression.

The reduction in terms of response equations for the extensive perturbations occurs at the expense of having to calculate higher-order response parameters for the intensive perturbations. Except for the smallest systems, however, the associated increase in the number of intensive parameters is insignificant compared with the reduction in the number of extensive parameters. This leads to an overall reduction in computational effort. We also note that the relative computational savings gained by eliminating extensive response parameters increase with molecular system size, and therefore the k_{2n+1} and $k_{2n+1,2n+2}$ rules are particularly important for large molecular systems.

Chapter 2

Density matrix-based self-consistent field response theory formulation

This chapter describes the work presented in **paper [2]**.

2.1 Introduction

The focus in theoretical and experimental chemistry has in the last few decades shifted towards larger molecular systems. For the treatment of time-dependent phenomena of large molecules, the method of choice today is time-dependent Kohn–Sham density functional theory (KS-DFT) [33–38] (including hybrid methods and HF) which offers reasonable accuracy at a low computational cost. In order to facilitate computations on increasingly larger systems, it is important that the computational time scales only linearly with the size of the system.

In conventional KS methods, the determination of the molecular orbital (MO) coefficients requires a diagonalization of the Fock matrix, a procedure that scales cubically with the size of the system. To obtain linear scaling, it is in general advantageous to abandon the MO description and work solely in terms of the density matrix in the atomic orbital (AO) representation, which becomes sparse for large molecular systems. Thus, by deriving working equations in the AO basis, linear scaling can be achieved when the molecular system becomes sufficiently large and sparse matrix algebra is used. Linear-scaling implementations have been developed for the different steps involved in the determination of the KS energy, i.e., the evaluation of the Fock matrix [39–43], the construction of the density matrix (see the reviews in Refs. [44, 45] and references therein), and the evaluation of the exchange-correlation terms [46, 47]. Linear-scaling AO-based KS-DFT response theory has been proposed by various authors [2, 48–55].

In this chapter we summarize the density-matrix based quasi-energy formulation of KS response theory developed in paper [2]. The advantage of this formulation compared to existing AO-based response formulations [48–55] is that static and frequency-dependent perturbations, as well as standard basis sets and perturbation-dependent basis sets (PDBSs), are treated on an equal footing. This is to be compared with traditional approaches, where derivations of

static molecular properties using PDBSs (e.g., molecular gradients and Hessians and magnetic properties calculated using so-called London atomic orbitals [56–58]) and frequency-dependent properties using standard basis sets have been performed independently of each other. In particular, the uniform description of static and time-dependent perturbations presented here also inherently includes the use of frequency-dependent PDBSs, which has been employed in some recent works [3, 59–61].

The presented derivation is a generalization of the developments by Helgaker *et al.* [48, 49], who introduced an unconstrained exponential parameterization of the density matrix in the AO basis and used this parameterization to determine response functions for standard basis sets. The exponential parameterization was also extended to PDBSs, but only for a static perturbation [50].

This chapter is organized as follows. In Section 2.2 we discuss the challenges that arise when attempting to apply the quasi-energy formulation within a density matrix framework. In Section 2.3 we present the working equation for the quasi-energy gradient, from which expressions for response functions in terms of perturbed density matrices may straightforwardly be obtained. The parameterization of the perturbed density matrix is outlined in Section 2.4, and Section 2.5 is devoted to response functions. Section 2.6 contains some concluding remarks.

2.2 Quasi-energy response theory in a density-matrix formulation

For the quasi-energy of Eq. (1.14), only the ket state is subject to time differentiation. The HF or KS quasi-energy is therefore not symmetric with respect to operations on the bra and ket states:

$$Q(t) = \left\langle \widetilde{\mathrm{SCF}} \left| H - \mathrm{i}\,\partial_t \right| \widetilde{\mathrm{SCF}} \right\rangle \tag{2.1}$$

where $|\widetilde{\mathrm{SCF}}\rangle$ is the time-dependent (phase-isolated) self-consistent field (SCF) single-determinant state, which may refer to a HF or a KS determinant.

In particular, the second term in Eq. (2.1) may be evaluated as

$$\left\langle \widetilde{\mathrm{SCF}} \left| -\mathrm{i}\,\partial_t \right| \widetilde{\mathrm{SCF}} \right\rangle = -\mathrm{i} \sum_J \int \phi_J^*(\mathbf{r},t)\dot{\phi}_J(\mathbf{r},t)\,\mathrm{d}\mathbf{r} \tag{2.2}$$

where the summation runs over all occupied spin MOs ϕ (denoted with index J). Note that only the ket orbital $\phi_J(\mathbf{r},t)$ is differentiated with respect to time. The electron density $\rho(\mathbf{r},t)$,

$$\rho(\mathbf{r},t) = \sum_J \phi_J^*(\mathbf{r},t)\phi_J(\mathbf{r},t) \tag{2.3}$$

and its time derivative,

$$\dot{\rho}(\mathbf{r},t) = \sum_J \Big(\dot{\phi}_J^*(\mathbf{r},t)\phi_J(\mathbf{r},t) + \phi_J^*(\mathbf{r},t)\dot{\phi}_J(\mathbf{r},t) \Big) \tag{2.4}$$

are symmetric in $\phi_J^*(\mathbf{r},t)$ and $\phi_J(\mathbf{r},t)$. Given that the time derivative term of the quasi-energy in Eq. (2.2) contains only the second term in the time-differentiated electron density, it is not straightforward to express the quasi-energy in terms of $\rho(\mathbf{r},t)$ and $\dot{\rho}(\mathbf{r},t)$.

Let us now consider the matrix representation of $\rho(\mathbf{r},t)$ in the AO basis. By expanding the MOs in AOs χ_μ, which may depend on the external (possibly time-dependent) perturbation,

$$\phi_J(\mathbf{r},t) = \sum_\mu C_{\mu J}(t)\chi_\mu(\mathbf{r},t) \tag{2.5}$$

we obtain

$$\rho(\mathbf{r},t) = \sum_{\mu\nu} D_{\mu\nu}(t)\chi_\mu^*(\mathbf{r},t)\chi_\nu(\mathbf{r},t) \tag{2.6}$$

where we have introduced the density matrix $\mathbf{D}$ with elements

$$D_{\mu\nu}(t) = \sum_J C_{\mu J}^*(t)C_{\nu J}(t) \tag{2.7}$$

The time-derivative of $\rho(\mathbf{r},t)$ may thus be expressed as

$$\dot{\rho}(\mathbf{r},t) = \sum_{\mu\nu}\Big(\dot{D}_{\mu\nu}(t)\chi_\mu^*(\mathbf{r},t)\chi_\nu(\mathbf{r},t) + D_{\mu\nu}(t)\dot{\chi}_\mu^*(\mathbf{r},t)\chi_\nu(\mathbf{r},t) + D_{\mu\nu}(t)\chi_\mu^*(\mathbf{r},t)\dot{\chi}_\nu(\mathbf{r},t)\Big) \tag{2.8}$$

with contributions from the density matrix as well as the AOs.

Even though the SCF quasi-energy cannot be expressed in terms of $\rho(\mathbf{r},t)$ and its time derivative (or, equivalently, in terms of $\mathbf{D}$ and its time derivative $\dot{\mathbf{D}}$), it is demonstrated in paper [2] that the *perturbation-strength derivative* of the time-averaged SCF quasi-energy can be written as a function of $\mathbf{D}$ and $\dot{\mathbf{D}}$:

$$\frac{d\mathcal{Q}}{d\varepsilon_A} = \frac{d\mathcal{Q}(\mathbf{D},\dot{\mathbf{D}})}{d\varepsilon_A} \equiv \mathcal{Q}^A(\mathbf{D},\dot{\mathbf{D}}) \tag{2.9}$$

The *quasi-energy derivative* $\mathcal{Q}^A(\mathbf{D},\dot{\mathbf{D}})$ (whose explicit form is given in Section 2.3) contains all information needed to determine response functions by further differentiation with respect to the perturbation strengths as in Eq. (1.34):

$$\langle\langle A;B\rangle\rangle_{\omega_B} = \left.\frac{\mathrm{d}\mathcal{Q}^A(\mathbf{D},\dot{\mathbf{D}})}{\mathrm{d}\varepsilon_B}\right|_{\{\varepsilon\}=0}, \quad \omega_A = -\omega_B \tag{2.10}$$

$$\langle\langle A;B,C\rangle\rangle_{\omega_B,\omega_C} = \left.\frac{\mathrm{d}^2\mathcal{Q}^A(\mathbf{D},\dot{\mathbf{D}})}{\mathrm{d}\varepsilon_B\mathrm{d}\varepsilon_C}\right|_{\{\varepsilon\}=0}, \quad \omega_A = -\omega_B - \omega_C \tag{2.11}$$

and so on. The quasi-energy derivative $\mathcal{Q}^A(\mathbf{D},\dot{\mathbf{D}})$ therefore provides an alternative starting point to the quasi-energy for identifying response functions in terms of perturbed density matrices.

For future convenience we extend the notation in Eq. (2.9) and adopt the following notation for the derivatives of a general function or matrix f:

$$f^{B_1\ldots B_m} = \frac{\mathrm{d}^m f}{\mathrm{d}\varepsilon_{B_1}\ldots\mathrm{d}\varepsilon_{B_m}} \tag{2.12}$$

$$f^{n,B_1\ldots B_m} = \frac{\partial^{n+m} f}{\partial(\mathbf{D}^{\mathrm{T}})^n\partial\varepsilon_{B_1}\ldots\partial\varepsilon_{B_m}} \tag{2.13}$$

with special cases $f^{0,B_1\ldots B_m} = \partial^m f/\partial\varepsilon_{B_1}\ldots\partial\varepsilon_{B_m}$ and $f^{n,0} = \partial^n f/\partial(\mathbf{D}^{\mathrm{T}})^n$. In some cases, the derivatives are evaluated at zero perturbation strengths, but this will always be clear from the context.

2.3 The quasi-energy gradient

When working with general time- and perturbation-dependent basis functions χ_μ, it is convenient to introduce the *generalized KS energy* E [2],

$$E = \mathrm{tr}\big(\mathbf{h} + \mathbf{V} + \tfrac{1}{2}\mathbf{G}^\eta(\mathbf{D}) - \tfrac{\mathrm{i}}{2}\mathbf{T}\big)\mathbf{D} + E_{\mathrm{xc}}[\rho] + h_{\mathrm{nuc}} \tag{2.14}$$

where the matrices are evaluated in the atomic spin orbital basis using (in general) perturbation-dependent basis sets χ at nonzero field strengths. In Eq. (2.14) $\mathbf{h}$ is the one-electron matrix without the external perturbation, $\mathbf{V}$ is the perturbation matrix, $\mathbf{G}^\eta(\mathbf{D})$ is the two-electron matrix containing a Coulomb contribution and an η-scaled exchange contribution, and $\mathbf{T}$ is an anti-Hermitian time-differentiated overlap matrix,

$$h_{\mu\nu} = \big\langle \chi_\mu \big| -\tfrac{1}{2}\nabla^2 - \sum\nolimits_K Z_K r_K^{-1} \big| \chi_\nu \big\rangle \tag{2.15}$$

$$V_{\mu\nu} = \langle \chi_\mu \, | V(t) | \, \chi_\nu \rangle \tag{2.16}$$

$$G^\eta_{\mu\nu}(\mathbf{D}) = \sum_{\alpha\beta} D_{\beta\alpha}(g_{\mu\nu\alpha\beta} - \eta g_{\mu\beta\alpha\nu}) \tag{2.17}$$

$$g_{\mu\nu\alpha\beta} = \iint \frac{\chi^*_\mu(\mathbf{x}_1)\chi^*_\alpha(\mathbf{x}_2)\chi_\nu(\mathbf{x}_1)\chi_\beta(\mathbf{x}_2)}{r_{12}} \, \mathrm{d}\mathbf{x}_1 \, \mathrm{d}\mathbf{x}_2 \tag{2.18}$$

$$T_{\mu\nu} = \langle \chi_\mu | \dot{\chi}_\nu \rangle - \langle \dot{\chi}_\mu | \chi_\nu \rangle \tag{2.19}$$

where the various distances and charges were defined in connection with Eq. (1.4), and where the integration variable $\mathbf{x}$ refers to both spatial $\mathbf{r}$ and spin coordinates. $E_{\mathrm{xc}}[\rho]$ is the exchange-correlation functional of the electron density $\rho = \rho(\mathrm{r}, t)$ in Eq. (2.3) and includes the remaining part of the energy contribution. It thus contains the effects of electron correlation and corrects the error made in the kinetic energy by evaluating it in terms of a single Slater determinant. Finally, h_{nuc} is the nuclear-nuclear repulsion term in Eq. (1.4d).

In the notation of Eqs. (2.12) and (2.13), the quasi-energy gradient $\mathcal{Q}^A = \mathcal{Q}^A(\mathbf{D}, \dot{\mathbf{D}})$ may be written in terms of partial derivatives of the generalized KS energy $E^{0,A}$ and a reorthonormalization term $\mathrm{tr}\,\mathbf{S}^A\mathbf{W}$ [2]

$$\mathcal{Q}^A = E^{0,A} - \mathrm{tr}\,\mathbf{S}^A\mathbf{W} \tag{2.20}$$

where $E^{0,A}$ is given by,

$$E^{0,A} = \mathrm{tr}\big(\mathbf{h}^A + \mathbf{V}^A + \frac{1}{2}\mathbf{G}^A(\mathbf{D}) - \tfrac{\mathrm{i}}{2}\mathbf{T}^A\big)\mathbf{D} + E^{0,A}_{\mathrm{xc}}[\rho] + h^A_{\mathrm{nuc}} \tag{2.21}$$

because $\mathbf{h}^{0,A} = \mathbf{h}^A$, etc. Note that only the two-electron integrals $g_{\mu\nu\alpha\beta}$ (and not $\mathbf{D}$) are differentiated with respect to ε_A in $\mathbf{G}^A(\mathbf{D})$. The $\mathbf{S}^A$ matrix in Eq. (2.20) is the derivative of the AO overlap matrix

$$S_{\mu\nu} = \langle \chi_\mu | \chi_\nu \rangle \tag{2.22}$$

and $\mathbf{W}$ is a generalized energy-and-frequency-weighted density matrix,

$$\mathbf{W} = \mathbf{DFD} + \frac{\mathrm{i}}{2}\big(\dot{\mathbf{D}}\mathbf{SD} - \mathbf{DS}\dot{\mathbf{D}}\big) \tag{2.23}$$

where $\mathbf{F}$ is the generalized time-dependent Fock matrix

$$\mathbf{F} = \mathbf{E}^{1,0} = \mathbf{h} + \mathbf{G}(\mathbf{D}) + \mathbf{V} - \tfrac{\mathrm{i}}{2}\mathbf{T} + \mathbf{F}_{\mathrm{xc}} \tag{2.24}$$

The functional derivative matrix $\mathbf{F}_{xc} = \mathbf{E}^{1,0}_{\mathrm{xc}}$ is given by

$$F_{xc,\mu\nu} = \int \chi^*_\mu \chi_\nu v_{xc}(\mathbf{r}, t) d\mathbf{x} \tag{2.25}$$

where the exchange-correlation potential $v_{xc}(\mathbf{r}, t)$

$$v_{xc}(\mathbf{r}, t) = \left.\frac{\delta E_{xc}}{\delta \rho(\mathbf{r})}\right|_{\rho(\mathbf{r})=\rho(\mathbf{r},t)} \tag{2.26}$$

have been introduced. In Eq. (2.26) the electron density is evaluated at $\rho(\mathbf{r}) = \rho(\mathbf{r}, t)$. This is the adiabatic approximation [36–38], where it is assumed that the exchange-correlation potential only depends on time through the electron density. We note that Eq. (2.20) reduces to the molecular gradient in the AO basis [62] in the time-independent limit.

If the perturbation A is not described using perturbation-dependent basis sets, most of the terms in Eq. (2.20) vanish and the following simple expression is obtained,

$$\mathcal{Q}^A = \operatorname{tr} \mathbf{V}^A \mathbf{D} \tag{2.27}$$

which represents the expectation value of the one-electron perturbation operator.

The quasi-energy gradient in Eq. (2.20) provides the starting point for generating response functions by further differentiation, according to Eq. (2.10) and (2.11). However, before considering response functions in Section 2.5, we now discuss the parameterization of the density matrix.

2.4 Parameterization of the time-dependent density matrix

The density matrix for a single-determinant SCF state must satisfy the trace, Hermiticity, and idempotency conditions [63]

$$\operatorname{tr} \mathbf{DS} = N \tag{2.28}$$

$$\mathbf{D}^\dagger = \mathbf{D} \tag{2.29}$$

$$\mathbf{DSD} = \mathbf{D} \tag{2.30}$$

where N is the number of electrons in the molecular system. Whereas the trace and Hermiticity conditions are automatically satisfied in the formulation given below, the idempotency relation requires special attention. Furthermore, the time-dependent density matrix must be a solution to the time-dependent SCF (TDSCF) matrix equation [2],

$$\Big(\mathbf{F} - \frac{\mathrm{i}}{2}\mathbf{S}\partial_t\Big)\mathbf{DS} - \Big(\mathbf{SDF} + \frac{\mathrm{i}}{2}\partial_t(\mathbf{SD})\mathbf{S}\Big) = \mathbf{0} \tag{2.31}$$

In the absence of a time-dependent perturbation Eq. (2.31) reduces to the well-known stationary conditions $\mathbf{F}_0\mathbf{D}_0\mathbf{S} = \mathbf{S}\mathbf{D}_0\mathbf{F}_0$ of SCF theory [63], where $\mathbf{F}_0$ and $\mathbf{D}_0$ are the Fock and density matrices for the unperturbed system (the subscript 0 referring to the unperturbed SCF state).

The density matrix is expanded in orders of the perturbation,

$$\mathbf{D} = \mathbf{D}_0 + \mathbf{D}^{(1)} + \mathbf{D}^{(2)} + \cdots \tag{2.32}$$

where the perturbed density matrices are written in terms of their frequency-operator components following Eq. (1.41),

$$\mathbf{D}^{(1)} = \sum_B \varepsilon_B \mathbf{D}^B e^{-\mathrm{i}\omega_B t} \tag{2.33}$$

$$\mathbf{D}^{(2)} = \frac{1}{2}\sum_{BC} \varepsilon_B \varepsilon_C \mathbf{D}^{BC} e^{-\mathrm{i}\omega_{BC} t} \tag{2.34}$$

The perturbed density matrices are partitioned into so-called *particular* and *homogeneous* components. The particular component is chosen such that the time-dependent density matrix satisfies the idempotency relation, whereas the homogeneous component ensures that the density matrix is a solution to the TDSCF equation.

To exemplify the partitioning scheme for the perturbed density matrices, let us consider the first-order perturbed density matrix $\mathbf{D}^B$, which is decomposed into a particular and a homogeneous component

$$\mathbf{D}^B = \mathbf{D}^B_{\mathrm{P}} + \mathbf{D}^B_{\mathrm{H}} \tag{2.35}$$

The inhomogeneous equation is the first-order idempotency condition obtained by differentiating Eq. (2.30) with respect to ε_B and evaluating at zero perturbation strengths,

$$\mathbf{D}^B\mathbf{S}_0\mathbf{D}_0 + \mathbf{D}_0\mathbf{S}_0\mathbf{D}^B - \mathbf{D}^B = \mathbf{N}^B, \quad \mathbf{N}^B = -\mathbf{D}_0\mathbf{S}^B\mathbf{D}_0 \tag{2.36}$$

A particular solution $\mathbf{D}^B_{\mathrm{P}}$ to this equation is given by:

$$\mathbf{D}^B_{\mathrm{P}} = \mathbf{N}^B\mathbf{S}_0\mathbf{D}_0 + \mathbf{D}_0\mathbf{S}_0\mathbf{N}^B - \mathbf{N}^B = -\mathbf{D}_0\mathbf{S}^B\mathbf{D}_0 \tag{2.37}$$

The homogeneous component $\mathbf{D}^B_{\mathrm{H}}$ is parameterized in terms of an unknown matrix $\mathbf{X}^B$ in the form,

$$\mathbf{D}^B_{\mathrm{H}} = \mathbf{D}_0\mathbf{S}_0\mathbf{X}^B - \mathbf{X}^B\mathbf{S}_0\mathbf{D}_0 \tag{2.38}$$

to ensure that $\mathbf{D}^B_{\mathrm{H}}$ is a solution to the homogeneous equation associated with Eq. (2.36),

$$\mathbf{D}^B_H\mathbf{S}_0\mathbf{D}_0 + \mathbf{D}_0\mathbf{S}_0\mathbf{D}^B_H - \mathbf{D}^B_H = \mathbf{0} \tag{2.39}$$

so that $\mathbf{D}^B$ in Eq. (2.35) satisfies the idempotency relation to first order. The matrix $\mathbf{X}^B$ in the homogeneous component $\mathbf{D}^B_{\mathrm{H}}$ is now determined such that $\mathbf{D}^B$ is also a solution to the first-order TDSCF equation. By differentiating Eq. (2.31) with respect to ε_B and evaluating at zero perturbation strengths, the following equation for $\mathbf{X}^B$ is obtained [2]:

$$(\mathbf{E}^{[2]} - \omega_B\mathbf{S}^{[2]})\mathbf{X}^B = \mathbf{R}^B \tag{2.40}$$

where $\mathbf{E}^{[2]}$ and $\mathbf{S}^{[2]}$ are generalized Hessian and metric matrices, respectively. As Eq. (2.40) is solved iteratively, it is not necessary to construct these matrices explicitly; it is sufficient to

know their products with a general matrix $\mathbf{X}$:

$$\begin{aligned}\mathbf{E}^{[2]}\mathbf{X} = {} & \mathbf{E}^{2,0}(\mathbf{X}\mathbf{S}_0\mathbf{D}_0 - \mathbf{D_0}\mathbf{S}_0\mathbf{X})\mathbf{D}_0\mathbf{S}_0 - \mathbf{S}_0\mathbf{D}_0\mathbf{E}^{2,0}(\mathbf{X}\mathbf{S}_0\mathbf{D}_0 - \mathbf{D}_0\mathbf{S}_0\mathbf{X}) \\ & + \mathbf{F}_0(\mathbf{X}\mathbf{S}_0\mathbf{D}_0 - \mathbf{D}_0\mathbf{S}_0\mathbf{X})\mathbf{S}_0 - \mathbf{S}_0(\mathbf{X}\mathbf{S}_0\mathbf{D}_0 - \mathbf{D_0}\mathbf{S}_0\mathbf{X})\mathbf{F}_0 \qquad (2.41)\\ \mathbf{S}^{[2]}\mathbf{X} = {} & \mathbf{S}_0(\mathbf{X}\mathbf{S}_0\mathbf{D}_0 - \mathbf{D}_0\mathbf{S}_0\mathbf{X})\mathbf{S}_0 \qquad (2.42)\end{aligned}$$

where the transformation of $\mathbf{E}^{2,0} = \partial^2 E/\partial(\mathbf{D}^{\mathrm{T}})^2$ on a general matrix $\mathbf{M}$ can be written in the form

$$\mathbf{E}^{2,0}(\mathbf{M}) = \mathbf{G}^{\eta}(\mathbf{M}) + \mathbf{G}^{\mathrm{xc}}(\mathbf{M}) \qquad (2.43)$$

where $\mathbf{G}^{\eta}(\mathbf{M})$ is defined by Eq. (2.17) and the exchange-correlation contribution is

$$G^{xc}_{\mu\nu}(\mathbf{M}) = \sum_{\alpha\beta} M_{\beta\alpha} \int \chi^*_\mu(\mathbf{r})\chi_\nu(\mathbf{r}) \Bigg(\int \chi^*_\alpha(\mathbf{r}_1)\chi_\beta(\mathbf{r}_1) \frac{\delta v_{xc}}{\delta\rho(\mathbf{r}_1)} d\mathbf{x}_1 \Bigg) d\mathbf{x} \qquad (2.44)$$

The right-hand side matrix of the response equations in Eq. (2.40) is given by

$$\begin{aligned}\mathbf{R}^B = {} & \big[\mathbf{E}^{1,B} + \mathbf{E}^{2,0}(\mathbf{D}^B_{\mathrm{P}})\big]\mathbf{D}_0\mathbf{S}_0 + \big(\mathbf{F}_0 - \tfrac{\omega_B}{2}\mathbf{S}_0\big)(\mathbf{D}^B_{\mathrm{P}}\mathbf{S}_0 + \mathbf{D}_0\mathbf{S}^B) \\ & - \mathbf{S}_0\mathbf{D}_0\big[\mathbf{E}^{1,B} + \mathbf{E}^{2,0}(\mathbf{D}^B_{\mathrm{P}})\big] - (\mathbf{S}_0\mathbf{D}^B_{\mathrm{P}} + \mathbf{S}^B\mathbf{D}_0)\big(\mathbf{F}_0 - \tfrac{\omega_B}{2}\mathbf{S}_0\big) \qquad (2.45)\end{aligned}$$

We note that the particular component $\mathbf{D}^B_{\mathrm{P}}$ only depends on the zeroth-order density matrix $\mathbf{D}_0$, whereas the homogeneous component $\mathbf{D}^B_{\mathrm{H}}$ requires the solution of the response equation in Eq. (2.40).

The first-order analysis given above may be generalized to arbitrary orders, decomposing the mth-order density matrix into particular and homogeneous components:

$$\mathbf{D}^{B_1\ldots B_m} = \mathbf{D}^{B_1\ldots B_m}_{\mathrm{P}} + \mathbf{D}^{B_1\ldots B_m}_{\mathrm{H}} \qquad (2.46)$$

The mth-order idempotency condition can be written as

$$\mathbf{D}^{B_1\ldots B_m}\mathbf{S}\mathbf{D}_0 + \mathbf{D}_0\mathbf{S}\mathbf{D}^{B_1\ldots B_m} - \mathbf{D}^{B_1\ldots B_m} = \mathbf{N}^{B_1\ldots B_m} \qquad (2.47)$$

where the inhomogeneity $\mathbf{N}^{B_1\ldots B_m}$ contains perturbed density matrices of order less than m. The mth order particular solution matrix $\mathbf{D}^{B_1\ldots B_m}_{\mathrm{P}}$ has the structure of Eq. (2.37), i.e.,

$$\mathbf{D}^{B_1\ldots B_m}_{\mathrm{P}} = \mathbf{N}^{B_1\ldots B_m}\mathbf{S}_0\mathbf{D}_0 + \mathbf{D}_0\mathbf{S}_0\mathbf{N}^{B_1\ldots B_m} - \mathbf{N}^{B_1\ldots B_m} \qquad (2.48)$$

The mth-order homogeneous component $\mathbf{D}^{B_1\ldots B_m}_{\mathrm{H}}$ is parameterized as in Eq. (2.38),

$$\mathbf{D}^{B_1\ldots B_m}_{\mathrm{H}} = \mathbf{D}_0\mathbf{S}\mathbf{X}^{B_1\ldots B_m} - \mathbf{X}^{B_1\ldots B_m}\mathbf{S}\mathbf{D}_0 \qquad (2.49)$$

where $\mathbf{X}^{B_1\ldots B_m}$ is determined so that the total density matrix in Eq. (2.46) satisfies the TDSCF equation to order m, by solving the mth-order response equation:

$$\big[\mathbf{E}^{[2]} - \omega_{B_1\ldots B_m}\mathbf{S}^{[2]}\big]\mathbf{X}^{B_1\ldots B_m} = \mathbf{R}^{B_1\ldots B_m} \qquad (2.50)$$

where $\omega_{B_1\ldots B_m}$=ω_{B_1}+ . . . +ω_{B_m}. Eq. (2.50) has the same form as the first-order equation in Eq. (2.40), with $\mathbf{R}^{B_1\ldots B_m}$ containing only lower-order density matrices. Since response equations

have the same structure to all orders, the solution matrices $\mathbf{X}$ can be determined using the same solver – for example, the linear-scaling solver of Coriani *et al.* [53], making the calculations suitable for large molecular systems.

In summary, to determine the mth-order density matrices $\mathbf{D}^{B_1 \dots B_m}$, we first construct the mth-order inhomogeneity $\mathbf{N}^{B_1 \dots B_m}$ from lower-order density matrices and determine the particular solutions $\mathbf{D}_{\mathrm{P}}^{B_1 \dots B_m}$. Next, the right-hand sides $\mathbf{R}^{B_1 \dots B_m}$ are constructed from $\mathbf{D}_{\mathrm{P}}^{B_1 \dots B_m}$ and lower-order density matrices, followed by the solution of the mth-order response equations to yield $\mathbf{X}^{B_1 \dots B_m}$ and the homogeneous components $\mathbf{D}_{\mathrm{H}}^{B_1 \dots B_m}$. Finally, the mth order density matrix $\mathbf{D}^{B_1 \dots B_m}$ is determined according to Eq. (2.46). We have thus established a recursive procedure for determining perturbed density matrices to arbitrary order, where the use of (frequency-dependent) PDBSs is an integrated part of the formulation. With the perturbed density matrices at hand, it is straightforward to evaluate response functions as we now discuss.

2.5 Response functions in terms of perturbed density matrices

Response functions may be identified by differentiation of the quasi-energy gradient in Eq. (2.20) according to Eqs. (2.10) and (2.11). In the notation of Eq. (2.13), the derivative of the first term in Eq. (2.20) may be written as (evaluation at zero perturbation strengths implicitly assumed)

$$\frac{dE^{0,A}}{d\varepsilon_B} = \frac{\partial E^{0,A}}{\partial \varepsilon_B} + \mathrm{tr}\, \frac{\partial E^{0,A}}{\partial \mathbf{D}^{\mathrm{T}}} \frac{\partial \mathbf{D}}{\partial \varepsilon_B} = E^{0,AB} + \mathrm{tr}\, \mathbf{E}^{1,A} \mathbf{D}^B \tag{2.51}$$

Including also the derivative of the second term in Eq. (2.20), we obtain the following expression for the linear response function

$$\langle\!\langle A; B \rangle\!\rangle_{\omega_B} = \mathcal{Q}^{AB} = E^{0,AB} + \mathrm{tr}\, \mathbf{E}^{1,A} \mathbf{D}^B - \mathrm{tr}\, \mathbf{S}^{AB} \mathbf{W}_0 - \mathrm{tr}\, \mathbf{S}^A \mathbf{W}^B \tag{2.52}$$

According to Eq. (2.24), the differentiated Fock matrix becomes

$$\mathbf{E}^{1,A} = \mathbf{F}^{0,A} = \mathbf{h}^A + \mathbf{G}^A(\mathbf{D}_0) + \mathbf{V}^A - \tfrac{\mathrm{i}}{2} \mathbf{T}^A + \mathbf{F}_{\mathrm{xc}}^{0,A} \tag{2.53}$$

and, using Eq. (2.23), the $\mathbf{W}$ matrices are given by

$$\mathbf{W}_0 = \mathbf{D}_0 \mathbf{F}_0 \mathbf{D}_0, \tag{2.54}$$

$$\mathbf{W}^B = \mathbf{D}_0 \mathbf{F}^B \mathbf{D}_0 + \mathbf{D}^B \big(\mathbf{F}_0 + \tfrac{\omega_B}{2} \mathbf{S}_0\big) \mathbf{D}_0 + \mathbf{D}_0 \big(\mathbf{F}_0 - \tfrac{\omega_B}{2} \mathbf{S}_0\big) \mathbf{D}^B \tag{2.55}$$

When the basis set does not depend on the external perturbations A and B, only the contribution involving $\mathbf{V}^A$ [see Eq. (2.20)] in the second term in Eq. (2.52) contributes, reducing the linear response function to the simple expression:

$$\langle\!\langle A; B \rangle\!\rangle_{\omega_B} = \mathrm{tr}\, \mathbf{V}^A \mathbf{D}^B \tag{2.56}$$

The quadratic response function in Eq. (2.11) is given by

$$\begin{aligned} \langle\!\langle A; B, C \rangle\!\rangle_{\omega_B, \omega_C} &= Q^{ABC} \\ &= E^{0,ABC} + \mathrm{tr}\big(\mathbf{E}^{1,AC} \mathbf{D}^B + \mathbf{E}^{1,AB} \mathbf{D}^C + \mathbf{E}^{2,A}(\mathbf{D}^B) \mathbf{D}^C + 2 \mathbf{E}^{1,A} \mathbf{D}^{BC}\big) \\ &\quad - \mathrm{tr}\big(\mathbf{S}^{ABC} \mathbf{W}_0 + \mathbf{S}^{AC} \mathbf{W}^B + \mathbf{S}^{AB} \mathbf{W}^C + \mathbf{S}^A \mathbf{W}^{BC}\big) \end{aligned} \tag{2.57}$$

where first-order densities $\mathbf{D}^B$ and $\mathbf{D}^C$, and second-order densities $\mathbf{D}^{BC}$ are required to determine the quadratic response function. This is in accordance with the 1_{2n+1} rule discussed in Section 1.7, see Table 1.1, where all terms involving response parameters referencing perturbation A are eliminated from the response function expression. It is also possible to obtain an expression for $\langle\langle A; B, C\rangle\rangle_{\omega_B,\omega_C}$ that complies with the standard $2n+1$ rule, where only first-order densities $\mathbf{D}^A$, $\mathbf{D}^B$, and $\mathbf{D}^C$ are required (the 3_{2n+1} rule using the notation in Table 1.1). This can be accomplished by constructing a *quasi-energy derivative Lagrangian*, where the idempotency relation in Eq. (2.30) and the TDSCF equation in Eq. (2.31) are added as constraints. With this Lagrangian at hand, it is straightforward to identify a $2n+1$ expression for the quadratic response function as demonstrated in paper [2]. More generally, the elimination rules discussed in Section 1.7 may be used to obtain a plethora of different expressions for cubic and higher order response functions. We refer to paper [2] for details.

2.6 Conclusion

We have presented a generalization of response theory at the HF and KS levels of theory to include (frequency-dependent) PDBSs on the same footing as standard basis sets. The inherent inclusion of PDBSs is advantageous for many molecular properties – for example for vibrational circular dichroism spectra, as we discuss in Chapter 3. The derivations are formulated exclusively in terms of variations in the density matrix in the AO basis with the idempotency relation for the density matrix as a constraint. We have thus established a framework for calculating response functions in the AO basis to arbitrary orders. The presented equations are prone to linear scaling when sparse matrix algebra can be applied.

Chapter 3

Variational response function formulation of vibrational circular dichroism

This chapter describes the work presented in **paper [3]**.

3.1 Introduction

Over the last decade vibrational circular dichroism (VCD) has become an increasingly used spectroscopic tool [64, 65] and is nowadays one of the most efficient and reliable spectroscopic techniques to assign the absolute configuration of chiral species. In VCD spectroscopy the difference in absorption between left and right circularly polarized light is measured for excitations involving vibrational states.

Molecular theories of VCD have been derived in different ways by several authors [66–71]. Implementations of these formulations involve the determination of wave-function parameters perturbed with respect to both the nuclear displacements ($3N$ components) and the magnetic perturbation (3 components), thus requiring the solution of $3N+3$ response equations (N being the number of atoms in the molecule).

In this chapter an alternative formula is discussed, where the atomic axial tensor (AAT) of VCD is recast as the frequency derivative of a linear response function. Using this alternative formula only six response equations are solved (rather than $3N+3$), namely three for the magnetic field responses plus, for each of the magnetic responses, an additional response equation for the "frequency-perturbed" density.

The formulation described here is particularly advantageous when combined with a computationally cheaper scheme to determine the vibrational modes and frequencies. For example, by computing the Hessian with smaller basis sets than used for the VCD tensors (due to the different basis set requirements), or using mode-tracking approaches for the exact calculation of normal modes of a pre-selected molecular vibration in a large molecule [72].

The chapter is organized as follows. In Section 3.2 the relevant VCD quantities are defined, and in Section 3.3 the determination of the AAT in exact response theory is presented. Section 3.4 describes the evaluation of the AAT using the density matrix-based response formulation of Chapter 2, where all contributions from PDBSs – required both to eliminate the gauge-origin problem [73, 74] using London orbitals [56, 57] and to account for the dependence on the Cartesian coordinates of the AOs – are inherently included. Section 3.5 contains some concluding remarks.

3.2 Definition of VCD quantities

We consider a molecular system described by the Born-Oppenheimer approximation, where the total wave function is written as a product of the electronic singlet ground state wave function $|\,\mathrm{o}\rangle$ and a nuclear vibrational wave function $|v\rangle$ (neglecting translation and rotation). In the vibrational ground state (all vibrational quantum numbers are zero), the total wave function is denoted $|o0\rangle$. If the nth vibrational degree of freedom (mode) is excited to the lowest excited vibrational state, the total wave function (still in the electronic ground state) is denoted $|o1_n\rangle$.

The intensity of the VCD-band for the $|o0\rangle\rightarrow|o1_n\rangle$ transition is determined by the rotational strength $R(o0 \rightarrow o1_n)$ [66]

$$R(o0 \rightarrow o1_n) = \sum_{\alpha} \mathrm{Im}\{\langle o0|\mu_\alpha|o1_n\rangle\langle o1_n|m_\alpha|o0\rangle\} \tag{3.1}$$

where μ_α ($\alpha = x, y, z$) are the Cartesian components of the electric dipole moment operator and m_α those of the magnetic dipole moment operator. The vibrational electric and magnetic dipole transition moments are

$$\langle o0|\mu_\beta|o1_n\rangle = \Big(\frac{1}{2\tilde{\omega}_n}\Big)^{\frac{1}{2}} \sum_{I,\alpha} S^I_{\alpha,n} P^I_{\alpha\beta} \tag{3.2}$$

$$\langle o0|m_\beta|o1_n\rangle = (2\tilde{\omega}_n)^{\frac{1}{2}} \sum_{I,\alpha} S^I_{\alpha,n} M^I_{\alpha\beta} \tag{3.3}$$

where I runs over the nuclei, $\tilde{\omega}_n$ is the harmonic angular frequency of the nth mode, and $S^I_{\alpha,n}$ is the transformation matrix from Cartesian nuclear displacements to mass-weighted normal mode displacements Q_n, i.e.,

$$R^I_\alpha - R^I_{\alpha,\mathrm{eq}} = \sum_n S^I_{\alpha,n} Q_n \tag{3.4}$$

The *atomic polar tensor* (APT) $P^I_{\alpha\beta}$ in Eq. (3.2) is the geometry-derivative of the electric dipole moment of the electronic ground state evaluated at the equilibrium geometry $\boldsymbol{R}_{\mathrm{eq}}$

$$P^I_{\alpha\beta} = \left(\frac{\partial \mu^{oo}_\beta}{\partial R^I_\alpha}\right)_{\mathrm{eq}}, \qquad \mu^{oo}_\beta = \langle o|\mu_\beta|o\rangle \tag{3.5}$$

The *atomic axial tensor* (AAT) $M^I_{\alpha\beta}$ in Eq. (3.3) is the derivative of the ground state magnetic moment with respect to the velocity of the nuclei [70]

$$M^I_{\alpha\beta} = \left(\frac{\partial m^{oo}_\beta}{\partial \dot{R}^I_\alpha}\right)_{\mathrm{eq}}, \qquad m^{oo}_\beta = \langle o|m_\beta|o\rangle \tag{3.6}$$

This may be written as a sum of an electronic ($I^I_{\alpha\beta}$) and a nuclear ($\mathcal{J}^I_{\alpha\beta}$) contribution [66]

$$M^I_{\alpha\beta} = I^I_{\alpha\beta} + \mathcal{J}^I_{\alpha\beta} \tag{3.7}$$

$$I^I_{\alpha\beta} = \left\langle \frac{\partial o}{\partial R^I_\alpha} \middle| \frac{\partial o}{\partial B_\beta} \right\rangle \tag{3.8}$$

$$\mathcal{J}^I_{\alpha\beta} = \frac{1}{4}\varepsilon_{\alpha\beta\gamma} Z_I R^I_{\gamma,\mathrm{eq}} \tag{3.9}$$

where B_β is a magnetic field strength component. Most existing procedures for computing the VCD rotational strength utilize Eqs. (3.8) and (3.9) for determining the AAT.

The APT may straightforwardly be evaluated as the geometric gradient of the electric dipole moment (see paper [3] for details), and the main challenge in VCD formulations is therefore to determine the electronic component of the AAT. In the following we focus solely on obtaining an efficient expression for $I^I_{\alpha\beta}$.

3.3 Response function formulation of the AAT

To determine $I^I_{\alpha\beta}$ within the response function formalism, it is convenient to introduce the geometrical gradient operator g^I_α (electronic part thereof),

$$g^I_\alpha = \left(\frac{\partial V_{\mathrm{Ne}}}{\partial R^I_\alpha}\right)_{\mathrm{eq}} \tag{3.10}$$

where V_{Ne} is the nuclei-electron attraction term in Eq. (1.4b). Consider next the linear response function $\langle\langle g^I_\alpha; m_\beta \rangle\rangle_\omega$, which may be written in the sum-over-states expression in Eq. (1.35a),

$$\begin{aligned}\langle\langle g^I_\alpha; m_\beta \rangle\rangle_\omega &= \sum_{j\neq o}\left(\frac{\langle o|g^I_\alpha|j\rangle\langle j|m_\beta|o\rangle}{\omega-\omega_j} - \frac{\langle o|m_\beta|j\rangle\langle j|g^I_\alpha|o\rangle}{\omega+\omega_j}\right) \\ &= -\sum_{j\neq o}\frac{2\omega}{\omega_j^2-\omega^2}\langle o|g^I_\alpha|j\rangle\langle j|m_\beta|o\rangle\end{aligned} \tag{3.11}$$

where ω_j is the excitation energy from the (electronic) ground state $|o\rangle$ to the (electronic) excited state $|j\rangle$. To obtain the last equality in Eq. (3.11) we have assumed that the excited states are real and used the fact that g^I_α is a real operator, whereas m_β is an imaginary operator.

The first-order expansion of a state $|o\rangle$ in the presence of a (static) magnetic field described by the perturbation $V = -\sum_\beta B_\beta m_\beta$ is [13]

$$|o\rangle = |o\rangle_0 + \sum_\beta \left|\frac{\partial o}{\partial B_\beta}\right\rangle B_\beta + \ldots \tag{3.12}$$

$$\left|\frac{\partial o}{\partial B_\beta}\right\rangle = -\sum_{j\neq o}|j\rangle\frac{\langle j|m_\beta|o\rangle}{\omega_j} \tag{3.13}$$

For a nuclear displacement perturbation $V = \sum_{I,\alpha}(R^I_\alpha - R^I_{\alpha,\mathrm{eq}})g^I_\alpha$ an equivalent expansion can

be introduced

$$|o\rangle = |o\rangle_{\text{eq}} + \sum_{I,\alpha} \left| \frac{\partial o}{\partial R^I_\alpha} \right\rangle (R^I_\alpha - R^I_{\alpha,\text{eq}}) + \cdots \tag{3.14}$$

$$\left| \frac{\partial o}{\partial R^I_\alpha} \right\rangle = \sum_{j \neq o} |j\rangle \frac{\langle j|g^I_\alpha|o\rangle}{\omega_j} \tag{3.15}$$

Using Eqs. (3.13) and (3.15), the electronic part of the AAT in Eq. (3.8) may be expressed as

$$\begin{aligned} I^I_{\alpha\beta} &= \left\langle \frac{\partial o}{\partial R^I_\alpha} \middle| \frac{\partial o}{\partial B_\beta} \right\rangle \\ &= -\sum_{j,k \neq o} \frac{\langle o|g^I_\alpha|j\rangle}{\omega_j} \langle j|k\rangle \frac{\langle k|m_\beta|o\rangle}{\omega_{ko}} \\ &= -\sum_{j \neq o} \frac{\langle o|g^I_\alpha|j\rangle\langle j|m_\beta|o\rangle}{\omega_j^2} \end{aligned} \tag{3.16}$$

Comparing Eq. (3.16) with Eq. (3.11) we obtain the following expression for the AAT,

$$I^I_{\alpha\beta} = \frac{1}{2} \frac{d}{d\omega} \langle\langle g^I_\alpha; m_\beta \rangle\rangle_\omega \Big|_{\omega=0} \tag{3.17}$$

Eq. (3.17) is the central equation for the AAT. It states that the AAT can be computed as the frequency derivative of the response function $\langle\langle g^I_\alpha; m_\beta \rangle\rangle_\omega$ evaluated at zero frequency.

3.4 The AAT in the density-matrix based quasi-energy formalism

We now summarize the determination of the AAT at the DFT level of theory within the density-matrix quasi-energy formalism described in Chapter 2. For reasons of brevity all the involved matrices are not presented here, and we refer to paper [3] for details. Rather, we focus on the overall structure of the response function used to determine the AAT and on the use of PDBSs.

Let us first consider the frequency-dependent response function $\langle\langle g^I_\alpha; m_\beta \rangle\rangle_\omega$ and then move on to evaluate its frequency-derivative in the static limit [the AAT in Eq. (3.17)].

3.4.1 Frequency-dependent linear response function

The general form of an external perturbation $V(t)$ is given in Eq. (1.18). Recalling that g^I_α is given by Eq. (3.10), the relevant perturbing operator $V(t)$ for determining $\langle\langle g^I_\alpha; m_\beta \rangle\rangle_\omega$ is given by

$$V(t) = \sum_{I,\alpha} \left(R^I_\alpha - R^I_{\alpha,\text{eq}}\right) g^I_\alpha - \sum_\alpha B_\alpha m_\alpha \tag{3.18}$$

with

$$R^I_\alpha - R^I_{\alpha,\text{eq}} = (R^I_{\alpha,\omega} e^{-i\omega t} + R^{I*}_{\alpha,\omega} e^{+i\omega t}) \tag{3.19}$$

$$B_\alpha = (B_{\alpha,\omega} e^{-i\omega t} + B^*_{\alpha,\omega} e^{+i\omega t}) \tag{3.20}$$

where $B_{\alpha,\omega}$ and $R^I_{\alpha,\omega}$ are perturbation strengths for the magnetic and geometric perturbations, respectively.

To ensure gauge-invariant results we employ (frequency-dependent) London atomic orbitals [56, 57] $\{\xi_\mu\}$, which depend both on the magnetic field and on the nuclear positions

$$\xi_\mu(\boldsymbol{r};\boldsymbol{R},\boldsymbol{B}) = \exp\left\{\tfrac{i}{2}(\boldsymbol{R}^{I(\mu)}-\boldsymbol{G})\times\boldsymbol{B}\cdot\boldsymbol{r}\right\}\chi_\mu(\boldsymbol{r}-\boldsymbol{R}^{I(\mu)}) \tag{3.21}$$

where $\{\chi_\mu\}$ are ordinary AOs, $I(\mu)$ indicates the nucleus on which ξ_μ is centered, and $\boldsymbol{G}$ is the magnetic gauge-origin. The relevant response function $\langle\langle g^I_\alpha; m_\beta\rangle\rangle_\omega$ is given by Eq. (2.52):

$$\begin{aligned}-\langle\langle g^I_\alpha; m_\beta\rangle\rangle_\omega &= E^{0,RB} + \operatorname{tr}\mathbf{E}^{1,R}\mathbf{D}^B - \operatorname{tr}\mathbf{S}^{RB}\mathbf{W}_0 - \operatorname{tr}\mathbf{S}^R\mathbf{W}^B \\ &= E^{0,RB} + \operatorname{tr}\mathbf{E}^{1,R}\mathbf{D}^B - \operatorname{tr}\mathbf{S}^R\mathbf{W}^B\end{aligned} \tag{3.22}$$

where superscripts R and B indicate differentiation with respect to the perturbation strengths $R^{I*}_{\alpha,\omega}$ and $B_{\alpha,\omega}$ associated with the nuclear displacements and the magnetic field, respectively. (The minus sign in Eq. (3.22) enters due to the conventional minus sign in the magnetic contribution in Eq. (3.18)). We note that the inclusion of frequency-dependent PDBSs in Eq. (3.22) – both the magnetic field dependence and the dependence on the nuclear positions – is an integrated part of the density matrix formulation in Chapter 2.

3.4.2 The atomic axial tensor in the density-matrix quasi-energy formulation

Within the density matrix based KS-DFT formalism the AAT in Eq. (3.17) is identified by differentiating Eq. (3.22) with respect to the optical frequency and evaluating in the static limit:

$$\begin{aligned}-\frac{d}{d\omega}\langle\langle g^I_\alpha; m_\beta\rangle\rangle_\omega\Big|_{\omega=0} &= -\tfrac{i}{2}\operatorname{tr}\mathbf{T}^{RB\omega}\mathbf{D}_0 + \operatorname{tr}\mathbf{S}^R\mathbf{W}^{B\omega} - \tfrac{i}{2}\operatorname{tr}\mathbf{T}^{R\omega}\mathbf{D}^B_{\omega=0} \\ &\quad + \operatorname{tr}\left[\mathbf{h}^R + \mathbf{V}^{t,R} - \tfrac{i}{2}\mathbf{T}^R + \mathbf{G}^{\eta,R}(\mathbf{D}_0) + \mathbf{E}^{1,R}_{\mathrm{xc}}\right]\mathbf{D}^{B\omega}\end{aligned} \tag{3.23}$$

where we have used the notation that,

$$\mathbf{D}^B_{\omega=0} = \mathbf{D}^B(\omega=0) \tag{3.24}$$

$$\mathbf{D}^{B\omega} = \frac{d\mathbf{D}^B(\omega)}{d\omega}\Big|_{\omega=0} \tag{3.25}$$

The important point is that only six response response equations of the form in Eq. (2.40) are required to determine all $3N\times 3$ components of the AAT using Eq. (3.23): three equations to determine the $\mathbf{D}^B_{\omega=0}$ components, and also three equations to determine the $\mathbf{D}^{B\omega}$ components. Specifically, the determination of $\mathbf{D}^B_{\omega=0}$ [see Eqs. (2.35)-(2.38)] requires the solution of three static magnetic field equations for the $\mathbf{X}^B_{\omega=0}$ matrix [Eq. (2.40) in the static limit],

$$\mathbf{D}^B_{\omega=0} = \mathbf{D}_0\mathbf{S}_0\mathbf{X}^B_{\omega=0} - \mathbf{X}^B_{\omega=0}\mathbf{S}_0\mathbf{D}_0 \tag{3.26}$$

$$\mathbf{E}^{[2]}\mathbf{X}^B_{\omega=0} = \mathbf{R}^B_{\omega=0} \tag{3.27}$$

and the determination of $\mathbf{D}^{B\omega}$ requires the solution of three response equations for $\mathbf{X}^{B\omega}$,

$$\mathbf{D}^{B\omega} = \mathbf{D}_0\mathbf{S}_0\mathbf{X}^{B\omega} - \mathbf{X}^{B\omega}\mathbf{S}_0\mathbf{D}_0 \tag{3.28}$$

$$\mathbf{E}^{[2]}\mathbf{X}^{B\omega} = \mathbf{R}^{B\omega} + \mathbf{S}^{[2]}\mathbf{X}^B \tag{3.29}$$

Eq. (3.29) is obtained by differentiating the frequency-dependent first order magnetic response equation in Eq. (2.40) with respect to ω and evaluating it in the static limit, see paper [3] for details.

3.5 Summary

We have presented an alternative formula to compute the AAT of VCD based on the frequency derivative of the linear response function $\langle\langle g^I_\alpha; m_\beta \rangle\rangle_\omega$. The formula for the AAT will of course yield the same results as existing VCD implementations based on alternative formulae [66–71]. and therefore no VCD numbers have been presented in this chapter.

The proposed formula has been implemented within the density matrix-based KS-DFT response formulation in Chapter 2, which – in contrast to existing AAT implementations – allows one to compute the AAT without solving any response equations for the $3N$ geometric displacements. Only six response equations are solved: three for the magnetic field perturbed densities, and three for the associated "frequency-perturbed" magnetic field-perturbed densities. The formalism naturally accounts for all contributions arising from the use of PDBSs. As only basic linear algebra operations of AO matrices are involved, the evaluation of the AAT is amenable to linear scaling provided that the matrices are sufficiently sparse and a linear-scaling response solver is used.

Chapter 4

Quasi-energy formulation of damped response theory

This chapter describes the work presented in **paper [4]**.

4.1 Introduction

Molecular response functions have singularities when one of the optical frequencies equals an excitation energy [see for example Eq. (1.35)]. This leads to an nonphysical behavior for calculated molecular properties in the resonance region, such as divergence of dispersion curves and absorption stick spectra. This nonphysical behavior is caused by the fact that the excited state lifetimes are assumed to be infinite when the standard molecular response functions are derived.

For a rigorous treatment of molecular properties, which reproduces the correct physical behavior at resonance frequencies, the finite lifetime of an excited molecular system has to be taken into account. This is not readily done using a standard quantum chemical description, and finite lifetimes have therefore been introduced using a phenomenological description by multiplying the excited states by a damping factor [75].

From a practical point of view, the introduction of finite excited-state lifetimes into the response functions allows broadened absorption (or dispersion) spectra in any frequency range to be calculated directly – that is, without explicit reference to transition strengths involving the individual excited states. The direct calculation of absorption spectra in damped response theory is particularly advantageous in cases where the standard response-theory approach is very cumbersome, mainly because many individual excited states need to be addressed. Such cases include electronic transitions to high-lying excited states in X-ray spectroscopy and absorption spectra of large molecules in general, where the density of the excited states is particularly high. To illustrate the latter case we have depicted energy levels for a "small" and a "large" molecule in Figure 4.1. Standard response theory uses a brute-force "bottom-up" approach for determining the excited state energies, starting with the energetically lowest lying excited state. Using this approach excitations involving, for example, the fifty lowest lying excited states can

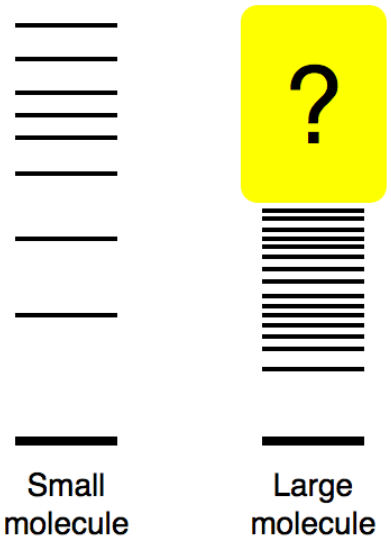

Figure 4.1: Schematic illustration of the excited states for a "small" molecule (left) and for a "large" molecule (right). The excited states hidden behind the question mark cannot be accessed using standard response theory, see the text for details.

be identified, and this is usually sufficient to determine absorption spectra in the frequency range of interest for a small molecule, see Figure 4.1 (left). However, due to the high density of excited states in a large molecule, only a very limited fraction of the absorption spectrum can be determined using the standard response theory approach, see Figure 4.1 (right). In contrast, using damped response theory, the absorption spectrum can be determined in any frequency range of interest without detailed knowledge about the excited state manifold. Thus, damped response theory allows one to investigate absorption processes involving excited states "behind the yellow curtain" in Figure 4.1.

In practice damped response theory may be formulated in different ways. In their complex propagator approach, Norman *et al.* [76] introduced a damping term into the Liouville equation to account for the finite lifetimes of excited states and identified damped response functions from this equation. Alternatively, damped response theory may be formulated by introducing finite lifetimes directly into the response functions in terms of complex excitation energies as described in paper [4]. These two formulations are equivalent, giving the same damped response function expressions. In both formulations, finite excited-state lifetimes are introduced by means of an *empirical* damping parameter. This parameter is input to the response calculation – the theory provides no recipe for determining the damping parameter. Below we discuss damped response theory in terms of complex excitation energies.

In Section 4.2 we discuss the introduction of empirical finite excited state lifetimes and the associated physical interpretations. In Section 4.3 we describe damped response theory with focus on damped linear response theory, and Section 4.4 contains some illustrate results. Finally, in Section 4.5 we give some concluding remarks.

4.2 Phenomenological damping of excited states

Assuming that the excited-state wave function $|n\rangle$ is a solution to the time-independent Schrödinger equation

$$H_0|n\rangle = E_n|n\rangle \tag{4.1}$$

the time-dependent excited state $|n(t)\rangle$

$$|n(t)\rangle = \mathrm{e}^{-iE_n t}|n\rangle \tag{4.2}$$

trivially satisfies the time-dependent Schrödinger equation,

$$\mathrm{i}\frac{\partial|n(t)\rangle}{\partial t} = H_0|n(t)\rangle = E_n|n(t)\rangle \tag{4.3}$$

The norm of $|n(t)\rangle$ is constant in time,

$$\langle n(t)|n(t)\rangle = \langle n|n\rangle = 1 \tag{4.4}$$

and therefore no decay occurs from the excited state to the ground state (or to other excited states). In other words, the lifetime of the excited state $|n(t)\rangle$ is infinite.

In reality, an excited state has a finite lifetime, but the decay mechanism between the excited state and the ground state is not readily described by the Hamiltonian H_0. However, a *phenomenological* description of the lifetime may be obtained by introducing a *damped excited state* $|\bar{n}(t)\rangle$ according to

$$|\bar{n}(t)\rangle = \mathrm{e}^{-\gamma t}|n(t)\rangle = \mathrm{e}^{-\mathrm{i}(E_n - \mathrm{i}\gamma)t}|n\rangle \tag{4.5}$$

The norm of the damped excited state $|\bar{n}(t)\rangle$ decays exponentially in time,

$$\langle\bar{n}(t)|\bar{n}(t)\rangle = \mathrm{e}^{-2\gamma t} \tag{4.6}$$

and $(2\gamma)^{-1}$ may therefore be interpreted as the effective lifetime of the excited state. The nondamped state $|n(t)\rangle$ in Eq. (4.3) possesses a real energy E_n; by contrast, the damped excited state $|\bar{n}(t)\rangle$ does not possess a well-defined real energy due to its finite lifetime (the energy-time uncertainty principle),

$$\mathrm{i}\frac{\partial|\bar{n}(t)\rangle}{\partial t} = (E_n - \mathrm{i}\gamma)|\bar{n}(t)\rangle \tag{4.7}$$

Comparing Eqs. (4.2) and (4.5) it is seen that damped excited states effectively can be introduced in terms of complex excited-state energies:

$$E_n \to E_n - \mathrm{i}\gamma \tag{4.8}$$

In the absence of external perturbations, the ground-state lifetime is infinite and the damping parameter associated with the ground-state energy E_0 is therefore zero. Thus, the substitution in Eq. (4.8) is equivalent to introducing complex excitation energies,

$$\omega_n \to \bar{\omega}_n = \omega_n - \mathrm{i}\gamma, \quad \omega_n = E_n - E_0 \tag{4.9}$$

From a pragmatic point of view, damped response theory is simply a matter of performing the substitution in Eq. (4.9) in the standard response function expressions to obtain a set of damped response functions. Here, and in Chapters 5 and 6, a bar indicates that the replacement in Eq. (4.9) has been carried out.

Let us comment on the physical interpretation of the damping parameter γ, which is an effective (inverse) lifetime common to all excited states. Due to the energy-time uncertainty principle this lifetime is related to the widths of peaks in absorption spectra. In standard response theory [13] transitions between the ground state and excited states are described in terms of oscillator strengths which are obtained from residues of response functions, see for example Eq. (1.38). This gives rise to a delta-peaked residue spectrum (absorption spectrum). In an experimental absorption spectrum the peaks are broadened and the oscillator strength is obtained by integration over the absorption band representing the electronic transition. The broadening of the electronic absorption bands is in general associated with contributions arising from very different physical phenomena:

- The isolated molecule possesses a finite lifetime due to spontaneous emission. This gives rise to an energy uncertainty manifested in a broadening of the absorption bands.
- The vibrational substructure of electronic absorption spectra leads to a broadening of the absorption bands.
- In an experiment the molecules are moving relative to the detector which leads to Doppler-broadening.
- Collisions among molecules perturb the electron densities and therefore the excited state energies, leading to a broadening of the absorption bands.

Unfortunately, it is essentially impossible to devise an accurate *ab initio* model, which takes into account the very many different broadening effects and provides a γ value tailored for each excited state. In any case, such a task is beyond the scope of this text. In this and the following chapters we therefore consider γ as a single empirical parameter, effectively encompassing all the broadening phenomena listed above.

We now discuss the implications of carrying out the replacement in Eq. (4.9) into the standard response function expressions to obtain the corresponding damped response functions.

4.3 Damped response theory

4.3.1 Damped response parameters

As discussed in Section 1.6, standard response functions may be written in terms of a set of response parameters x. The response equations in exact response theory all have the same form of Eq. (1.46). A more detailed derivation [4] shows that $\mathcal{Q}^{2,0}$ contains a (frequency-independent)

Hessian term $\mathbf{E}^{[2]}$ and a frequency-dependent metric term $\omega\mathbf{S}^{[2]}$. Specifically, using matrix notation the m'th order response equation for the $x^{B_1\ldots B_m}$ parameters may be written as,

$$(\mathbf{E}^{[2]} - \omega_{B_1\ldots B_m}\mathbf{S}^{[2]})\mathbf{x}^{B_1\ldots B_m} = \mathbf{g}^{B_1\ldots B_m} \tag{4.10}$$

where the right-hand side vector $\mathbf{g}^{B_1\ldots B_m}$ contains response parameters of order $m-1$ and below. In general, the Hessian $\mathbf{E}^{[2]}$ and metric $\mathbf{S}^{[2]}$ matrices have the paired structures:

$$\mathbf{E}^{[2]} = \begin{pmatrix} \mathbf{A} & \mathbf{B} \\ \mathbf{B}^* & \mathbf{A}^* \end{pmatrix} \tag{4.11}$$

$$\mathbf{S}^{[2]} = \begin{pmatrix} \boldsymbol{\Sigma} & \boldsymbol{\Delta} \\ -\boldsymbol{\Delta}^* & -\boldsymbol{\Sigma}^* \end{pmatrix} \tag{4.12}$$

where an asterisk denotes complex conjugation. In exact theory $\mathbf{E}^{[2]}$ and $\mathbf{S}^{[2]}$ are diagonal,

$$\mathbf{E}^{[2]} = \begin{pmatrix} \boldsymbol{\omega}_k & \mathbf{0} \\ \mathbf{0} & \boldsymbol{\omega}_k^* \end{pmatrix} \tag{4.13}$$

$$\mathbf{S}^{[2]} = \begin{pmatrix} \mathbf{1} & \mathbf{0} \\ \mathbf{0} & -\mathbf{1} \end{pmatrix} \tag{4.14}$$

where $\boldsymbol{\omega}_k$ is a diagonal matrix containing the excitation energies. Using the diagonal representation the m'th order response parameters may be written out explicitly,

$$\begin{pmatrix} {}^1\mathbf{x}^{B_1\ldots B_m} \\ {}^2\mathbf{x}^{B_1\ldots B_m} \end{pmatrix} = \begin{pmatrix} (\boldsymbol{\omega}_k - \boldsymbol{\omega}_{B_1\ldots B_m})^{-1} & \mathbf{0} \\ \mathbf{0} & (\boldsymbol{\omega}_k^* + \boldsymbol{\omega}_{B_1\ldots B_m})^{-1} \end{pmatrix} \begin{pmatrix} {}^1\mathbf{g}^{B_1\ldots B_m} \\ {}^2\mathbf{g}^{B_1\ldots B_m} \end{pmatrix} \tag{4.15}$$

Although the excitation energies are real in standard response theory, we have retained the complex conjugation in the lower right blocks in Eqs. (4.13) and (4.15). In this way we impose the requirement that the paired structure of the Hessian matrix in standard response theory is retained also in damped response theory. Specifically, by introducing complex excitation energies according to Eq. (4.9) the *damped generalized Hessian* $\bar{\mathbf{E}}^{[2]}$ becomes:

$$\mathbf{E}^{[2]} \rightarrow \bar{\mathbf{E}}^{[2]} = \begin{pmatrix} \bar{\boldsymbol{\omega}}_k & \mathbf{0} \\ \mathbf{0} & \bar{\boldsymbol{\omega}}_k^\star \end{pmatrix} = \begin{pmatrix} \boldsymbol{\omega}_k - i\boldsymbol{\gamma} & \mathbf{0} \\ \mathbf{0} & \boldsymbol{\omega}_k + i\boldsymbol{\gamma} \end{pmatrix} = \mathbf{E}^{[2]} - i\gamma\mathbf{S}^{[2]} \tag{4.16}$$

where we have used Eq. (4.14), and where $\boldsymbol{\gamma}$ is a diagonal matrix with γ on all diagonal entries. The damped counterpart of the mth order response equation in Eq. (4.10) determines the mth order *damped response vector* $\bar{\mathbf{x}}^{B_1\ldots B_m}$,

$$[\mathbf{E}^{[2]} - (\omega_{B_1\ldots B_m} + i\gamma)\mathbf{S}^{[2]}]\bar{\mathbf{x}}^{B_1\ldots B_m} = \bar{\mathbf{g}}^{B_1\ldots B_m} \tag{4.17}$$

where we have also carried out the replacement in Eq. (4.9) in the right-hand side vector $\mathbf{g}^{B_1\ldots B_m}$ whenever an excitation energy occurs to obtain the damped right-hand side vector $\bar{\mathbf{g}}^{B_1\ldots B_m}$. Inversion of Eq. (4.17) yields the damped analogue of the standard response equation in Eq. (4.15):

$$\begin{pmatrix} {}^1\bar{\mathbf{x}}^{B_1\ldots B_m} \\ {}^2\bar{\mathbf{x}}^{B_1\ldots B_m} \end{pmatrix} = \begin{pmatrix} (\boldsymbol{\omega}_k - \boldsymbol{\omega}_{B_1\ldots B_m} - i\boldsymbol{\gamma})^{-1} & \mathbf{0} \\ \mathbf{0} & (\boldsymbol{\omega}_k + \boldsymbol{\omega}_{B_1\ldots B_m} + i\boldsymbol{\gamma})^{-1} \end{pmatrix} \begin{pmatrix} {}^1\bar{\mathbf{g}}^{B_1\ldots B_m} \\ {}^2\bar{\mathbf{g}}^{B_1\ldots B_m} \end{pmatrix} \tag{4.18}$$

A comparison of the standard response equation in Eq. (4.15) and the damped response equation in Eq. (4.18) illustrates the main differences between standard response theory and damped response theory:

- Standard response vectors and standard response functions are either purely real or purely imaginary (depending on the perturbing operators in question), whereas damped response vectors and damped response functions are complex quantities.
- When the optical frequency approaches an excitation energy, $\omega_{B_1 \ldots B_m} \rightarrow \omega_k$, the standard response vector $x_k^{B_1 \ldots B_m}$ diverges. In contrast, the corresponding element of the damped response vector $\bar{x}_k^{B_1 \ldots B_m}$ is well-defined at all frequencies, including $\omega_{B_1 \ldots B_m} = \omega_k$.
- Comparing Eq. (4.15) and Eq. (4.18) it is seen that damped response theory effectively corresponds to introducing complex frequencies, e.g.,

$$\omega_{B_1 \ldots B_m} \rightarrow \omega_{B_1 \ldots B_m} + \mathrm{i}\gamma. \tag{4.19}$$

  In practice, therefore, damped response theory is a matter of solving response equations with complex frequencies [4, 76, 77].

In general, the real and imaginary components of a damped response function contains information about dispersion and absorption processes, respectively (or vice versa, depending on the nature of the operators). To exemplify this we now consider the damped linear response function.

4.3.2 Damped linear response theory

By carrying out the replacement in Eq. (4.19) into the linear response function in Eq. (1.35a), we obtain a sum-over-states expression for the *damped linear response function* $\overline{\langle\langle A; B \rangle\rangle}_{\omega_B}$:

$$\overline{\langle\langle A; B \rangle\rangle}_{\omega_B} = -\sum_j \left(\frac{A^{oj} B^{jo}}{\omega_j - (\omega_B + i\gamma)} + \frac{A^{jo} B^{oj}}{\omega_j + (\omega_B + i\gamma)} \right) \tag{4.20}$$

where we have used the short-hand notation for transition matrix elements in Eq. (1.36). To illustrate the underlying structure of the damped linear response function, let us consider the case where $A{=}B{=}\mu_\alpha$ is a component of the electric dipole operator and write out in detail the real and imaginary components of the damped response function,

$$\begin{aligned} \overline{\langle\langle \mu_\alpha; \mu_\alpha \rangle\rangle}_{\omega_B} = -\sum_j \Big(& \mu_\alpha^{oj} \mu_\alpha^{jo} d_j(\omega_B) + \mu_\alpha^{oj} \mu_\alpha^{jo} d_j(-\omega_B) \\ & + \mathrm{i}\big[\mu_\alpha^{oj} \mu_\alpha^{jo} a_j(\omega_B) - \mu_\alpha^{oj} \mu_\alpha^{jo} a_j(-\omega_B) \big] \Big) \end{aligned} \tag{4.21}$$

where we have introduced the *dispersion and absorption lineshape functions* $d_j(\pm\omega)$ and $a_j(\pm\omega)$,

$$d_j(\omega) = \frac{\omega_j - \omega}{(\omega_j - \omega)^2 + \gamma^2}, \qquad d_j(-\omega) = \frac{\omega_j + \omega}{(\omega_j + \omega)^2 + \gamma^2} \tag{4.22a}$$

$$a_j(\omega) = \frac{\gamma}{(\omega_j - \omega)^2 + \gamma^2}, \qquad a_j(-\omega) = \frac{\gamma}{(\omega_j + \omega)^2 + \gamma^2} \tag{4.22b}$$

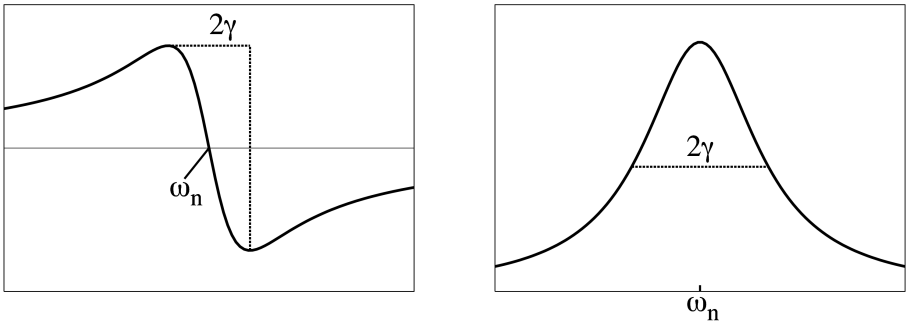

Figure 4.2: Dispersion $d_n(\omega)$ (left) and absorption $a_n(\omega)$ (right) lineshape functions entering in damped response theory.

The dispersion and absorption lineshape functions are plotted in Figure 4.2. Note that γ determines the width of the lineshape functions; in particular 2γ is full width at half maximum (FWHM) for the Lorentzian absorption lineshape function.

In the *nonresonant region* the real component of $\overline{\langle\langle \mu_\alpha; \mu_\alpha \rangle\rangle}_{\omega_B}$ is – for practical purposes – identical to the standard response function $\langle\langle \mu_\alpha; \mu_\alpha \rangle\rangle_{\omega_B}$ [4]. A plot of (minus) $\overline{\langle\langle \mu_\alpha; \mu_\alpha \rangle\rangle}_{\omega_B}$ against ω_B thus yields a spectrum of the polarizability. In the *resonant region* $\langle\langle \mu_\alpha; \mu_\alpha \rangle\rangle_{\omega_B}$ diverges [see Eq. (1.35a)], whereas the real component of $\overline{\langle\langle \mu_\alpha; \mu_\alpha \rangle\rangle}_{\omega_B}$ is well-defined and has the qualitatively correct dispersion shape in Figure 4.2 (left). The real part of the damped linear response function thus provides a physically reasonable description of the polarizability at all frequencies, whereas the standard response function is well-behaved only in the nonresonant region.

The *imaginary* part of $\overline{\langle\langle \mu_\alpha; \mu_\alpha \rangle\rangle}_{\omega_B}$ plotted against ω_B describes a one-photon absorption spectrum, where Lorentzian lineshape functions a_j are superimposed onto the electric-dipole transition strengths $|\mu_\alpha^{0j}|^2$. In other words, in damped linear response theory the residue stick spectrum of the standard linear response function in Eq. (1.38) with superimposed lineshape functions is effectively projected onto the imaginary axis. We emphasize that, using damped response theory, absorption spectra may be obtained in any frequency range of interest simply by calculating $\overline{\langle\langle A; B \rangle\rangle}_{\omega_B}$ for a set of frequencies ω_B in this frequency range and plotting $\mathrm{Im}(\overline{\langle\langle A; B \rangle\rangle}_{\omega_B})$ against ω_B.

4.3.3 Higher-order damped response theory

For the damped linear response function discussed above, the introduction of complex excitation energies is equivalent to introducing complex frequencies. Likewise, for higher order response functions, complex frequencies are effectively introduced in accordance with Eq. (4.19) for each frequency entering the response function. In general, the introduction of damping terms into a nonlinear damped response function can be interpreted in a similar way as for the polarizability in Section 4.3.2, where one component describes dispersion and the other absorption. In Chapters 5 and 6 we consider examples of damped quadratic and damped cubic response theory, respectively, and we therefore refrain from discussing damped nonlinear response theory in this chapter.

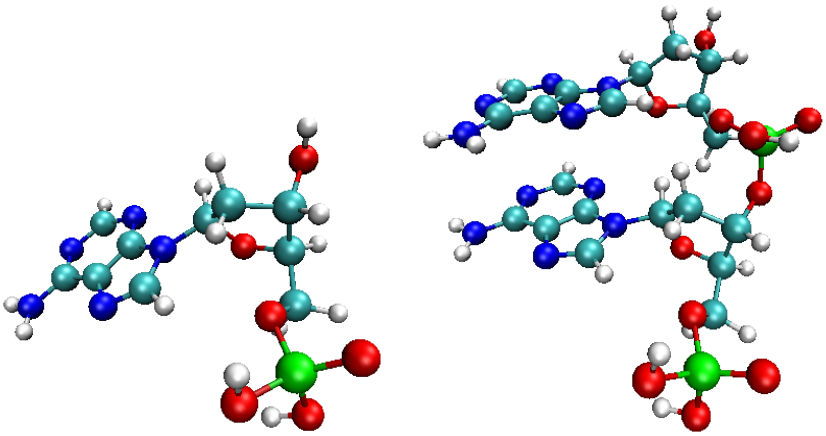

Figure 4.3: Single adenosine monophosphate nucleotide A_1 (left) and single DNA string containing two adenosine monophosphate nucleotides A_2 (right).

4.3.4 Damped response theory for a variational approximate state

For reasons of brevity the reader is referred to paper [4] for a detailed discussion of damped response theory for a variational approximate state. Here we just state that the damped response equations in approximate theory have the same form as in exact theory, see Eq. (4.17). For example, within the density matrix based KS-DFT formalism of Chapter 2, the damped counterpart of the mth order response equation in Eq. (2.50) takes the following form:

$$\left[\mathbf{E}^{[2]} - (\omega_{B_1 \ldots B_m} + i\gamma)\mathbf{S}^{[2]}\right]\bar{\mathbf{X}}^{B_1 \ldots B_m} = \bar{\mathbf{R}}^{B_1 \ldots B_m}. \tag{4.23}$$

where $\bar{\mathbf{X}}^{B_1 \ldots B_m}$ and $\bar{\mathbf{R}}^{B_1 \ldots B_m}$ are the mth order damped response matrix and damped right-hand side matrix, respectively. We note that an efficient algorithm for solving damped response equations was recently developed [78].

4.4 Illustrative results

In this section it is demonstrated that damped response theory is a very useful tool for obtaining absorption spectra for large molecular systems – in particular, when combined with the AO-based density matrix formulation in Chapter 2.

We present proof-of-concept calculations of absorption spectra obtained using standard and damped response theory. The calculations were carried out for a single adenosine monophosphate nucleotide (referred to as A_1 in the following) and for a DNA oligomer containing two adenosine monophosphate nucleotides (referred to as A_2 in the following) for the frequency range up to 0.6 a.u. Molecular structures are given in Figure 4.3. A_1 and A_2 are representations of the small and large molecules, respectively, in Figure 4.1. The calculations have been carried out at the HF/6-31G level of theory using a single-stranded DNA geometry obtained from the Maestro program [79] without carrying out additional optimizations.

In Figure 4.4 results for A_1 (first column) and A_2 (second column) are given. In the first row panels (from the top) the absorption spectra obtained from damped response theory (the

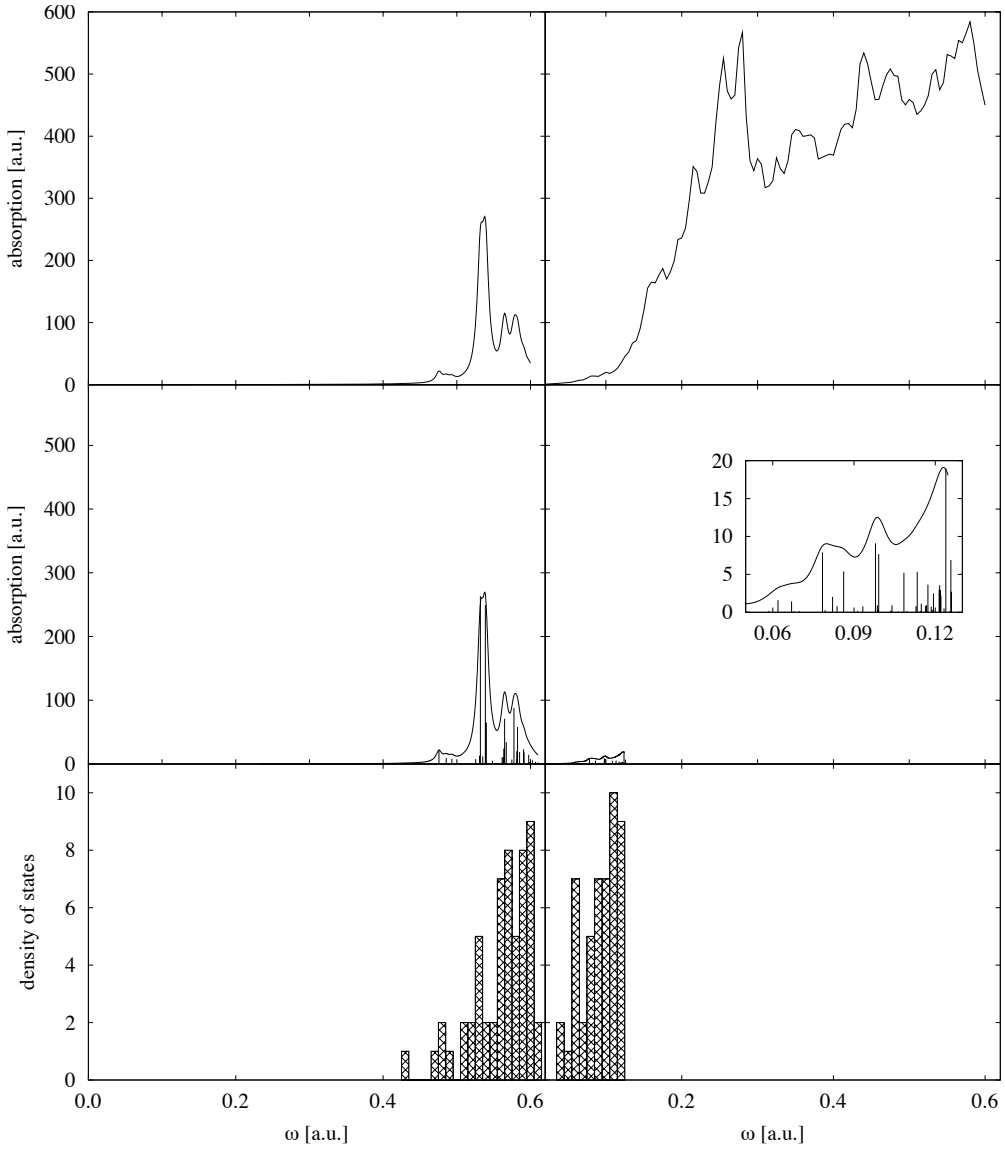

Figure 4.4: Absorption spectra (xx component) for A_1 (first column) and A_2 (second column), $\gamma = 0.005$ a.u. **Top panel:** Absorption spectra obtained using the damped response theory approach; **Middle panel:** First 50 excitation energies stick spectrum obtained using standard response theory with superimposed Lorentzian lineshape functions; **Bottom panel:** Density of the first 50 excited states.

imaginary component of the damped linear response function) are shown. In the second row panels absorption stick spectra containing the first 50 excitations are presented (obtained from the linear response function residues of standard response theory, see Eq. (1.38)). The Lorentzian lineshape functions of Eq. (4.22b) have been superimposed onto the residue stick spectrum. The third row panels show the density of the first 50 excited states, i.e., the number of excited states with excitation energies in a given frequency interval $[\omega; \omega + \Delta\omega]$. It is seen that the density of the excited states increases drastically at higher frequencies and for larger systems.

For A_1 (an example of the small molecule in Figure 4.1) the first 50 excitation energies give the absorption spectrum up to a frequency of about 0.6 a.u. The standard residue stick spectrum with superimposed Lorentzian lineshape functions (second row, left column panel) is identical to the spectrum obtained using damped response theory (first row, first column panel) in accordance with the theoretical prediction (Section 4.3.2).

For A_2 (an example of the large molecule in Figure 4.1), the first 50 excited states only include low lying states up to 0.1 a.u. (second row, right column panel). Because the density of states increases significantly with increasing frequency, it is virtually impossible to calculate all the excited states in the frequency range between 0.1-0.6 a.u. Therefore, standard response theory cannot be applied to evaluate the absorption spectrum for this frequency range. Larger molecules, such as DNA strings containing more than two nucleotides, will have even more low lying excited states, which will complicate the use of standard response theory even further. However, damped response theory can be successfully used for obtaining the absorption spectra for larger systems in all frequency ranges, as can be seen in the first row, second column panel of Figure 4.4, where the damped absorption spectrum for A_2 is given up to a frequency of 0.6 a.u. Thus, damped response theory allows one to investigate absorption spectra involving excited states "behind the yellow curtain" in Figure 4.1.

4.5 Concluding remarks and perspectives

Summarizing, damped response theory is a very useful tool for calculation absorption spectra, in particular for large molecules, where the use of standard response theory is problematic. A drawback of using damped response theory is that we only get a convoluted absorption spectrum and no information about the individual excited states. Alternatively, if the individual excitation energies and associated absorption strengths are of interest, standard and damped response theory can potentially be combined: first, the largest peaks in the absorption spectrum are located using damped response theory, and subsequently the individual excited states corresponding to these particular peaks are accessed in standard response theory using, for example, root homing techniques [80, 81].

Chapter 5

Damped response formulation of Magnetic Circular Dichroism

This chapter describes the work presented in **paper [5]**.

5.1 Introduction

In recent years an increasing number of quantum chemistry publications have dealt with the subject of Magnetic Circular Dichroism (MCD) [82–98]. MCD is the difference in extinction coefficients for left and right circularly polarized light traveling through a sample of (non-chiral) molecules in the direction of a static magnetic field. The phenomenon originates from a differential interaction of the sample with left and right circularly polarized light induced by the external magnetic field. As a consequence, when plane polarized light impinges on the sample, its two circularly polarized components are absorbed to different extents [23, 99–103]. This is referred to as the ellipticity of the sample.

The MCD spectrum is usually decomposed and analyzed in terms of three different spectral features corresponding to three molecular parameters known as the Faraday $\mathcal{A}$, $\mathcal{B}$ and $\mathcal{C}$ terms [102–108]. For closed-shell molecules only the Faraday $\mathcal{A}$ and $\mathcal{B}$ terms contribute to the MCD spectrum, although the $\mathcal{A}$ term only contributes if the system possesses degenerate excited states. The $\mathcal{C}$ term only appears for open-shell systems, i.e., systems with a degenerate ground state. In this chapter we consider MCD for closed shell molecules and refrain from further discussion of the $\mathcal{C}$ term.

Once the Faraday $\mathcal{A}$ and $\mathcal{B}$ terms have been calculated for the electronic transitions, one can simulate the MCD spectrum by attaching suitable lineshape functions to each individual term and adding them together. For near degenerate states this procedure is numerically unstable, because two very large $\mathcal{B}$ terms with associated lineshape functions are subtracted from each other. These instability problems are encountered in standard response theory and may be remedied using damped response theory as will be discussed in this chapter.

In Section 5.2 we describe how MCD spectra can be calculated using damped or standard

response theory. In Section 5.3 we demonstrate that a molecule with near-degenerate excited states may be subject to numerical instabilities arising when calculating MCD spectra using the standard response theory approach, whereas the damped response theory approach is numerically stable. Finally, Section 5.4 contains some concluding remarks.

5.2 Methodology

5.2.1 Ellipticity using damped response theory

For plane-polarized light traveling in the Z direction of a space-fixed frame of reference, the ellipticity θ of a sample of randomly moving molecules in the presence of a static magnetic field B_Z directed along the Z axis is given by (see Ref. [23] or paper [5] for details),

$$\theta = \frac{1}{2}\omega C \,\mathrm{Re}\left(\varepsilon_{\alpha\beta\gamma}\overline{\langle\langle \mu_\gamma; m_\beta, \mu_\alpha\rangle\rangle}_{0,\omega+i\gamma}\right) \tag{5.1}$$

where

$$C = \frac{1}{6}\mu_0 c l N B_Z \tag{5.2}$$

Here, m_α and μ_α are the α'th component of the magnetic and electric dipole operators in the molecular-fixed frame, respectively, ω is the optical (laser) frequency, N is the number density of molecules in the sample, μ_0 is the permeability in vacuum, l is the length of the sample, c is the speed of light in vacuum, and $\overline{\langle\langle \mu_\gamma; m_\beta, \mu_\alpha\rangle\rangle}_{0,\omega+i\gamma}$ is a *damped quadratic response function*. We have used the Einstein summation convention in connection with the Levi-Civita tensor $\varepsilon_{\alpha\beta\gamma}$.

By introducing complex excitation energies according to Eq. (4.9) and using Eq. (1.35b), the damped quadratic response function $\overline{\langle\langle \mu_\gamma; m_\beta, \mu_\alpha\rangle\rangle}_{0,\omega+i\gamma}$ may be expressed as [5],

$$\begin{aligned}
\overline{\langle\langle \mu_\gamma; m_\beta, \mu_\alpha\rangle\rangle}_{0,\omega_C+i\gamma} = &\sum_{p\neq o}\sum_{q\neq o}\frac{m_\beta^{op}\tilde{\mu}_\gamma^{pq}\mu_\alpha^{qo}}{\omega_p(\omega_q-\omega_C-i\gamma)} \\
&+\sum_{p\neq o}\sum_{q\neq o}\frac{\mu_\gamma^{op}\tilde{m}_\beta^{pq}\mu_\alpha^{qo}}{(\omega_p-\omega_C-i\gamma)(\omega_q-\omega_C-i\gamma)}+\sum_{p\neq o}\sum_{q\neq o}\frac{\mu_\gamma^{op}\tilde{\mu}_\alpha^{pq}m_\beta^{qo}}{(\omega_p-\omega_C-i\gamma)\omega_q} \\
&+\sum_{p\neq o}\sum_{q\neq o}\frac{\mu_\alpha^{oq}\tilde{m}_\beta^{qp}\mu_\gamma^{po}}{(\omega_q+\omega_C+i\gamma)(\omega_p+\omega_C+i\gamma)}+\sum_{p\neq o}\sum_{q\neq o}\frac{m_\beta^{oq}\tilde{\mu}_\alpha^{qp}\mu_\gamma^{po}}{\omega_q(\omega_p+\omega_C+i\gamma)} \\
&+\sum_{p\neq o}\sum_{q\neq o}\frac{\mu_\alpha^{oq}\tilde{\mu}_\gamma^{qp}m_\beta^{po}}{(\omega_q+\omega_C+i\gamma)\omega_p}
\end{aligned} \tag{5.3}$$

where we have used the notation for transition matrix elements introduced in Eq. (1.36), the p, q summations run over all excited states, and we have inserted $\omega_A = -\omega_C$ since $\omega_B = 0$.

Let us now introduce the Faraday $\mathcal{A}$ and $\mathcal{B}$ terms for the transition from the ground state $|o\rangle$ to an excited state $|j\rangle$ in accordance with Ref. [23]:

$$\mathcal{A}(o\to j) = \frac{1}{2}\sum_{st}\varepsilon_{\alpha\beta\gamma}\,\mathrm{Im}\left(m_\beta^{j_t j_s}\mu_\alpha^{j_s o}\mu_\gamma^{o j_t}\right) = \frac{1}{2}\varepsilon_{\alpha\beta\gamma}\sum_{s} m_\beta^{\tilde{j}_s\tilde{j}_s}\,\mathrm{Im}\left(\mu_\gamma^{o\tilde{j}_s}\mu_\alpha^{\tilde{j}_s o}\right) \tag{5.4a}$$

$$\mathcal{B}(o\to j) = \sum_{s}\varepsilon_{\alpha\beta\gamma}\left(\sum_{p\neq o}\frac{\mathrm{Im}(m_\beta^{op}\mu_\gamma^{pj_s}\mu_\alpha^{j_s o})}{\omega_p}+\sum_{p\neq\{j\}}\frac{\mathrm{Im}(m_\beta^{pj_s}\mu_\alpha^{j_s o}\mu_\gamma^{op})}{\omega_p-\omega}\right) \tag{5.4b}$$

In Eq. (5.4b), $\{j\}$ refers to the set of (possibly) degenerate states with excitation energy ω_j, and the real states j_s have been expanded in terms of complex states $\tilde{j}_s$ which diagonalize the imaginary m_β operator. In paper [5] it is shown that if the excited state $|j\rangle$ is fairly isolated in the energy spectrum, then the ellipticity in Eq. (5.1) may be expressed in terms of the $\mathcal{A}(o \to j)$ and $\mathcal{B}(o \to j)$ terms as:

$$\theta \approx -C\omega\left(\mathcal{B}(o \to j)a_j(\omega) + \mathcal{A}(o \to j)\frac{\partial a_j(\omega)}{\partial \omega}\right) \qquad (\omega \approx \omega_j) \tag{5.5}$$

where the absorption lineshape function $a_j(\omega)$ is given in Eq. (4.22b).

We recognize that the Faraday $\mathcal{B}$ terms are associated with an absorption lineshape function, and that the $\mathcal{A}$ terms are associated with a differentiated lineshape function in agreement with previous findings [102]. The damped response theory expression for the ellipticity in Eq. (5.1) will therefore an MCD spectrum with contributions from both the Faraday $\mathcal{A}$ and $\mathcal{B}$ terms, where the former is multiplied by the frequency derivative of an absorption lineshape function and the latter is multiplied by an absorption lineshape function. In damped response theory the $\mathcal{A}$ and $\mathcal{B}$ contributions can in general not be separated from each other.

5.2.2 Faraday $\mathcal{A}$ and $\mathcal{B}$ terms using standard response theory

We now discuss how the individual Faraday $\mathcal{A}$ and $\mathcal{B}$ terms can be calculated as a double and a single residue, respectively, of a *standard quadratic response function*. The advantage of this approach is that one directly calculates the individual $\mathcal{A}$ and $\mathcal{B}$ terms for each excited state.

To display the underlying structure of the quadratic response function, it is convenient to write out the sum-over-states expression in Eq. (1.35b) in detail for A=μ_γ, B=m_β, and C=μ_α:

$$\begin{aligned}
\langle\langle \mu_\gamma; m_\beta, \mu_\alpha \rangle\rangle_{\omega_B,\omega_C} = &\sum_{p\neq o}\sum_{q\neq o}\frac{m_\beta^{op}\tilde{\mu}_\gamma^{pq}\mu_\alpha^{qo}}{(\omega_p+\omega_B)(\omega_q-\omega_C)} \\
&+\sum_{p\neq o}\sum_{q\neq o}\frac{\mu_\gamma^{op}\tilde{m}_\beta^{pq}\mu_\alpha^{qo}}{(\omega_p-\omega_B-\omega_C)(\omega_q-\omega_C)}+\sum_{p\neq o}\sum_{q\neq o}\frac{\mu_\gamma^{op}\tilde{\mu}_\alpha^{pq}m_\beta^{qo}}{(\omega_p-\omega_B-\omega_C)(\omega_q-\omega_B)} \\
&+\sum_{p\neq o}\sum_{q\neq o}\frac{\mu_\alpha^{oq}\tilde{m}_\beta^{qp}\mu_\gamma^{po}}{(\omega_q+\omega_C)(\omega_p+\omega_B+\omega_C)}+\sum_{p\neq o}\sum_{q\neq o}\frac{m_\beta^{oq}\tilde{\mu}_\alpha^{qp}\mu_\gamma^{po}}{(\omega_q+\omega_B)(\omega_p+\omega_B+\omega_C)} \\
&+\sum_{p\neq o}\sum_{q\neq o}\frac{\mu_\alpha^{oq}\tilde{\mu}_\gamma^{qp}m_\beta^{po}}{(\omega_q+\omega_C)(\omega_p-\omega_B)}
\end{aligned} \tag{5.6}$$

where we have inserted $\omega_A = -\omega_B - \omega_C$.

In the case where $\omega_B = 0$ (static magnetic field) inspection of Eq. (5.6) reveals that double poles are present; for example in the second term when $\omega_C = \omega_j$ and $p = q = j$. To treat also such cases correctly we recall that the residue of a general function $f(\omega_C)$ at $\omega_C = \omega_j$ is given by [109]

$$R\Big(f(\omega_C);\omega_j\Big) = \frac{1}{(n-1)!}\lim_{\omega_C\to\omega_j}\frac{d^{n-1}}{d\omega_C^{n-1}}\Big((\omega_C-\omega_j)^n f(\omega_C)\Big) \tag{5.7}$$

where n denotes the order of the pole[1]. Considering Eq. (5.6) at $\omega_B = 0$, the first three terms have first-order ($n = 1$) poles at $\omega_C = \omega_j$, while the second term also has a contribution from a second-order pole ($n = 2$). Using this information and the definition of the $\mathcal{A}$ and $\mathcal{B}$ terms in Eq. (5.4), it can be shown [5] that the $\mathcal{B}$ term can be identified from a *single residue* of the quadratic response function at $\omega_B = 0$ and $\omega_C = \omega_j$,

$$\mathcal{B}(o \to j) = -\frac{1}{2}\,\mathrm{Im}\left\{ R\left(\varepsilon_{\alpha\beta\gamma} \langle\langle \mu_\gamma; m_\beta, \mu_\alpha \rangle\rangle_{0,\omega_C}; \omega_j \right) \right\} \tag{5.8}$$

while the $\mathcal{A}$ term can be determined as a *double residue*,

$$\mathcal{A}(o \to j) = \frac{1}{2}\varepsilon_{\alpha\beta\gamma}\,\mathrm{Im}\left\{ \left[\lim_{\omega_{BC}\to\omega_j} (\omega_{BC} - \omega_j) \left(\lim_{\omega_C \to \omega_j} (\omega_C - \omega_j) \langle\langle \mu_\gamma; m_\beta, \mu_\alpha \rangle\rangle_{\omega_B,\omega_C} \right) \right] \right\} \tag{5.9}$$

where $\omega_{BC} = \omega_B + \omega_C$.

5.3 Numerical instabilities for near-degenerate states

In Section 5.2 it was established that the damped quadratic response function $\overline{\langle\langle \mu_\gamma; m_\beta, \mu_\alpha \rangle\rangle}_{0,\omega+i\gamma}$ directly provides an MCD spectrum with contributions from both the Faraday $\mathcal{B}$ and $\mathcal{A}$ terms with associated lineshape functions, see Eqs. (5.1) and (5.5), while the individual $\mathcal{B}$ and $\mathcal{A}$ terms can be obtained as single and double residues, respectively, of the standard quadratic response function $\langle\langle \mu_\gamma; m_\beta, \mu_\alpha \rangle\rangle_{\omega_B,\omega_C}$, see Eqs. (5.8) and (5.9). If the excited states are energetically well-separated the MCD spectrum obtained using damped response theory is identical to the MCD spectrum obtained by superimposing lineshape functions onto the $\mathcal{A}$ and $\mathcal{B}$ terms determined using standard response theory. However, in the case of near-degeneracies the standard expression for the $\mathcal{B}$ term becomes artificially large, and the MCD spectrum obtained using standard response theory may be numerically unstable. To see this, consider the second term in the sum-over-states expression for the $\mathcal{B}$ term in Eq. (5.4b). At exact resonance we have $\omega = \omega_j$. This does not pose a problem, because the (possibly degenerate) state $|j\rangle$ is not included in the summation ($p \neq j$). However, if the two excited states $|j\rangle$ and $|f\rangle$ are nearly degenerate – i.e., $|\omega_j - \omega_f| < \delta$ (where δ is a very small number) – the term with $p = f$ in the second term of Eq. (5.4b) will blow up, leading to instabilities. Such instability problems are avoided in damped response theory, where the lineshape functions are built into the theory, rather than superimposed onto the residue stick spectrum after the calculation, as is done using standard response theory.

5.3.1 Cyclopropane: theoretical analysis

To exemplify the above discussion consider the cyclopropane molecule (Figure 5.1, right), which has a doubly-degenerate state g with two components g_f and g_j. Changing one of the $\widehat{\mathrm{CCC}}$ angles of this molecule lowers the molecular symmetry from D_{3h} to C_{2v} (Figure 5.1, left). This

[1] In passing we note that the simple residue definition used in Eqs. (1.38) and (1.39) is a special case of the general definition in Eq. (5.7), which is necessary to treat double (and higher order) poles correctly.

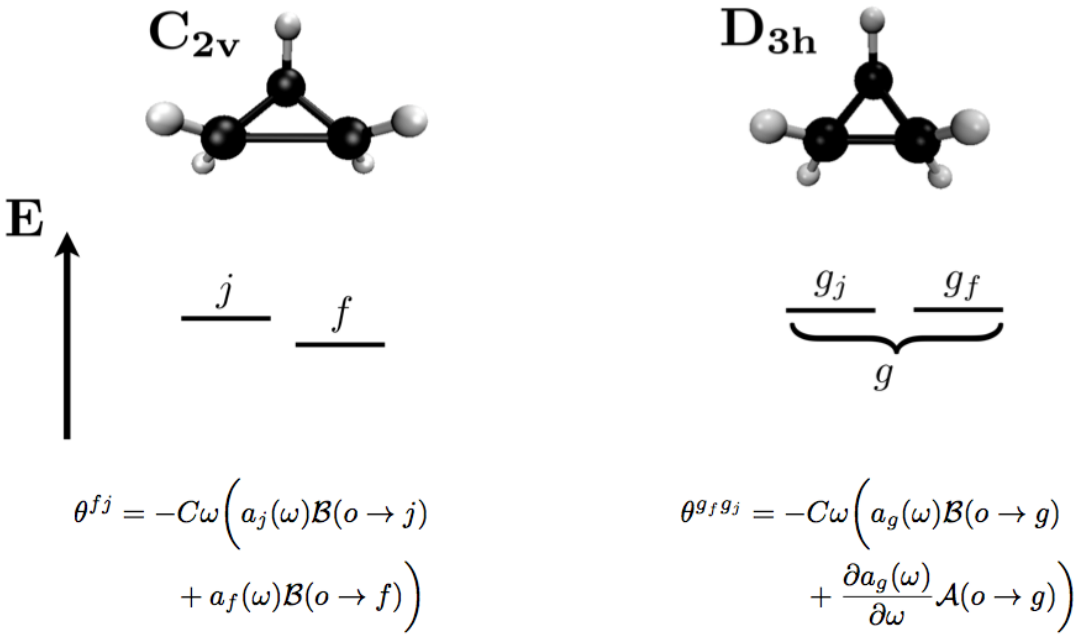

Figure 5.1: The degenerate E′ state (g) of cyclopropane in a D_{3h} configuration (depicted on the right) has both an $\mathcal{A}$ and a $\mathcal{B}$ term contribution to the ellipticity. Increasing one of the $\widehat{\text{CCC}}$ angles breaks the D_{3h} symmetry and gives rise to the C_{2v} configuration (depicted on the left), thereby lifting the degeneracy of the E′ state, which then evolves into two separate states (f and j) of A_1 and B_2 symmetry. These two states both contribute with a $\mathcal{B}$ term to the ellipticity.

causes the degenerate state g to split into two non-degenerate states f and j. The f and j states both have a $\mathcal{B}$ term contribution to the ellipticity, i.e., the contribution to the ellipticity arising from the states f and j on the left of Figure 5.1 may be written as:

$$\theta^{fj} \approx -C\omega\Big(a_j(\omega)\mathcal{B}(o \to j) + a_f(\omega)\mathcal{B}(o \to f)\Big) \tag{5.10}$$

Consider the change in the ellipticity in Eq. (5.10) as the states $|f\rangle$ and $|j\rangle$ become degenerate (i.e., going from left to right in Figure 5.1). In this case damped response theory ensures a *smooth transition* of the two $\mathcal{B}$ terms in Eq. (5.10) into one $\mathcal{A}$ term and one $\mathcal{B}$ term for the degenerate $|g\rangle$ state:

$$\theta^{g_f g_j} \approx -C\omega\Big(a_g(\omega)\mathcal{B}(o \to g) + \frac{\partial a_g(\omega)}{\partial \omega}\mathcal{A}(o \to g)\Big) \tag{5.11}$$

In paper [5] it is shown explicitly that damped response theory ensures a smooth transition of Eq. (5.10) into Eq. (5.11). In contrast, in standard response theory, the individual $\mathcal{B}$ terms as defined in Eq. (5.4b) are divergent as the $\widehat{\text{CCC}}$ angle approaches 60°. Thus, for near-degenerate states f and j, the $\mathcal{B}(o{\to}f)$ and $\mathcal{B}(o{\to}j)$ terms of standard response theory approaches infinity. Superimposing lineshape functions onto the $\mathcal{B}(o{\to}f)$ and $\mathcal{B}(o{\to}j)$ terms leads to large cancellation effects in the MCD spectrum, because these $\mathcal{B}$ terms are both very large but with opposite signs. This procedure is thus numerically unstable, as the accuracy of the resulting spectrum is significantly reduced compared to the accuracy of the individual $\mathcal{B}$ terms. Only when lineshape functions are built into the theory, as is the case in damped response theory, the numerical instabilities are removed.

5.3.2 Cyclopropane: numerical results

To illustrate the above discussion we now report numerical results obtained for cyclopropane using both standard and damped response theory. The equilibrium geometry in the D_{3h} configuration has been optimized at the DFT/B3LYP level of theory using the cc-pVTZ basis set. Distorted geometries have been obtained by changing the $\widehat{\text{CCC}}$ angle, while keeping all other geometry parameters fixed. All MCD calculations have been carried out in the gas phase using the B3LYP functional and the aug-cc-pVDZ basis set. A value of $\gamma = 0.005$ a.u. was used in the damped response calculations. In our implementation we apply the density matrix-based KS-DFT response formulation discussed in Chapter 2, where we use London atomic orbitals [56, 57] to ensure gauge-invariant results. The reader is referred to paper [5] for implementation details.

In Figure 5.2 we have plotted damped and standard MCD spectra, where residual norm thresholds (RNTs) of 10^{-5} a.u. and 10^{-9} a.u. in the response equations were used in the left and right plots, respectively. The upper plots show the spectra at a $\widehat{\text{CCC}}$ angle of 60° (D_{3h} configuration, depicted on the right of Figure 5.1), while the $\widehat{\text{CCC}}$ angle is increased as indicated in the figure for the remaining plots (C_{2v} configuration, depicted on the left of Figure 5.1). Clearly, the damped spectra (red) vary smoothly with the $\widehat{\text{CCC}}$ angle, regardless of the RNT, whereas the standard spectra (green) using RNT = 10^{-5} a.u. change dramatically for small variations of the $\widehat{\text{CCC}}$ angle, indicating numerical instabilities. A closer analysis of the individual $\mathcal{B}$ terms used for simulating the standard spectra (see paper [5]) reveals that the instabilities are caused by two very large $\mathcal{B}$ terms with opposite signs – in accordance with the analysis in Section 5.3.1. By increasing significantly the accuracy in the calculation it is possible to quench the numerical instability problems such that the two very large $\mathcal{B}$ terms cancel each other in the correct manner. This is illustrated by the standard spectra obtained using the very tight RNT of 10^{-9} a.u. in Figure 5.2 (right). These spectra change smoothly as a function of the $\widehat{\text{CCC}}$ angle and are very similar to the corresponding damped spectra. We note that these numerically stable standard response results were obtained with a RNT for the response equations, which is far below what is conventionally used in MCD calculations.

5.4 Summary

An MCD spectrum can be directly obtained from damped quadratic response theory, where the MCD spectrum encompasses both $\mathcal{A}$ and $\mathcal{B}$ terms with different associated lineshape functions. In general, the information about the individual $\mathcal{A}$ and $\mathcal{B}$ terms is lost in damped response theory. In standard quadratic response theory the individual $\mathcal{A}$ and $\mathcal{B}$ terms may be obtained from a residue analysis of the appropriate quadratic response function. However, for near-degenerate states the MCD spectra obtained using standard response theory are numerically unstable. In contrast, the MCD spectra obtained using damped response theory are numerically stable and changes smoothly when lifting a degeneracy, for example, by distorting the molecular geometry. We therefore conclude that the combination of the damped and standard response

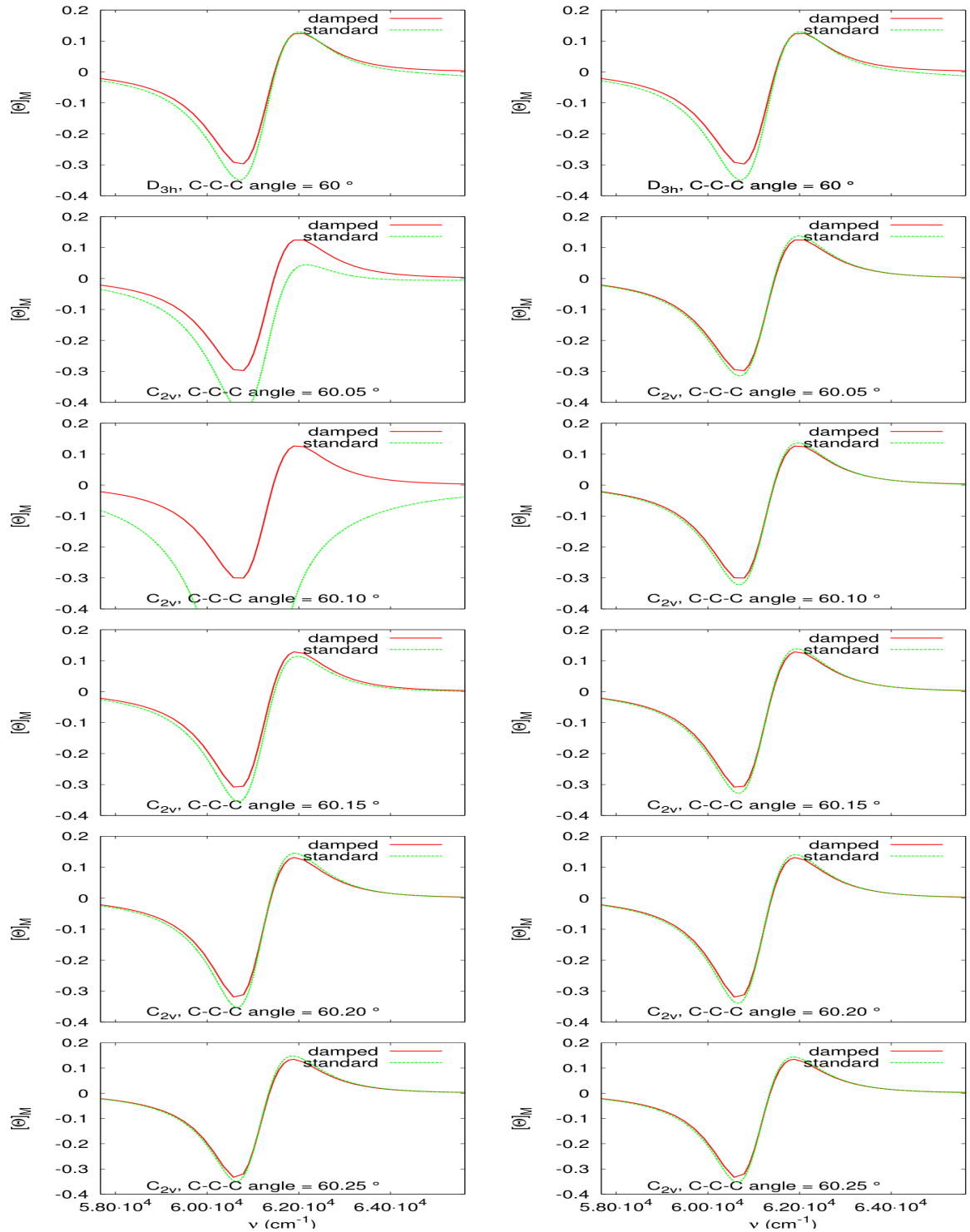

Figure 5.2: Comparison of the MCD spectra obtained directly from damped response theory (red-solid line) and the simulated standard spectra (green-dashed lines) obtained by superimposing lineshape functions onto explicitly calculated individual $\mathcal{A}$ and $\mathcal{B}$ terms. Residual norm thresholds in the response equations of 10^{-5} and 10^{-9} (a.u.) were used in the left and right plots, respectively.

theory approaches constitutes a potent tool for analyzing MCD spectra providing both: values for the individual $\mathcal{A}$ and $\mathcal{B}$ terms (using standard response theory, only well-defined in the absence of near-degenerate states) and a full MCD spectrum (using damped response theory, always possible).

Chapter 6

Damped response theory description of two-photon absorption

This chapter describes the work presented in **paper [6]**.

6.1 Introduction

In Chapters 4 and 5 examples of damped *linear* and *quadratic* damped response theory were discussed as exemplified by one-photon absorption (OPA) and MCD, respectively. We now turn our attention to an example of damped *cubic* response theory, namely *two-photon absorption (TPA)* spectroscopy.

Introduced by Goeppert-Mayer in 1931 [110], TPA was first studied experimentally about fifty years ago [111, 112]. Since then TPA has become a powerful tool in numerous fields of science and technology, due to its applications, among others, in 3D fluorescence microscopy [113–115], optical limiting [114, 116], optical data storage [117, 118], and 3D micro-fabrication [113]. Two-photon (and more generally multi-photon) spectroscopy exhibits greater 3D spatial selectivity, higher resolution and penetration than usual one-photon absorption spectroscopy, in turn leading to reduced scattering loss, photo-bleaching and background fluorescence effects. The latest developments in the field of TPA materials – with emphasis on both the experimental and theoretical aspects and on the strategies for the design and characterization of efficient chromophores – are discussed in detail in recent reviews [119–121].

This chapter is organized as follows. In Section 6.2 we define the relevant TPA quantities, and in Sections 6.3 and 6.4 we discuss the determination of TPA using standard and damped response theory, respectively. The standard and damped approaches are compared in Section 6.5, and Section 6.6 contains some concluding remarks.

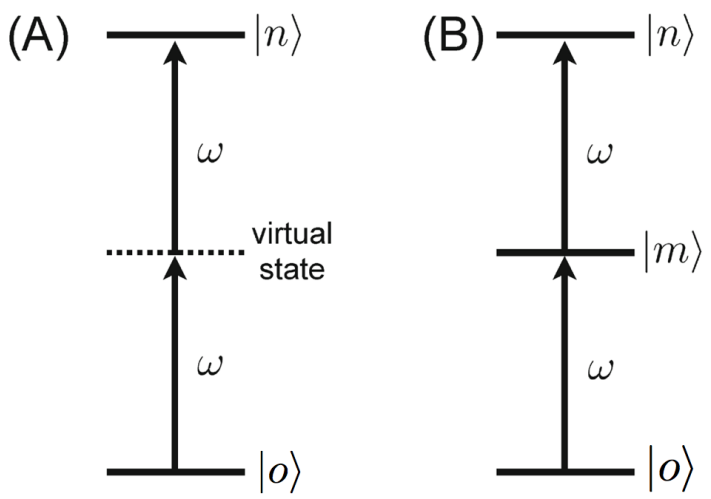

Figure 6.1: Illustration of the TPA $|o\rangle \rightarrow |n\rangle$ transition via (A) a so-called virtual state (single-resonance case), and (B) via an actual intermediate state $|m\rangle$ (double-resonance case).

6.2 Two-photon absorption

We consider the process where a molecular system in the ground state $|o\rangle$ undergoes a transition to the excited state $|n\rangle$ by absorbing two photons of frequencies ω_1 and ω_2, i.e., ω_1+ω_2=ω_n, where ω_n is the nth excitation energy. The (A,B)th component $(A,B = x,y,z)$ of the *two-photon transition amplitude tensor* $T^{on}_{AB}(\omega_1,\omega_2)$ may be written in the sum-over-states expression [110, 122]

$$T^{on}_{AB}(\omega_1,\omega_2) = \sum_{p\neq o}\left(\frac{\mu^{op}_A\tilde{\mu}^{pn}_B}{\omega_p-\omega_1}+\frac{\mu^{op}_B\tilde{\mu}^{pn}_A}{\omega_p-\omega_2}\right) \tag{6.1}$$

where the summation index runs over all excited states (assumed to be real), μ_A and μ_B are components of the electric dipole operator, and where we have used the notation for transition matrix elements introduced in Eq. (1.36).

For the remainder of this chapter we assume that the two photons have the same energy, i.e., ω_1=ω_2=ω. In this case 2ω=ω_n, and $T^{on}_{AB}(\omega_n/2,\omega_n/2)$ becomes,

$$T^{on}_{AB}(\omega_n/2,\omega_n/2) = \sum_{p\neq o}\left(\frac{\mu^{op}_A\tilde{\mu}^{pn}_B}{\omega_p-\omega_n/2}+\frac{\mu^{op}_B\tilde{\mu}^{pn}_A}{\omega_p-\omega_n/2}\right) \tag{6.2}$$

The isotropically averaged expression for the *TPA strength* $\bar{\delta}_{on}$ in a sample of randomly tumbling molecules – where both photons are linearly polarized with parallel propagation – is given by [122],

$$\bar{\delta}_{on} = \frac{1}{30}\sum_{A,B}\Big(2T^{on}_{AA}(\omega_n/2,\omega_n/2)T^{on}_{BB}(\omega_n/2,\omega_n/2) + 4T^{on}_{AB}(\omega_n/2,\omega_n/2)T^{on}_{AB}(\omega_n/2,\omega_n/2)\Big) \tag{6.3}$$

where the sums run independently over the x,y,z components of the molecular axes.

The TPA transition $|o\rangle \rightarrow |n\rangle$ is usually interpreted as the absorption of one photon to a so-called "virtual" state, followed by a second one-photon transition from the virtual state to the final state $|n\rangle$ as depicted in Figure 6.1(A). This interpretation is useful when $|n\rangle$ is one of the lower lying excited states. If $|n\rangle$ is a higher lying excited state there might exist an intermediate state $|m\rangle$ halfway between the ground state $|o\rangle$ and $|n\rangle$ as shown in Figure 6.1(B), i.e., $\omega_m = \omega_n/2$. If the laser frequency ω is chosen such that $\omega = \omega_m = \omega_n/2$, the *one-photon* transitions $|o\rangle \rightarrow |m\rangle$ and $|m\rangle \rightarrow |n\rangle$ will be simultaneously resonant. We refer to this situation as a *double-resonance*. In this case the mth term in the expression for the TPA amplitude in Eq. (6.2) diverges. This divergence is caused by the fact that the excited state lifetimes in standard response theory are assumed to be infinite. An empirical solution to this problem is to introduce a phenomenological lifetime for the excited states as will be discussed in the context of damped response theory in Chapter 6.4. Before doing so we consider the determination of TPA in standard response theory in Section 6.3 below.

For reasons of brevity, we focus only on the sum-over-state expressions in the following discussions and leave out derivation details, focusing instead on the difference between TPA spectra obtained using standard and damped response theory and on the associated physical interpretations. We also omit implementation details; the reader is referred to paper [6] for a discussion of these.

6.3 Two-photon absorption in standard response theory

6.3.1 Two-photon absorption from quadratic response theory

The TPA *amplitude* component $T^{on}_{AB}(\omega_n/2, \omega_n/2)$ may formally be determined from the residue in Eq. (1.39) of the *quadratic response function* $\langle\langle \mu_A; \mu_B, \mu_C \rangle\rangle_{\omega_B, \omega_C}$:

$$\left(\lim_{\omega_C \rightarrow \omega_n} (\omega_C - \omega_n) \langle\langle \mu_A; \mu_B, \mu_C \rangle\rangle_{\omega_B, \omega_C} \right) \Bigg|_{\omega_B = -\omega_n/2} = -T^{on}_{AB}(\omega_n/2, \omega_n/2) \mu^{no}_C \tag{6.4}$$

The residue in Eq. (6.4) is thus the product of a TPA amplitude and an OPA amplitude (a dipole matrix element). In standard response theory it is straightforward to separate the $T^{on}_{AB}(\omega_n/2, \omega_n/2)$ and μ^{no}_C contributions and subsequently evaluate the TPA strength simply by squaring the TPA amplitudes as in Eq. (6.3). In damped quadratic response theory a spectrum of the residues in Eq. (6.4) with superimposed lineshape functions is obtained [4], and it is not possible to separate out the individual TPA and OPA amplitude components from this spectrum. However, as we show in Section 6.3.2 below, the TPA strength (the TPA amplitude squared) equals a residue of a cubic response function, and the corresponding damped cubic response function thus directly yields a spectrum of TPA strengths as will be detailed in Section 6.4.

6.3.2 Two-photon absorption from cubic response theory

Let us now consider the residue of the cubic response function $\langle\langle \mu_A; \mu_B, \mu_C, \mu_D \rangle\rangle_{\omega_B, \omega_C, \omega_D}$ at $\omega_{CD} \equiv \omega_C + \omega_D = \omega_n$, which, as we shall see, equals a component of the TPA strength ten-

sor for the two-photon $|o\rangle \rightarrow |n\rangle$ transition. To this end we turn our attention to the sum-over-states expression for the cubic response function in Eq. (1.35c). It is clear that only the terms in the cubic response function containing ω_{CD} in the denominator will contribute to this particular residue. We therefore define a simplified *standard TPA response function* $\langle\langle \mu_A; \mu_B, \mu_C, \mu_D \rangle\rangle_{\omega_B,\omega_C,\omega_D}(\omega_{CD})$, where only terms involving ω_{CD} in the total cubic response function are retained. In paper [6] it is shown that this modified cubic response function may be written as:

$$\langle\langle \mu_A; \mu_B, \mu_C, \mu_D \rangle\rangle_{\omega_B,\omega_C,\omega_D}(\omega_{CD}) = -\sum_{q\neq o}\left\{ \frac{T^{oq}_{AB}(-\omega_A, -\omega_B)T^{oq}_{CD}(\omega_C, \omega_D)}{\omega_q - \omega_{CD}} + \frac{T^{oq}_{AB}(\omega_A, \omega_B)T^{oq}_{CD}(-\omega_C, -\omega_D)}{\omega_q + \omega_{CD}} \right\} \tag{6.5}$$

By construction the residue of $\langle\langle \mu_A; \mu_B, \mu_C, \mu_D \rangle\rangle_{\omega_B,\omega_C,\omega_D}(\omega_{CD})$ at $\omega_{CD} = \omega_n$ equals the residue of the full cubic response function, which may thus be identified as:

$$\begin{aligned} &\lim_{\omega_{CD}\rightarrow\omega_n}(\omega_{CD} - \omega_n)\langle\langle \mu_A; \mu_B, \mu_C, \mu_D \rangle\rangle_{\omega_B,\omega_C,\omega_D} \\ =&\lim_{\omega_{CD}\rightarrow\omega_n}(\omega_{CD} - \omega_n)\langle\langle \mu_A; \mu_B, \mu_C, \mu_D \rangle\rangle_{\omega_B,\omega_C,\omega_D}(\omega_{CD}) \\ =&T^{on}_{AB}(-\omega_A, -\omega_B)T^{on}_{CD}(\omega_C, \omega_D) \end{aligned} \tag{6.6}$$

where $\omega_C{+}\omega_D{=}\omega_n$ and consequently $\omega_A{+}\omega_B{=}-\omega_n$. We may still consider ω_A (or ω_B) and ω_C (or ω_D) as independent parameters. By choosing $\omega_C{=}\omega$ and $\omega_A{=}{-}\omega$ (where ω is the (positive) optical laser frequency) we obtain the following frequency relations,

$$\omega_A = \omega_B = -\omega; \qquad \omega_C = \omega_D = \omega; \qquad \omega_{CD} = \omega_C + \omega_D = 2\omega \tag{6.7}$$

and Eq. (6.6) becomes

$$\lim_{2\omega\rightarrow\omega_n}(2\omega - \omega_n)\langle\langle \mu_A; \mu_B, \mu_C, \mu_D \rangle\rangle_{-\omega,\omega,\omega} = T^{on}_{AB}(\omega_n/2, \omega_n/2)T^{on}_{CD}(\omega_n/2, \omega_n/2) \tag{6.8}$$

Thus, the residue of the cubic response function at $\omega_{CD}{=}\omega_n$ yields the (A, B, C, D)th component of the TPA strength tensor $T^{on}_{AB}(\omega_n/2, \omega_n/2)T^{on}_{CD}(\omega_n/2, \omega_n/2)$ for the $|o\rangle \rightarrow |n\rangle$ transition.

6.4 Two-photon absorption in damped response theory

Let us now introduce phenomenological finite excited state lifetimes in terms of complex excitation energies [see Eq. (4.9)] into the standard TPA response function in Eq. (6.5). In paper [6] it is demonstrated that the resulting *damped TPA response function* $\langle\langle \overline{\mu_A; \mu_B, \mu_C, \mu_D} \rangle\rangle_{-\omega,\omega,\omega}(\omega_{CD})$ may be expressed as:

$$\langle\langle \overline{\mu_A; \mu_B, \mu_C, \mu_D} \rangle\rangle_{-\omega,\omega,\omega}(\omega_{CD}) = -\sum_{q\neq o}\left(\frac{T^{oq}_{AB}(\omega - i\gamma, \omega - i\gamma)T^{oq}_{CD}(\omega + i\gamma, \omega + i\gamma)}{\omega_q - 2\omega - i\gamma} + \frac{T^{oq}_{AB}(-\omega + i\gamma, -\omega + i\gamma)T^{oq}_{CD}(-\omega - i\gamma, -\omega - i\gamma)}{\omega_q + 2\omega + i\gamma} \right) \tag{6.9}$$

where we have allowed for complex frequency arguments in the general TPA amplitude definition in Eq. (6.1) and used the frequency relations in Eq. (6.7).

In paper [6] Eq. (6.9) is analyzed, and the following expression is derived:

$$\langle\langle\overline{\mu_A;\mu_B,\mu_C,\mu_D}\rangle\rangle_{-\omega,\omega,\omega}(\omega_{CD}) = -\sum_{q\neq o}\big[\Phi^q_{ABCD}(\omega)+\Lambda^q_{ABCD}(\omega)\big]\big[d_q(2\omega)+ia_q(2\omega)\big] \tag{6.10}$$

where the dispersion $d_q(\omega)$ and absorption $a_q(\omega)$ lineshape functions are defined in Eq. (4.22), and where we have introduced the *damped TPA strength functions* $\Phi^q_{ABCD}(\omega)$ and $\Lambda^q_{ABCD}(\omega)$ according to

$$\Phi^q_{ABCD}(\omega) = P(A,B)P(C,D)\sum_{p\neq o,r\neq o}\mu^{op}_A\tilde{\mu}^{pq}_B\mu^{or}_C\tilde{\mu}^{rq}_D d_p(\omega)d_r(\omega) \tag{6.11a}$$

$$\Lambda^q_{ABCD}(\omega) = P(A,B)P(C,D)\sum_{p\neq o,r\neq o}\mu^{op}_A\tilde{\mu}^{pq}_B\mu^{or}_C\tilde{\mu}^{rq}_D a_p(\omega)a_r(\omega) \tag{6.11b}$$

The permutation operator $P(A,B)$ is defined in Eq. (1.37a).

Before proceeding let us consider the damped linear response function in Eq. (4.21), which is the one-photon analogue of the damped TPA response function in Eq. (6.10). The terms where lineshape functions enter with positive frequency arguments are the main contributors to Eq. (4.21), and we may therefore approximate Eq. (4.21) as

$$\overline{\langle\langle\mu_A;\mu_B\rangle\rangle}_\omega \approx -\sum_{q\neq o}\mu^{oq}_A\mu^{qo}_B\big[d_q(\omega)+\mathrm{i}a_q(\omega)\big] \tag{6.12}$$

As discussed in Section 4.3.2, the imaginary part of the damped linear response function represents a spectrum of the (A,B)th component of the OPA tensor $[\mu^{oq}_A\mu^{qo}_B]$ with superimposed Lorentzian lineshape functions $a_q(\omega)$, whereas the real part describes a dispersion spectrum. Noticing the similarities between Eqs. (6.10) and (6.12) we therefore define a *damped TPA function* $\delta^{ABCD}_D(\omega)$, which equals minus the *imaginary* part of Eq. (6.10),

$$\begin{aligned}\delta^{ABCD}_D(\omega) &\equiv -\operatorname{Im}\big[\langle\langle\overline{\mu_A;\mu_B,\mu_C,\mu_D}\rangle\rangle_{-\omega,\omega,\omega}(\omega_{CD})\big]\\ &= \sum_{q\neq o}\Phi^q_{ABCD}(\omega)a_q(2\omega)+\sum_{q\neq o}\Lambda^q_{ABCD}(\omega)a_q(2\omega)\end{aligned} \tag{6.13}$$

The isotropically averaged damped TPA spectrum $\bar{\delta}_D(\omega)$ is now obtained as in Eq. (6.3)

$$\bar{\delta}_D(\omega) = \frac{1}{30}\sum_{A,B}\Big(2\delta^{AABB}_D(\omega)+4\delta^{ABAB}_D(\omega)\Big) \tag{6.14}$$

We note that the imaginary part of the damped linear response function in Eq. (6.12) is *identical* to a one-photon stick spectrum with superimposed lineshape functions. In general, the damped TPA function $\bar{\delta}_D(\omega)$ is not completely identical to the standard TPA strengths in Eq. (6.2) with superimposed lineshape functions. However, in Section 6.5.1 it is shown that in the single-resonance case [Figure 6.1(A)] the damped and standard TPA spectra are – for all practical purposes – identical. In contrast, in the double-resonance case depicted in Figure 6.1(B), the standard TPA spectrum diverges, whereas the damped TPA spectrum is still well-defined and physically meaningful, as discussed in Section 6.5.2.

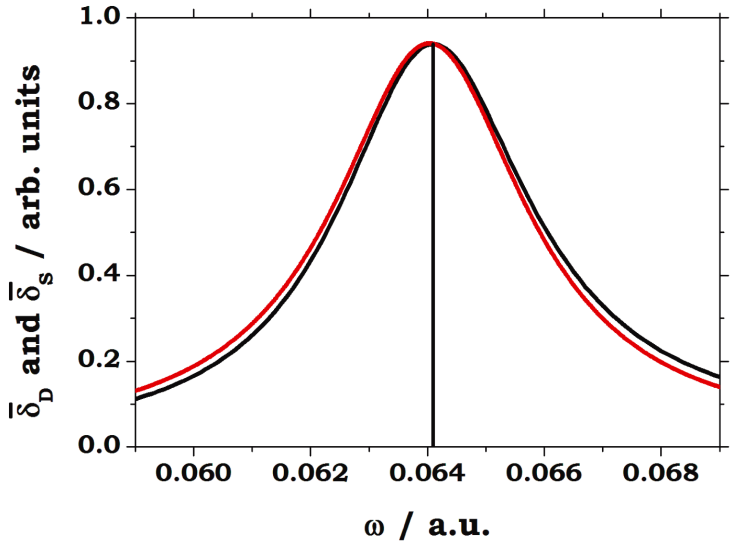

Figure 6.2: Standard (red) and damped (black) TPA spectra for LiH at the CAM-B3LYP/aug-cc-pVTZ level of theory using the experimental equilibrium geometry 1.5957 Å [123]. The broadening parameter $\gamma = 0.004$ a.u. Note that the optical frequency ω corresponds to a one-photon frequency.

6.5 Comparison of standard and damped TPA

6.5.1 The single-resonance case

In paper [6] it was shown that in the single-resonance case depicted in Figure 6.1(A) (i.e., the laser frequency ω is far-off-resonance), the damped TPA function in Eq. (6.13) is approximately given by:

$$\delta_D^{ABCD}(\omega) \approx \sum_{q \neq o} T_{AB}^{oq}(\omega,\omega) T_{CD}^{oq}(\omega,\omega) a_q(2\omega) \qquad (\omega \text{ far-off-resonance}) \tag{6.15}$$

This expression is very similar but not identical to the corresponding standard TPA residue spectrum with superimposed lineshape functions $\delta_S^{ABCD}(\omega)$, which, using Eq. (6.8), has the form

$$\delta_S^{ABCD}(\omega) = \sum_{q \neq o} T_{AB}^{oq}(\omega_q/2,\omega_q/2) T_{CD}^{oq}(\omega_q/2,\omega_q/2) a_q(2\omega) \tag{6.16}$$

The TPA amplitudes in the damped TPA spectrum in Eq. (6.15) depend on the optical frequency ω, whereas the frequencies entering the standard TPA amplitudes in Eq. (6.16) equal exactly half the excitation energies $\omega_q/2$. In the single-resonance case the damped and standard TPA spectra will thus be very similar, but not identical.

To illustrate the discussion above we have in Figure 6.2 plotted the isotropically averaged damped TPA spectrum in Eq. (6.14) and the corresponding averaged standard TPA spectrum $\bar{\delta}_S(\omega)$,

$$\bar{\delta}_S(\omega) = \frac{1}{30} \sum_{A,B} \left(2\delta_S^{AABB}(\omega) + 4\delta_S^{ABAB}(\omega) \right) \tag{6.17}$$

for a CAM-B3LYP calculation on the LiH molecule using the aug-cc-pVTZ basis. The first excited state in LiH (ω_1=0.128 a.u.) is energetically isolated, and therefore the $|o\rangle\rightarrow|1\rangle$ two-photon transition is appropriate to illustrate the single-resonance case. Thus, the frequency range in Figure 6.2 is centered around $\omega_1/2$ to probe the two-photon excitation to $|1\rangle$. Clearly, for all practical purposes the standard and damped spectra are identical, but a closer inspection reveals that they differ slightly for the reasons discussed above.

6.5.2 The double-resonance case

Consider the double-resonance case, where ω and 2ω are both close to resonance in the sense that $\omega\approx\omega_m$ and $2\omega\approx\omega_n$, see Figure 6.1(B). In this case the standard expression for the TPA amplitude in Eq. (6.2) becomes artificially large, and it diverges in the limit where $\omega=\omega_m=\omega_n/2$. In damped response theory the singularity problems of standard response theory are effectively avoided by introducing a factor $i\gamma$ in the denominator of the standard TPA amplitudes, see Eq. (6.9). We now discuss the implications of this empirical solution to the singularity problem in the double-resonance case.

In the double-resonance case, the damped TPA function in Eq. (6.13) may be approximated by [6]:

$$\delta_D^{ABCD}(\omega) \approx P(A,B)P(C,D)\big(\mu_A^{om}\mu_B^{mn}\mu_C^{om}\mu_D^{mn}\big)a_m(\omega)^2 a_n(2\omega) \qquad (\omega \approx \omega_m \approx \omega_n/2) \quad (6.18)$$

To investigate in more detail the physical content of Eq. (6.18) let us consider the *exact* double-resonance case $\omega=\omega_m=\omega_n/2$, see Figure 6.1(B), and assume that $A=B=C=D=x$ (TPA absorption along the x axis):

$$\delta_D^{xxxx}(\omega) \approx 4|\mu_x^{om}|^2|\mu_x^{mn}|^2(8\tau^3) \qquad (\omega = \omega_m = \omega_n/2) \quad (6.19)$$

where we have used Eq. (4.22b) and inserted the empirical lifetime $\tau=(2\gamma)^{-1}$. A simple physical interpretation of the TPA process described by Eq. (6.19) is the following two-step process:

(i) First, the one-photon excitation $|o\rangle\rightarrow|m\rangle$ occurs with transition strength $|\mu_x^{om}|^2$, corresponding to the first transition in Figure 6.1(B). This process is proportional to the lifetime of $|m\rangle$ (τ);

(ii) Following the $|o\rangle\rightarrow|m\rangle$ transition, a second one-photon transition $|m\rangle\rightarrow|n\rangle$ occurs with transition strength $|\mu_x^{mn}|^2$ [the second transition in Figure 6.1(B)]. This process is proportional to the lifetime of $|m\rangle$ (τ) *and* to the lifetime of $|n\rangle$ (also τ because we simply assume that all excited states have the same lifetime).

The total TPA process is therefore proportional to $|\mu_x^{om}|^2\tau$ (first transition) times $|\mu_x^{mn}|^2\tau^2$ (second transition). We emphasize, however, that no real information is contained in the lifetime τ, because it is an empirical parameter, and consequently the interpretation given above is only qualitative.

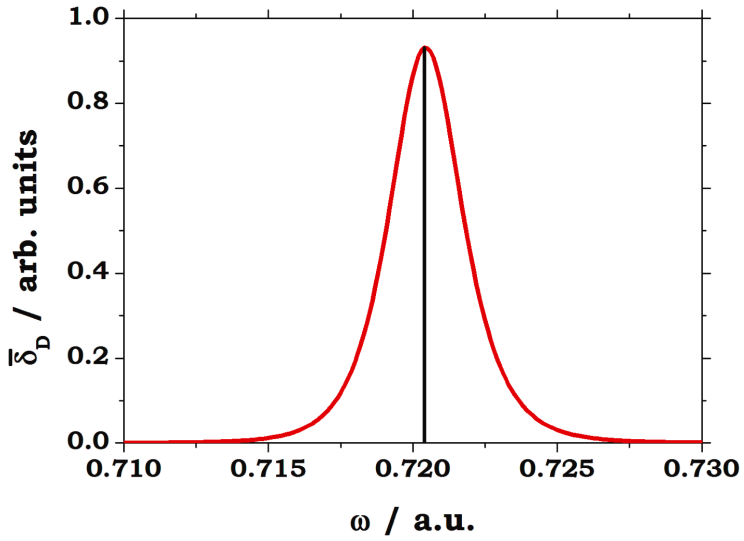

Figure 6.3: Damped absorption spectra for the artificial hydrogen fluoride test system described in the text, where the third excitation energy ω_3 equals half the fourth excitation energy $\omega_4/2$ (indicated by black stick). The broadening parameter $\gamma = 0.004$ a.u. Note that the optical frequency ω corresponds to a one-photon frequency.

Consider now the exact double-resonance case for a small test calculation on hydrogen fluoride with an H-F bond length of 1.95477 a.u., and with 6-31G basis functions on F and an STO-3G basis function on H. This very artificial system is of course not realistic representation of the hydrogen fluoride molecule; however, it serves as a useful test system, because the third and fourth excitation energies are related by ω_3=$\omega_4/2$=0.7204 a.u. at the Hartree-Fock level of theory. This system thus illustrates the structure of damped TPA spectra in the general double-resonance case. A standard TPA calculation of the $|o\rangle \rightarrow |4\rangle$ two-photon transition for this HF molecule will give meaninglessly large numbers, if the response equations converge at all. In contrast, the damped TPA calculation gives a smooth spectrum centered at ω=ω_3=$\omega_4/2$=0.7204 a.u. as shown in Figure 6.3. The damped TPA formulation thus provides a well-defined spectrum, also in double-resonance cases.

6.5.3 The two-photon absorption spectrum of BINOL

Having considered isolated single- and double-resonance peaks in TPA spectra for small test systems in Section 6.5.1 and 6.5.2, respectively, we now turn our attention to the TPA spectrum for a molecule of a relatively large size, namely R-(+)-1,1'-bi(2-naphtol) (BINOL). The TPA and two-photon circular dichroism spectra of BINOL were reported recently [124, 125] for the species dissolved in tetrahydrofuran (THF). The one- and two-photon spectra of both gas-phase and solvated BINOL have also been studied computationally, see Refs. [124–126].

In Figure 6.4 we have plotted the standard and damped TPA spectra calculated at the DFT/B3LYP level using the cc-pVDZ basis set and the geometrical parameters from Ref. [127]. Also plotted are the experimental TPA data (measured in THF solution) taken from Ref. [126].

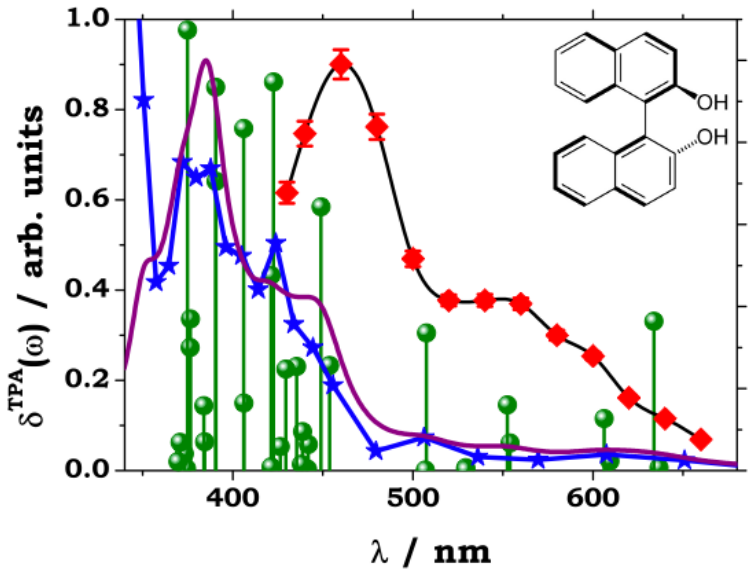

Figure 6.4: BINOL, cc-pVDZ basis set. Damped (γ=0.004 a.u., blue curve with blue stars) vs. standard (vertical green sticks) TPA results. The convoluted standard spectrum, obtained with the same γ is given by the purple curve. Also reported are the experimental data from Ref. [126] (black line with red diamonds). To make comparison easier, the computed damped TPA, standard convoluted and experimental spectra were all normalized in intensity.

The experimentally determined TPA spectrum $\delta^{\mathrm{TPA}}(\omega)$ is related to the calculated standard TPA spectrum by [128]

$$\delta^{\mathrm{TPA}}(\omega) \approx 5.31678 \times 10^{-4} \omega^2 \bar{\delta}_X(\omega) \tag{6.20}$$

where X=S for standard TPA [see Eq. (6.17)], and X=D for damped TPA [see Eq. (6.14)]. Eq. (6.20) yields the TPA spectrum in Göppert-Mayer (GM) units, when all the quantities on the right hand side are given in atomic units. For standard TPA, the sum in Eq. (6.16) was in the considered case restricted to the 35 first excited states:

$$\delta_S^{ABCD}(\omega) = \sum_{q=1}^{35} T_{AB}^{oq}(\omega_q/2, \omega_q/2) T_{CD}^{oq}(\omega_q/2, \omega_q/2) a_q(2\omega) \tag{6.21}$$

Considering Figure 6.4, the standard and damped spectra are reasonably close to each other although not identical for the reasons discussed in Section 6.5.1 and 6.5.2. However, below 400 nm the standard spectrum dies out abruptly, because only 35 excited states have been considered, see Eq. (6.21). In contrast, the damped TPA spectrum by construction gets contributions from *all excited states* and thus also from strong TPA absorbers well below 400 nm, which have not been determined using the standard approach.

Our simulated spectra show qualitatively the behavior observed in experiment, although with a net blue shift of the peak observed by experimentalists around 450 nm (by at least 70–75 nm if we assume that it can be mimicked by the relative maximum at ≈375 nm in the simulated spectra). A more in depth comparison with experiment is given in Ref. [126].

6.6 Conclusion and perspectives

We have demonstrated how TPA spectra can be calculated in damped response theory by introducing complex excitation energies into the standard response theory expressions. By construction, standard and damped TPA spectra are not completely identical. However, in the single-resonance case standard and damped response theory provide – for practical purposes – the same TPA spectra. In contrast, the occurrence of double-resonances causes the standard TPA spectrum to blow up, whereas the damped TPA spectrum is well-defined and provides physically motivated TPA spectra at all optical frequencies.

Damped response theory provides a complete and reasonable description of TPA spectra without detailed knowledge of the excited electronic state manifold and of their two-photon responses. This is of extreme importance in large molecules, where the density of excited states in regions of relevance for two-photon spectroscopy might be particularly large (see the discussion in connection with Figure 4.1). We thus consider damped response theory as a viable tool to investigate TPA properties of large molecular systems.

PART B: Linear-scaling formulation of coupled-cluster theory – the Divide-Expand-Consolidate approach

Chapter 7

The DEC method I: Foundation and proof of concept

This chapter describes the work presented in **paper [7]**.

7.1 Introduction

In Chapters 2-6 molecular properties were treated within the DFT (or HF) framework. In many cases DFT provides a qualitatively correct description of the energetics and molecular properties of a molecular system at a relatively low computational cost. In particular, using linear-scaling techniques [39–47], it is possible to perform calculations on large molecular systems at the DFT level. However, the empirical nature of the correction terms and the neglect of dispersion forces[1] in standard DFT functionals make it difficult to systematically improve the accuracy of DFT. In this and the following chapters we consider the more accurate coupled-cluster (CC) method [63, 130], which is usually a better and safer choice.

Assuming that the electronic structure is dominated by a single HF reference determinant, the well-known hierarchy of CC models constitutes a systematic way of obtaining increasingly accurate energetics and molecular properties [63]. Furthermore, in contrast to standard DFT functionals, the CC models provide a correct description of dispersion forces which is crucial for a proper description of, e.g., the intramolecular interactions in large biomolecules including proteins and DNA. Unfortunately, the application of CC methods in their standard formulations has been limited to small molecules, because the computational time scales dramatically with molecular size. For example, the computational times of the increasingly accurate models in the CC energy hierarchy MP2 [131] (second order Møller-Plesset perturbation theory), CCSD [132] (CC with singles and doubles excitations), CCSD(T) [133] (CCSD with approximate triples), and CCSDT [134, 135] (CC with singles, doubles, and triples) scale as N^5, N^6, N^7, and N^8, respectively, where N is a measure of the molecular system size. The red curve in Figure 7.1

[1] It should be noted that empirical dispersion-corrections to the "standard DFT energy" have been suggested, see Ref. [129] for a recent review.

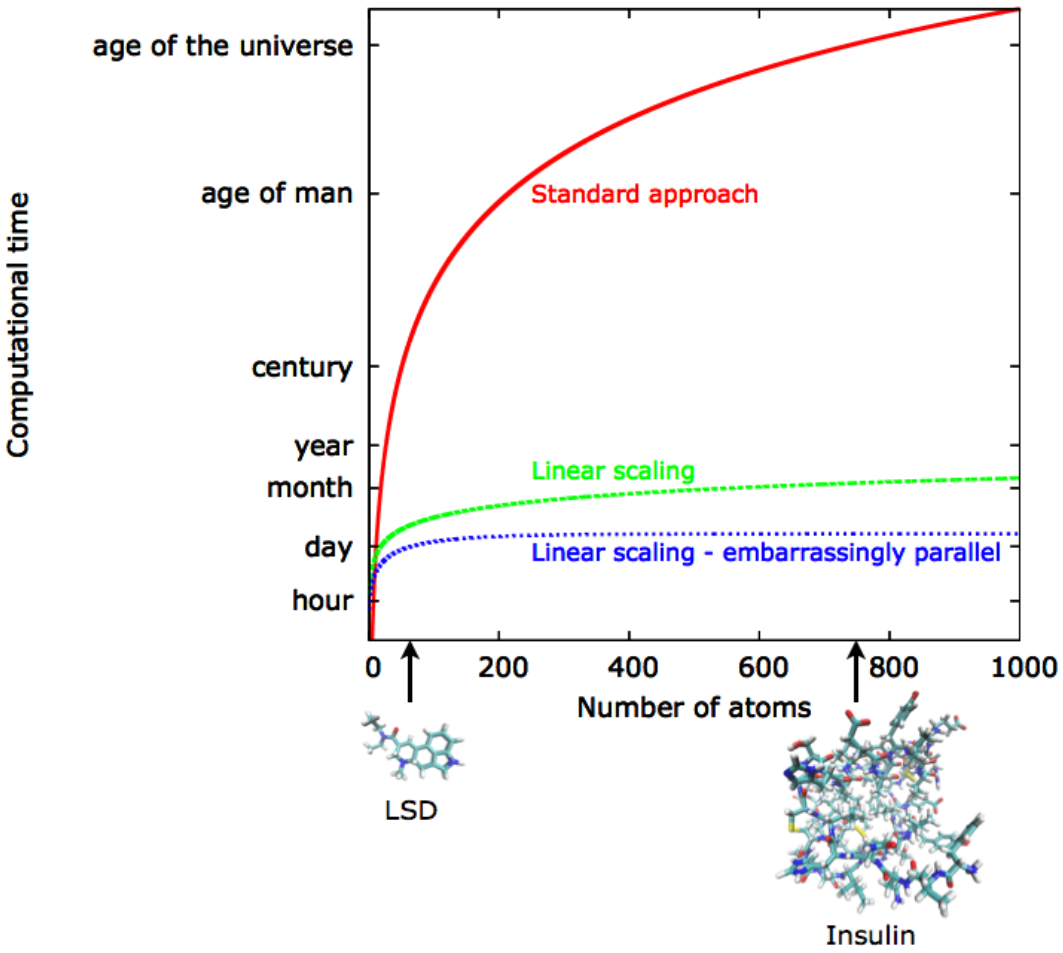

Figure 7.1: Estimated computational time as a function of system size for the CCSD(T) method using the standard approach (red curve), a linear-scaling approach (green curve), and a linear-scaling *and* embarrassingly parallel approach (blue curve).

gives the estimated computational time plotted against system size for standard CCSD(T) calculations. It is clear that, using a standard implementation, accurate CC calculations on large molecules (such as the insulin molecule displayed in Figure 7.1) will forever be out of reach.

This so-called scaling wall of conventional CC algorithms arises because standard CC calculations are expressed in the nonlocal canonical HF basis (Figure 7.2, top), whereas the major task of the CC calculation is to improve the mean-field HF treatment by describing the local electron-electron interactions (dynamical correlation). However, using a set of local orbitals (Figure 7.2, bottom) it should be possible to capture the local nature of the electron correlation effects in an efficient manner, such that the computational time of a CC calculation ideally scales only *linearly* with the system size (green curve in Figure 7.1). This would allow highly accurate calculations to be carried out on systems with a thousand atoms within a few months. Better still, if the CC calculation is also *embarrassingly parallel* – in the sense that the full CC calculation may be carried out in terms of small independent fragment calculations – it would be possible to carry out highly accurate CC calculations in a few days (blue curve in Figure 7.1). Naturally, this idealized case assumes that a sufficient number of processors are available for the

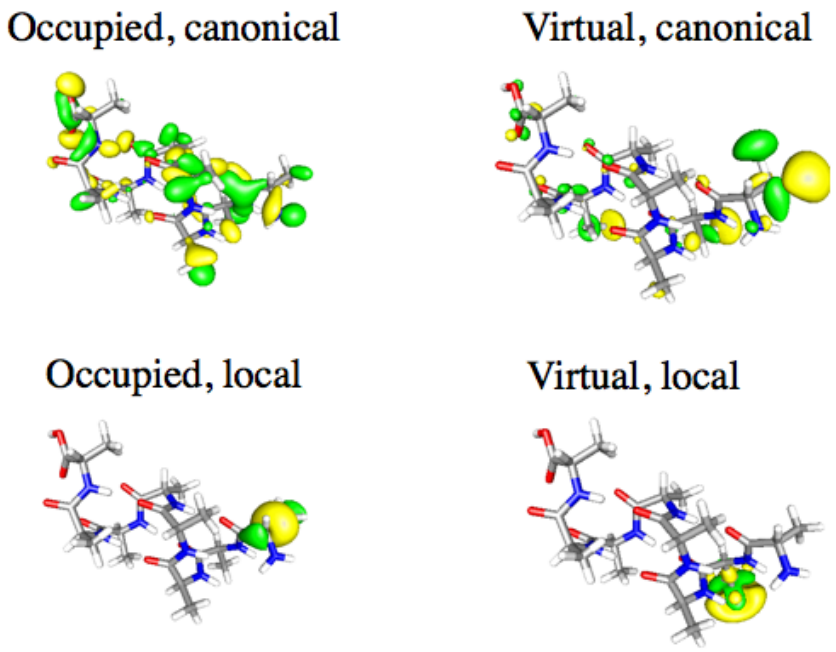

Figure 7.2: Least local occupied and virtual canonical orbitals and least local occupied and virtual localized orbitals for an alpha-helix peptide containing 8 alanine residues. The local orbitals were obtained using the localization procedure described in Chapter 10.

fragment calculations, and that the fragments are only of modest size.

The goal of this chapter is to present the foundation for the linear-scaling and embarrassingly parallel Divide-Expand-Consolidate (DEC) CC method, which is an attempt to approach the idealized blue curve in Figure 7.1. In Chapter 8 we discuss additional features of the DEC method and compare it method to existing local CC methods. The main motivation for the DEC scheme is not to be able to compete with conventional CC implementations for small and medium-sized molecules. Rather, the aim is to develop a method which enables CC calculations on large molecular systems – where conventional CC calculations encounter a scaling wall – and which reproduces the standard CC results. At this stage the DEC method has been developed for the MP2 and CCSD models. For completeness, the discussion in this chapter is initiated by summarizing standard CC theory.

7.2 Standard coupled-cluster theory

The CC wave function may be written in the form [63]

$$|\mathrm{CC}\rangle = \exp(T)\,|\mathrm{HF}\rangle \tag{7.1}$$

where $|\mathrm{HF}\rangle$ is the HF reference state and the *cluster operator* T is written as

$$T = T_1 + T_2 + \cdots \tag{7.2}$$

The T_1 operator produces single excitations from the HF reference state, T_2 produces double excitations, and so on:

$$T_1 = \sum_{ai} t_i^a E_{ai} \tag{7.3}$$

$$T_2 = \frac{1}{2} \sum_{aibj} t_{ij}^{ab} E_{ai} E_{bj} \tag{7.4}$$

where t_i^a and t_{ij}^{ab} denote singles and doubles amplitudes, respectively. E_{ai} is a singlet excitation operator describing an excitation from the occupied orbital ϕ_i to the virtual orbital ϕ_a, and it can be written in terms of the elementary creation operators $a_{a\sigma}^\dagger$ and annihilation operators $a_{i\sigma}$ (with σ denoting spin) according to [63]

$$E_{ai} = a_{a\alpha}^\dagger a_{i\alpha} + a_{a\beta}^\dagger a_{i\beta} \tag{7.5}$$

In this and the following chapters only closed-shell molecules are considered and indices $i, j, \ldots$ refer to occupied HF molecular orbitals, indices $a, b, \ldots$ refer to virtual HF molecular orbitals, while indices $p, q, \ldots$ are reserved to molecular orbitals of general type. Finally, Greek indices $\mu, \nu, \tau, \epsilon, \ldots$ refer to atomic orbitals.

The CC energy E_{CC} is not determined variationally. Rather, the time-independent Schrödinger equation written in the form

$$H_0 \exp(T) |\mathrm{HF}\rangle = E_{\mathrm{CC}} \exp(T) |\mathrm{HF}\rangle \tag{7.6}$$

is multiplied from the left by $\exp(-T)$ and projected by the HF reference state $\langle \mathrm{HF}|$ to yield E_{CC},

$$E_{\mathrm{CC}} = \langle \mathrm{HF} | \exp(-T) H_0 \exp(T) | \mathrm{HF} \rangle \tag{7.7}$$

Multiplication of Eq. (7.6) by $\exp(-T)$ followed by projection against the excited state determinants $\langle \mu|$ gives the nonlinear CC amplitude equations,

$$\langle \mu | \exp(-T) H_0 \exp(T) | \mathrm{HF} \rangle = 0 \tag{7.8}$$

whose solution yield the CC amplitudes and thus the CC wave function.

If all $T_1, \ldots, T_n$ excitation operators (n being the number of electrons in the system) are included in Eq. (7.2), the CC model is equivalent to the so-called full configuration interaction (FCI) model, i.e., $E_{\mathrm{CC}} = E_{\mathrm{FCI}}$. In practice the expansion in Eq. (7.2) is truncated. For example, if Eq. (7.2) is truncated after the T_2 operator, the CCSD model [132] is obtained. Note that, due to the exponential parameterization in Eq. (7.1), higher than second order excitations are also included in the CCSD model – for example, quadruple excitations are introduced in terms of disconnected cluster operator terms, such as $\frac{1}{2}T_2^2$. Importantly, the exponential ansatz also ensures that the approximate CC models are *size-extensive*. Therefore, small and large systems are described with the same accuracy in the sense that the relative error in the CC energy compared to the FCI energy is the same for a single monomer and for an arbitrary number of noninteracting monomers.

It is convenient to express the total CC energy E_{CC} as a sum of a HF contribution E_{HF} and an electron correlation contribution E_{corr},

$$E_{\mathrm{CC}} = E_{\mathrm{HF}} + E_{\mathrm{corr}} \tag{7.9}$$

By evaluating Eq. (7.7), an expression for the correlation energy may be obtained as [63]

$$E_{\mathrm{corr}} = \sum_{ijab} (t_{ij}^{ab} + t_i^a t_j^b) L_{iajb} \tag{7.10}$$

where

$$L_{iajb} = 2g_{iajb} - g_{ibja} \tag{7.11}$$

and g_{iajb} is a two-electron integral in the HF orbital basis given by (assuming real orbitals),

$$g_{iajb} = \iint \phi_i(\mathbf{r}_1)\phi_a(\mathbf{r}_1)\frac{1}{r_{12}}\phi_j(\mathbf{r}_2)\phi_b(\mathbf{r}_2)d\mathrm{r}_1 d\mathrm{r}_2 \tag{7.12}$$

The expression for the correlation energy in Eq. (7.10) applies to all standard CC models. By carrying out a perturbation theory analysis of the CCSD model and retaining only the first order terms, the CCSD model reduces to the much simpler MP2 model [63], where only doubles excitations are present. Thus, an expression for the MP2 correlation energy can be identified by omitting the singles contributions from Eq. (7.10).

The CC amplitude equations in Eq. (7.8) may be evaluated for the different excitation levels $\langle\mu|$. For example, the MP2 amplitude equation becomes [63],

$$g_{aibj} + \sum_c t_{ij}^{cb} F_{ac} + \sum_c t_{ij}^{ac} F_{bc} - \sum_k t_{kj}^{ab} F_{ki} - \sum_k t_{ik}^{ab} F_{kj} = 0 \tag{7.13}$$

where F_{rs} is an element of the Fock matrix. The MP2 equation is a subset of the CCSD doubles amplitude equation. For explicit expressions for the singles and doubles CCSD amplitude equations, see Ref. [63] or Table 2 in paper [7].

7.3 The Divide-Expand-Consolidate scheme

In this section the DEC strategy for obtaining the MP2 and CCSD correlation energies is described. It is assumed that a set of orthogonal, local HF orbitals is available for both the occupied and virtual orbital spaces. In Chapter 10 we describe how such local orbitals may be obtained in practice. By exploiting the locality of the orbitals and rewriting the CC equations it will be demonstrated that it is possible to evaluate E_{corr} in a linear-scaling and embarrassingly parallel manner. The HF contribution to the energy may also be evaluated in a linear-scaling manner as discussed elsewhere [39–45].

After the initial HF calculation, the first step in the DEC scheme is to assign each local HF orbital to the atomic site where it has the largest Mulliken charge. In this way each atomic site is assigned a set of local occupied and a set of local virtual HF orbitals. The set of occupied HF orbitals assigned to atomic site P is denoted $\underline{P}$ and the set of virtual HF orbitals assigned to

Table 7.1: Overview of the notation used in the DEC method.

Symbol	Short description
P,Q,R, ...	Labels for atomic sites
$E^{\mathrm{o}}_{\mathrm{P}}$	Atomic fragment energy
$\Delta E^{\mathrm{o}}_{\mathrm{PQ}}$	Pair interaction energy
$\mathcal{E}_{\mathrm{P}}$	Energy orbital space (EOS) for evaluating $E^{\mathrm{o}}_{\mathrm{P}}$
$\mathcal{A}_{\mathrm{P}}$	Amplitude orbital space (AOS) for calculating CC amplitudes
$\{\mathcal{A}_{\mathrm{P}}\}$	Atomic fragment extent where MO coefficients are expanded
$\underline{P}$	Set of occupied orbitals assigned to site P (occupied orbitals in $\mathcal{E}_{\mathrm{P}}$)
$\overline{P}$	Set of virtual orbitals assigned to site P
$[\underline{P}]$	Set of occupied orbitals local to P
$[\overline{P}]$	Set of virtual orbitals local to P (virtual orbitals in $\mathcal{E}_{\mathrm{P}}$)
$\mathcal{B}_{\underline{\mathrm{P}}}$	Occupied buffer orbital space
$\mathcal{B}_{\overline{\mathrm{P}}}$	Virtual buffer orbital space
FOT	Fragment optimization threshold defining the accuracy of $E^{\mathrm{o}}_{\mathrm{P}}$

atomic site P is denoted $\overline{P}$. Table 7.1 contains an overview of the DEC notation. An illustration of how a one-dimensional model system is divided into atomic sites and assigned a set of occupied and virtual HF orbitals is given in Figure 7.3(A). As a specific example we present the orbital assignment for the $C_{14}H_2$ molecule (cc-pVDZ basis) in Figure 7.3(B). The orbitals are not evenly distributed because the local orbitals do not reflect the symmetry of the molecule. However, this uneven distribution is unproblematic because the DEC algorithm automatically adjusts the sizes of the orbital spaces according to the specific assignment of orbitals as will be detailed in Section 7.4.2.

Having assigned the local HF orbitals to atomic sites, the correlation energy in Eq. (7.10) can be expressed in terms of atomic fragment energies $E^{\mathrm{o}}_{\mathrm{P}}$ and pair interaction energies $\Delta E^{\mathrm{o}}_{\mathrm{PQ}}$

$$E^{\mathrm{o}}_{\mathrm{P}} = \sum_{\substack{ij\in\underline{P}\\ab}} (t^{ab}_{ij} + t^a_i t^b_j) L_{iajb} \tag{7.14}$$

$$\Delta E^{\mathrm{o}}_{\mathrm{PQ}} = \sum_{\substack{i\in\underline{P}\\ j\in\underline{Q}}} \sum_{ab} (t^{ab}_{ij} + t^a_i t^b_j) L_{iajb} + \sum_{\substack{i\in\underline{Q}\\ j\in\underline{P}}} \sum_{ab} (t^{ab}_{ij} + t^a_i t^b_j) L_{iajb} \tag{7.15}$$

giving

$$E_{\mathrm{corr}} = \sum_{\mathrm{P}} E^{\mathrm{o}}_{\mathrm{P}} + \sum_{P>Q} \Delta E^{\mathrm{o}}_{\mathrm{PQ}} \tag{7.16}$$

where the summations run over all atomic sites. No approximations have been made in Eq. (7.16); the summations in Eq. (7.16) have simply been reordered compared to Eq. (7.10).

In a conventional CC calculation, the CC wave function is expanded in the nonlocal canonical HF orbital basis, and therefore the integrals g_{iajb} entering Eqs. (7.14) and (7.15) are generally nonvanishing for any choice of indices i, a, j, b, see Figure 7.4 (left). The evaluation of E_{corr} thus

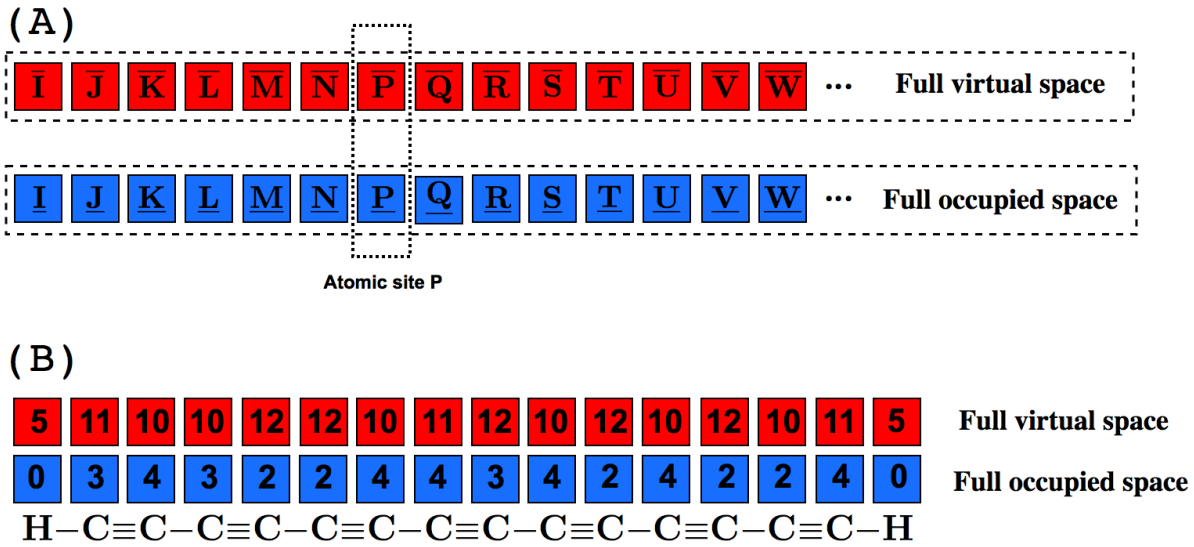

Figure 7.3: (A) Molecular system divided into atomic sites I,J, . . . ,P, . . . where each site has been assigned a set of occupied (blue) and a set of virtual (red) HF orbitals. (B) Example of orbital assignments for the $C_{14}H_2$ molecule, where the numbers of occupied and virtual orbitals assigned to each atom are given above the atoms.

scales with the fourth power of the system size. However, the computational effort required to evaluate Eqs. (7.14) and (7.15) may be greatly reduced by using a local HF basis. Specifically, an integral g_{iajb} is nonvanishing only if the $\phi_i\phi_a$ and $\phi_j\phi_b$ charge distributions are both nonzero – i.e., ϕ_i and ϕ_a are close to each other in space and likewise for ϕ_j and ϕ_b, see Figure 7.4 (right). To be more specific with respect to the summation restrictions for local orbitals depicted in Figure 7.4 (right), let us consider the g_{iajb} integral for the case where $i \in \underline{P}$ and $j \in \underline{Q}$. This integral is nonvanishing only if $a \in [\overline{P}]$ and $b \in [\overline{Q}]$, where $[\overline{P}]$ refers to the set of virtual HF orbitals local to $\overline{P}$ (including $\overline{P}$):

$$g_{iajb} \neq 0: \quad i \in \underline{P}\,,\, a \in [\overline{P}]\,,\, j \in \underline{Q}\,,\, b \in [\overline{Q}] \tag{7.17}$$

By applying the locality restriction in Eq. (7.17), Eqs. (7.14) and (7.15) may be written as

$$E^{\mathrm{o}}_{\mathrm{P}} = \sum_{\substack{ij\in\underline{P}\\ ab\in[\overline{P}]}} (t_{ij}^{ab} + t_i^a t_j^b) L_{iajb} \tag{7.18}$$

$$\Delta E^{\mathrm{o}}_{\mathrm{PQ}} = \Big(\sum_{\substack{i\in\underline{P}\\ j\in\underline{Q}}} + \sum_{\substack{i\in\underline{Q}\\ j\in\underline{P}}}\Big) \sum_{ab\in[\overline{P}]\cup[\overline{Q}]} (t_{ij}^{ab} + t_i^a t_j^b) L_{iajb} \tag{7.19}$$

We refer to the set of orbitals in $\underline{P}$ and $[\overline{P}]$ as the *energy orbital space* (EOS) $\mathcal{E}_{\mathrm{P}}$ for the atomic site P,

$$\mathcal{E}_{\mathrm{P}} = \underline{P} \cup [\overline{P}] \tag{7.20}$$

since $\underline{P}$ and $[\overline{P}]$ contain the set of occupied and virtual orbitals, respectively, required to determine $E^{\mathrm{o}}_{\mathrm{P}}$. The sizes of the EOSs for the different fragments are not known *a priori*. Rather,

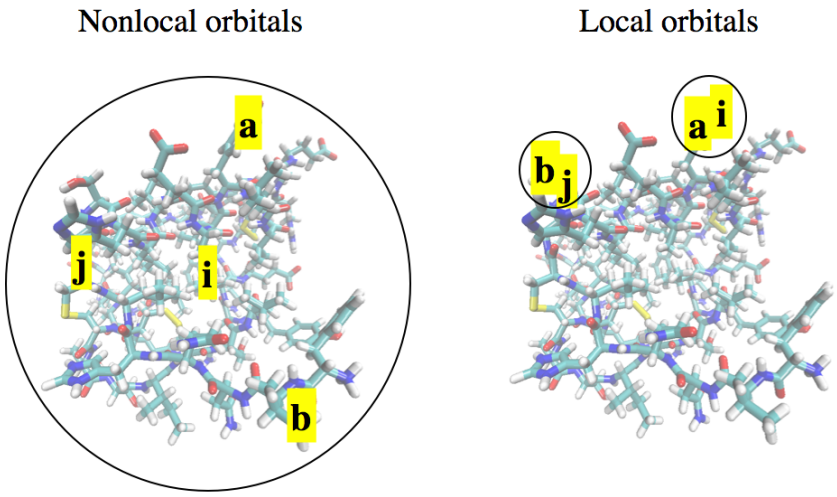

Figure 7.4: For nonlocal orbitals (left) g_{iajb} integrals are in general nonvanishing for any choice of indices i, a, j, b. Using local orbitals (right) the g_{iajb} integrals are nonvanishing only if the local $\phi_i\phi_a$ and $\phi_j\phi_b$ charge distributions are simultaneously nonvanishing.

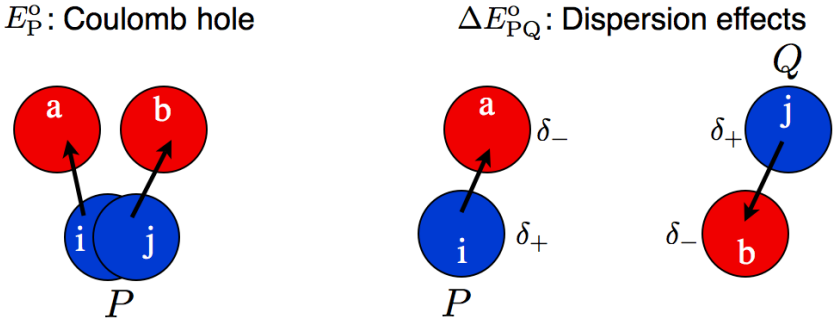

Figure 7.5: Illustrations of excitations from occupied orbitals ϕ_i and ϕ_j (blue) into virtual orbitals ϕ_a and ϕ_b (red). Left: Short-range electron-electron repulsion described by the atomic fragment energy $E^{\mathrm{o}}_{\mathrm{P}}$ (Coulomb hole). Right: Dispersion effects described by pair interaction energy $\Delta E^{\mathrm{o}}_{\mathrm{PQ}}$.

the sizes of the orbital fragments are determined during the calculation in a black box manner to ensure that the standard CC energy is determined to a preset threshold as discussed in Section 7.4.2.

A qualitative physical interpretation of the fragment energies in Eqs. (7.18) and (7.19) is the following. The atomic fragment energy $E^{\mathrm{o}}_{\mathrm{P}}$ describes short-range electron-electron repulsion in terms of excitations from two overlapping occupied orbitals ϕ_i and ϕ_j into two neighbouring virtual orbitals ϕ_a and ϕ_b, see Figure 7.5 (left). This ultimately describes the so-called Coulomb hole in the wave function. For larger pair distances the pair interaction energy $\Delta E^{\mathrm{o}}_{\mathrm{PQ}}$ describes dispersion effects (also known as induced dipole-induced dipole interactions), which decays with the inverse pair distance to the sixth power r^{-6}_{PQ}. As indicated by the induced partial charges in Figure 7.5 (right) dispersion effects are in general attractive.

Having introduced the DEC partitioning of the energy as defined by Eqs. (7.16), (7.18), and (7.19), we are now in position to summarize the *Divide-Expand-Consolidate scheme* for the determination of the correlation energy:

- **Divide** the orbital space among the atomic sites (Figure 7.3).
- **Expand** the orbital spaces of the individual atomic fragments to obtain converged atomic fragment energies E°_{P}. Pair fragments are then formed as unions of atomic fragments to calculate the pair interaction energies $\Delta E^{\circ}_{\mathrm{PQ}}$.
- **Consolidate** the calculated atomic fragment energies and pair interaction energies according to Eq. (7.16) to get the correlation energy for the full molecular system.

This scheme is summarized in Figure 7.6.

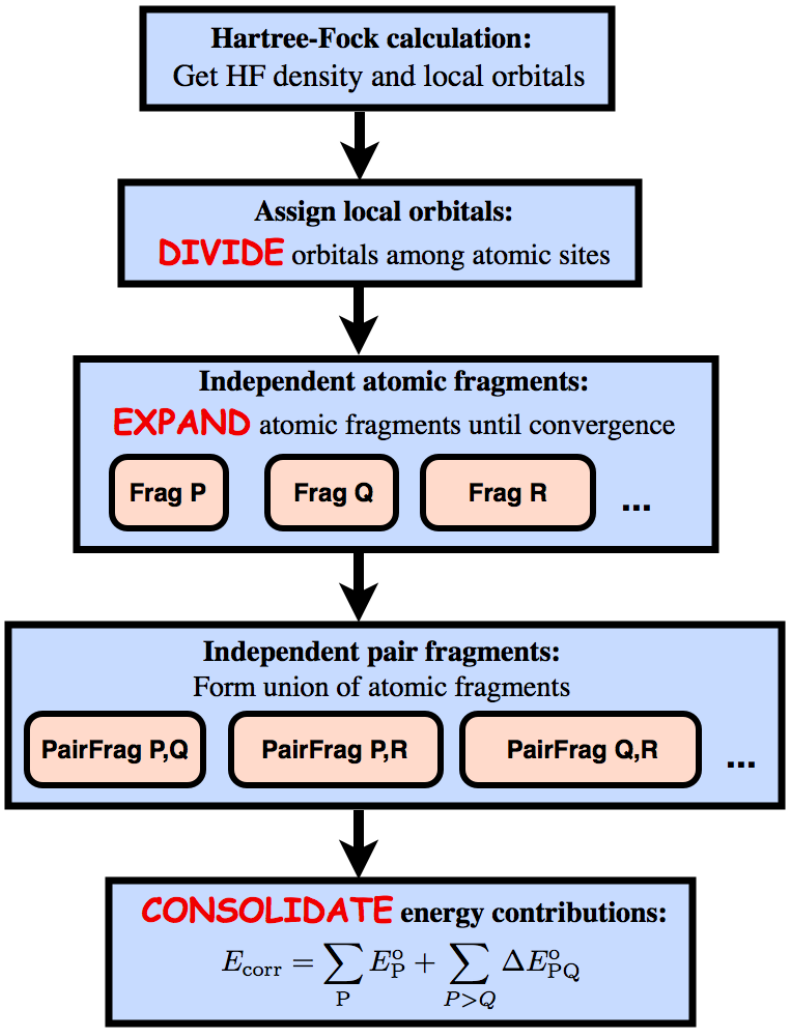

Figure 7.6: Overview of the Divide-Expand-Consolidate (DEC) scheme for evaluating the correlation energy.

Consider the computational scaling of the DEC method. The number of atomic fragments equals the number of atoms N in the molecule, while there are $N(N-1)/2$ pair fragments, leading to a quadratic scaling with system size. However, since $\Delta E^{\circ}_{\mathrm{PQ}}$ describes dispersion effects decaying with the inverse pair distance to the sixth power, distant pairs may be omitted from the DEC calculation with a negligible effect on the correlation energy. For a large (homogeneous) molecular system each atomic site thus interacts with a fixed number of other atomic sites N_{int},

and the total number of pair fragments to consider is $N_{\text{int}}N/2$ (neglecting boundary effects). Assuming that the orbital fragment sizes are independent of the molecular system size (which follows from the theoretical locality analysis in Section 7.4.1 and is supported by the numerical results in Section 7.5.2), it follows that the DEC scheme becomes linear-scaling for large molecular systems. Furthermore, both the atomic fragment calculations as well as the subsequent pair fragment calculations are independent. Therefore, the DEC scheme is also embarrassingly parallel in the sense that the fragment calculations may be carried out on different nodes of a supercomputer with no communication between the nodes. Thus, in the ideal case where a sufficient number of processors are available, the total time for a DEC CC calculation (not considering the initial HF calculation) is simply the sum of the times required for the largest atomic fragment calculation and the largest pair fragment calculation – independently of the molecular system size.

7.4 Fragment orbital spaces in the DEC method

7.4.1 Locality analysis of the amplitude equations

Eq. (7.18) states that the fragment energy E^{o}_{P} may be evaluated in a small local EOS containing the occupied orbitals assigned to atom P and virtual orbitals in the $[\overline{P}]$ space. In order to evaluate Eq. (7.18) the corresponding CC amplitudes must of course be known. In this section it is described how the locality of the orbitals can be exploited to determine the amplitudes inside the EOS without invoking a full molecular calculation. Details are given in paper [7], where a locality analysis of the MP2 and CCSD amplitude equations is carried out. The main results are summarized here.

Consider an EOS amplitude $t^{ab}_{ij,\text{P}}$ used for evaluating the atomic fragment energy E^{o}_{P}. When the amplitude equations involving $t^{ab}_{ij,\text{P}}$ are solved, $t^{ab}_{ij,\text{P}}$ couples strongly to other amplitudes inside the EOS. However, $t^{ab}_{ij,\text{P}}$ couples only weakly to amplitudes outside the EOS. In particular, the coupling effects between $t^{ab}_{ij,\text{P}}$ and an amplitude t^{cd}_{kl} outside the EOS decrease rapidly with increasing distance between atomic site P and the MOs ϕ_k, ϕ_l, ϕ_c, and ϕ_d. Therefore, the EOS amplitudes for atomic fragment P can be determined accurately by solving the CC amplitude equations in a small local orbital fragment space, including only orbitals which are spatially close to the atomic site P. However, due to coupling effects it is necessary to include some surrounding buffer atoms outside the EOS to ensure that the amplitudes inside the EOS are determined with sufficient accuracy. By denoting the occupied and virtual buffer spaces as $\mathcal{B}_{\underline{\text{P}}}$ and $\mathcal{B}_{\overline{\text{P}}}$, respectively, the *amplitude orbital space* (AOS) $\mathcal{A}_{\text{P}}$ used to solve the amplitude equations for atomic fragment P is the union of the EOS in Eq. (7.20) and these buffer spaces:

$$\mathcal{A}_{\text{P}} = \mathcal{E}_{\text{P}} \cup \mathcal{B}_{\underline{\text{P}}} \cup \mathcal{B}_{\overline{\text{P}}} \tag{7.21}$$

To carry out the DEC fragment calculations in an efficient manner it is also necessary to restrict the MOs inside $\mathcal{A}_{\text{P}}$ to a localized region of space. In general, a MO ϕ^X_r assigned to an

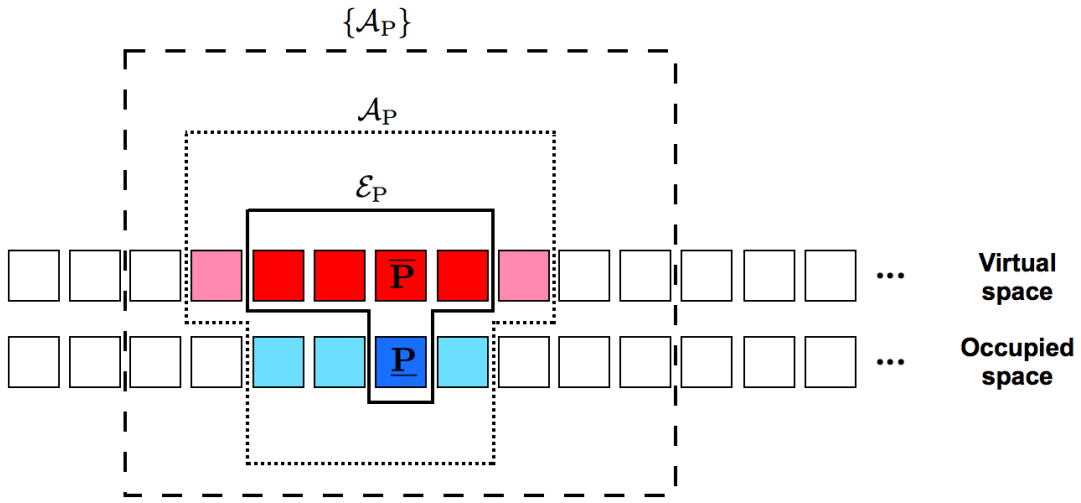

Figure 7.7: Atomic fragment P. The atomic fragment energy E_P^o is evaluated in the *energy orbital space* (EOS) $\mathcal{E}_P$ (dark-blue and dark-red markings). The CC amplitude equation is solved in the *amplitude orbital space* $\mathcal{A}_P$, where occupied $\mathcal{B}_{\underline{P}}$ (light-blue) and virtual $\mathcal{B}_{\overline{P}}$ (pink) buffer spaces are added to the EOS. The expansion coefficients for the molecular orbitals in the $\mathcal{A}_P$ space are confined to the atoms in the *atomic fragment extent* {$\mathcal{A}_P$}.

atom X inside the AOS is expanded in terms of atomic orbitals χ,

$$\phi_r^X = \sum_\mu \chi_\mu C_{\mu r}; \qquad (X \in \mathcal{A}_P) \tag{7.22}$$

Even though the MOs are localized in space (see, for example, Figure 7.2), there may be very small – but nonzero – orbital coefficients $C_{\mu r}$ on distant atoms far away from X. Therefore, the μ summation in Eq. (7.22), in principle, runs over all atoms in the molecule. However, it is possible to remove the very small orbital tails on distant atoms without compromising the accuracy of the correlated calculation. This can be done by approximating ϕ_r^X by an orbital $\tilde{\phi}_r^X$, where the μ summation index in Eq. (7.22) runs only over a limited part of the molecule, denoted the *atomic fragment extent* {$\mathcal{A}_P$}:

$$\tilde{\phi}_r^X = \sum_{\tilde{\mu} \in \{\mathcal{A}_P\}} \chi_{\tilde{\mu}} \tilde{C}_{\tilde{\mu} r}; \qquad (X \in \mathcal{A}_P) \tag{7.23}$$

The atomic fragment extent contains the atoms in $\mathcal{A}_P$ and some additional boundary atoms to ensure a proper description of the MOs inside $\mathcal{A}_P$. Thus, for atomic fragment P, two-electron integrals in the atomic orbital basis need to be calculated for atoms in the {$\mathcal{A}_P$} space. The details for determining {$\mathcal{A}_P$} and the approximate MO coefficients $\tilde{C}_{\tilde{\mu} r}$ such that the approximate orbital $\tilde{\phi}_r^X$ is a good representation of the true orbital ϕ_r^X are given in paper [7].

In summary, the fragment energy is evaluated inside the EOS $\mathcal{E}_P^o$, the amplitude equations are solved in the AOS $\mathcal{A}_P$, and the MOs are expanded on atoms in the atomic fragment extent {$\mathcal{A}_P$}. Figure 7.7 gives an illustration of the spaces employed in an atomic fragment calculation for a one-dimensional system. The pair fragments are formed as unions of the atomic fragments. For a given AOS the amplitudes equations are solved as standard MP2 or CCSD calculations

inside that limited orbital space. We now describe how the EOS and AOS are determined in a practical calculation in a manner which ensures that the atomic fragment energies – and therefore also the total correlation energy – are determined to a preset accuracy.

7.4.2 Determination of fragment orbital spaces

As discussed in Section 7.4.1, the effects on the atomic fragment energy $E_{\mathrm{P}}^{\mathrm{o}}$ from local orbitals surrounding P fall of rapidly with increasing distance to the P center. Thus, by gradually expanding the orbital fragments to include orbitals located further and further away from P, each expansion step will include orbitals with still smaller effects on the fragment energy $E_{\mathrm{P}}^{\mathrm{o}}$. This orbital expansion procedure can therefore be repeated until the atomic fragment energy is converged to a predefined energy tolerance, denoted the *fragment optimization threshold* (FOT). The orbital fragment expansion procedure determining the AOS may be carried out as depicted in Figure 7.8. Each of the orbital spaces – i.e., the EOS $[\overline{P}]$ (dark-red), the occupied buffer space $\mathcal{B}_{\underline{\mathrm{P}}}$ (light-blue), and the virtual buffer space $\mathcal{B}_{\overline{\mathrm{P}}}$ (pink) – is gradually increased to ensure that $E_{\mathrm{P}}^{\mathrm{o}}$ is determined to the accuracy defined by the FOT. When the change in the atomic fragment energy for a given expansion step is larger than the FOT, the step is accepted, otherwise it is rejected. Continuing in this manner the cycle in Figure 7.8(B-D) is repeated until one full optimization round is carried through where the sizes of the EOS, the occupied buffer space, and the virtual buffer space all remain unchanged.

In practice the fragment expansions may be controlled by including all atoms which are closer to P than a certain orbital space radius (with a different orbital space radius for $[\overline{P}]$, $\mathcal{B}_{\underline{\mathrm{P}}}$, and $\mathcal{B}_{\overline{\mathrm{P}}}$). New atoms are then included in the fragment by increasing the orbital space radii for $[\overline{P}]$, $\mathcal{B}_{\underline{\mathrm{P}}}$, and $\mathcal{B}_{\overline{\mathrm{P}}}$. Alternatively, new atoms may be introduced by including the nearest-neighbours to the atoms which are already included in the fragment. A more sophisticated fragment optimization scheme is currently being developed [136]. However, the general features of the fragment optimization procedure are captured by the simple representation in Figure 7.8.

7.5 Illustrative results

In Section 7.5.1 we present proof-of-concept calculations demonstrating that the total MP2 and CCSD correlation energies may be determined from DEC fragment calculations with control of the errors introduced compared to a full molecular calculation. In Section 7.5.2 it is shown that the fragment sizes and the relative energy errors in DEC-MP2 calculations are independent of the size of the molecular system, and also that distant atom pairs may be omitted from the DEC calculation. In all calculations the cc-pVDZ basis [137] has been applied.

7.5.1 DEC-MP2 and DEC-CCSD calculations on $C_{14}H_2$

The discussion regarding the accuracy of the DEC-MP2 and DEC-CCSD calculations compared to full molecular MP2 and CCSD calculations is initiated by considering the $C_{14}H_2$ molecule.

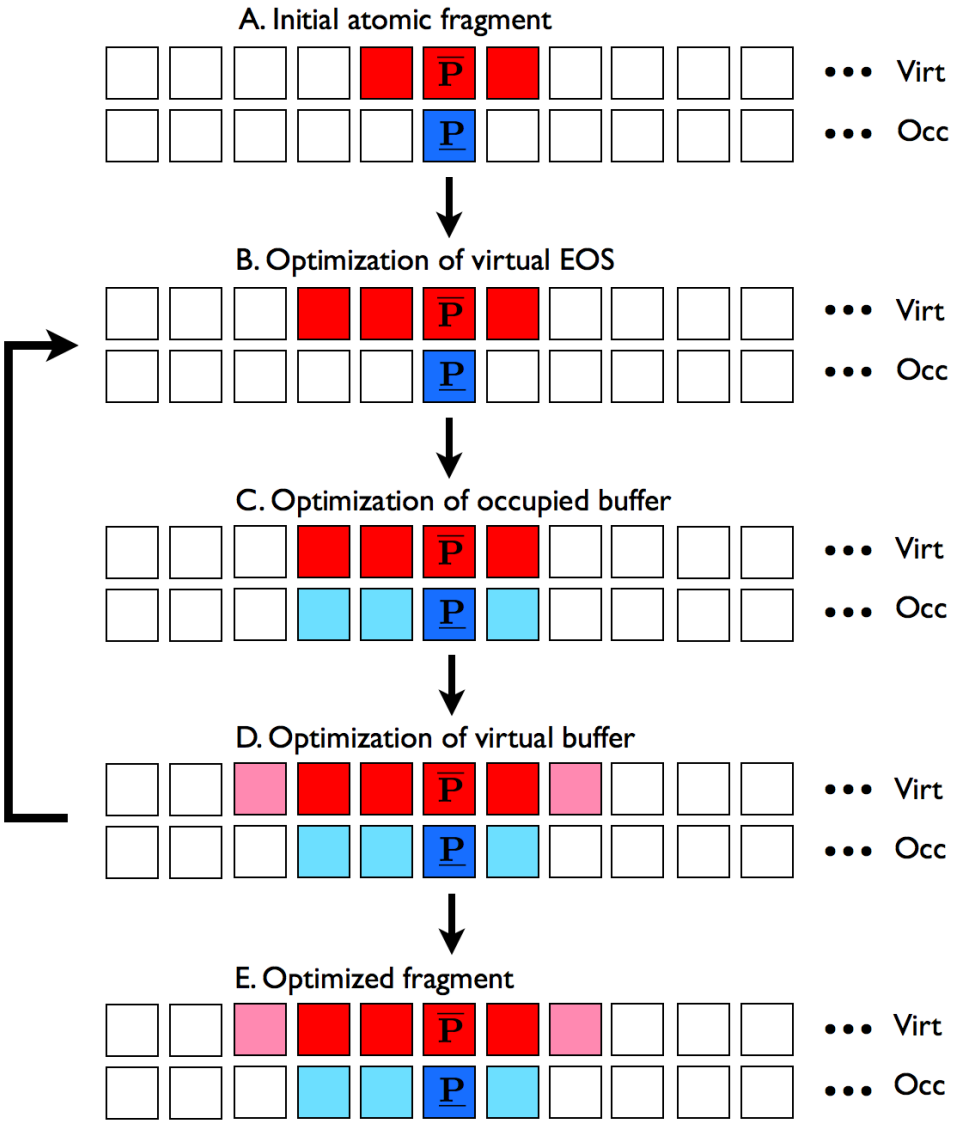

Figure 7.8: Main steps in the fragment optimization procedure for atomic fragment P. Initially a starting guess is made for the size of the orbital fragment space for evaluating $E_{\mathrm{P}}^{\mathrm{o}}$. The virtual energy orbital space (EOS) (dark-red) is then determined (B), followed by an optimization of the occupied (light-blue) and virtual (pink) buffer spaces (C and D). It is then checked that the spaces are still optimal going through the steps in B, C and D again until the sizes of all orbital spaces remain unchanged to yield the optimized fragment (E).

In Table 7.2 the total energy errors (fourth column) compared to full molecular MP2 (A) and CCSD (B) calculations for various FOTs are listed. In general, the errors decrease by an order of magnitude, when the FOT is lowered by an order of magnitude, even though some deviance from this general result is observed for CCSD (to be explained below).

Table 7.2: Energy errors [a.u.] compared to a full molecular calculation for single, pair, and total correlation energies as a function of the fragment optimization threshold (FOT).

(A) MP2

FOT	$\Delta(\sum_{\mathrm{P}} E^{\mathrm{o}}_{\mathrm{P}})$	$\Delta(\sum_{\mathrm{P>Q}} \Delta E^{\mathrm{o}}_{\mathrm{PQ}})$	ΔE_{corr}	% of E_{corr}
10^{-3}	0.013063	0.016875	0.029938	98.278
10^{-4}	0.001601	0.001775	0.003377	99.806
10^{-5}	0.000121	0.000139	0.000260	99.985
10^{-6}	0.000023	0.000014	0.000037	99.998

(B) CCSD

FOT	$\Delta(\sum_{\mathrm{P}} E^{\mathrm{o}}_{\mathrm{P}})$	$\Delta(\sum_{\mathrm{P>Q}} \Delta E^{\mathrm{o}}_{\mathrm{PQ}})$	ΔE_{corr}	% of E_{corr}
10^{-3}	-0.000811	0.000369	-0.000442	100.025
10^{-4}	-0.000255	0.000067	-0.000189	100.011
10^{-5}	-0.000059	0.000046	-0.000013	100.001
10^{-6}	-0.000021	0.000006	-0.000015	100.001

The second and third columns in Table 7.2 contain the sum of the single atomic fragment energy errors and the sum of the pair interaction energy errors, respectively, compared to a conventional calculation. Henceforth we denote $\sum_{\mathrm{P}} E^{\mathrm{o}}_{\mathrm{P}}$ as the total single energy and $\sum_{\mathrm{P>Q}} \Delta E_{\mathrm{PQ}}$ as the total pair interaction energy. For both MP2 and CCSD the errors in the total single energy and in total pair interaction energy decrease when tightening the FOT.

In general, the MP2 fragmentation errors are positive, i.e., the fragment energies calculated using the DEC scheme are larger than the fragment energies calculated in the full orbital space. Therefore, the total energy error ΔE_{corr} compared to a full molecular calculation decreases systematically when the FOT is lowered. In contrast, for CCSD the total single energy errors are negative, whereas the total pair interaction energy errors are positive for the molecule under consideration. This leads to cancellation of errors for CCSD, and consequently the total energy errors for CCSD are smaller than those for MP2. This cancellation of errors is also the reason why the error (accidentally) is smaller when the FOT is 10^{-5} than 10^{-6} for the CCSD case, even though the total single and total pair interaction energy errors both decrease when lowering the FOT. A closer look at the individual fragment energy errors reveals that these are always positive for MP2, whereas their signs vary for CCSD. This will in general lead to cancellation of errors for DEC-CCSD compared to DEC-MP2. Thus, in a sense, DEC-MP2 demonstrates the "worst case scenario", where all individual fragment errors are added, whereas DEC-CCSD in general give smaller errors due to cancellation effects. However, if the amplitudes are used

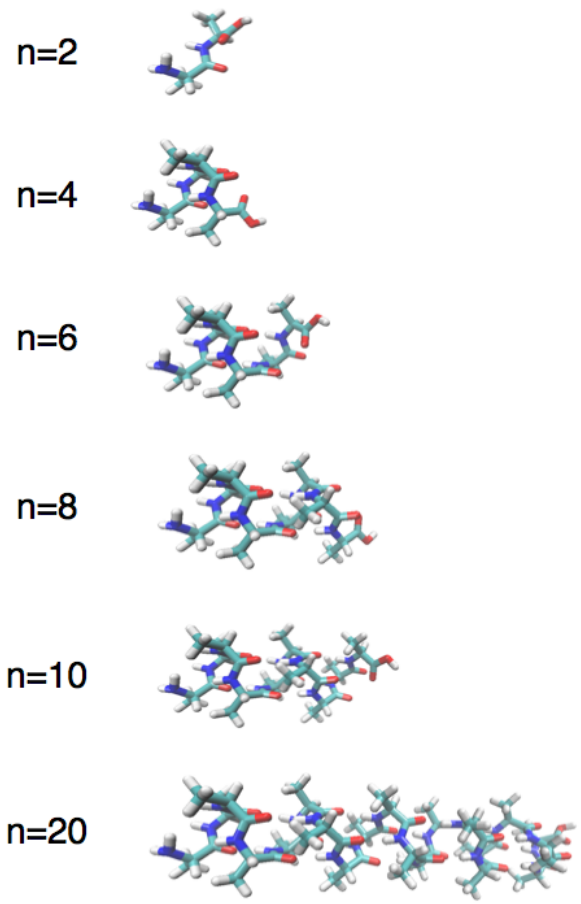

Figure 7.9: Alanine alpha-helix oligomers, where n is the number of alanine residues.

to evaluate for example molecular gradients, errors of similar size will be obtained for MP2 and CCSD as the cluster amplitudes are of similar quality.

In summary, it is a crucial feature of the DEC model that the full molecular correlation energy may be determined to any desired accuracy simply by tightening the FOT. For CCSD the error may be smaller than expected due to fortuitous cancellation of fragment energy errors. It should be noted that when the FOT is decreased to yield increasingly accurate energies, the fragment sizes increase to improve the description of the individual fragment amplitudes. Thus, an increased accuracy as defined by the FOT comes at the price that the individual fragment calculations become more expensive.

7.5.2 DEC-MP2 calculations on alanine oligomers

Having demonstrated that, for a given molecule, the error in the correlation energy in a DEC calculation may be controlled by the FOT, we now investigate how the fragment sizes and the correlation energy error are affected when the molecular size is systematically increased using a fixed FOT of 10^{-4}. The molecules under investigation are alpha-helix peptide oligomers containing 2, 4, 6, 8, 10, or 20 alanine residues – see Figure 7.9. The geometries were obtained using the Maestro program [79] without carrying out additional optimizations. The calculations

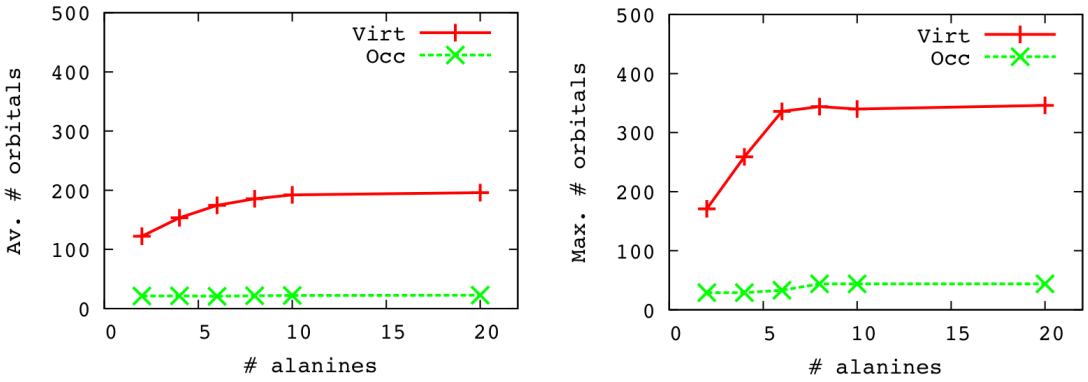

Figure 7.10: Average (left) and maximum (right) number of occupied (green-dashed) and virtual (red-solid) orbitals in the amplitude orbital space as a function of the number of alanine residues.

presented in this section[2] have been carried out using the MP2 model.

Sizes of orbital spaces

Figure 7.10 gives the average (left) and maximum (right) number of occupied and virtual orbitals in the AOS for the atomic fragments as a function of the molecular size. For the largest molecules the orbital fragment sizes are independent on the system size. This is crucial for the applicability of the DEC scheme to the calculation of correlation energies for large molecular systems – the individual fragment calculations are of similar cost, regardless of the total molecular size.

The behavior in Figure 7.10 can be understood by considering the locality of the HF orbitals which ultimately defines the sizes of the orbital fragments. The maximum orbital spread (MOS) for a set of orbitals is a measure of the locality of these orbitals (see Chapter 10). For all the considered alanine oligomers in Figure 7.9 the MOS is 2.34 a.u. The HF orbitals are thus equally local, and therefore the sizes of the orbital fragment spaces are independent of molecular size for the largest molecules in Figure 7.10. For the smallest molecules in Figure 7.10 many atoms are located near the edges of the molecule. Such edge atoms, in general, require only relatively small orbital fragment spaces. Consequently, the sizes of the orbital fragment spaces in Figure 7.10 increases with molecular system size for small molecules, while they saturate for the larger molecules where the relative number of edge atoms is small.

Energy errors

In Table 7.3 we present the errors in the correlation energy obtained in DEC-MP2 calculations compared to full molecular MP2 calculations. For alanine(6), alanine(8), and alanine(10) the absolute energy errors (third column) increases linearly with system size, while the percentage of E_{corr} that is recovered (fourth column) remains constant at approximately 99.88%. For the

[2]These calculations have been carried out solely to be presented in this thesis using an improved version of the DEC program compared to the one used in paper [7]. However, the conclusions derived from these calculations are the same as those presented in Section 7.2 of paper [7].

smallest alanine oligomers the energy errors are somewhat smaller since many fragments (in particular the pair fragments) include a very large fraction of the full molecular orbital space.

The fact that the absolute error increases with molecular size for larger molecules can be understood by recalling that the total correlation energy is calculated as a sum of atomic fragment and atomic pair fragment interaction energies, see Eq. (7.16). For MP2 calculations the fragment energy errors are all positive (see the discussion in Section 7.5.1). Therefore, the errors accumulate rather than cancel, and in effect the total energy error increases with system size.

In conclusion, the absolute MP2 energy errors are positive and size-extensive, whereas the relative energy errors are independent of the system size. Cluster amplitudes, and therefore also molecular properties (e.g., molecular gradients), can thus be determined with similar accuracy independently of the system size.

Table 7.3: Absolute (ΔE_{corr}) and relative (% of E_{corr}) energy errors of DEC-MP2/cc-pVDZ calculations on alanine oligomers of increasing size compared to full molecular calculations.

# alanines	E_{corr} (a.u.)	ΔE_{corr} (a.u.)	% of E_{corr}
2	-1.74291	0.00056	99.97
4	-3.29833	0.00220	99.93
6	-4.85900	0.00533	99.89
8	-6.41841	0.00744	99.88
10	-7.97682	0.00974	99.88
20	-15.72189	—	—

Pair interaction energies

As discussed in connection with Figure 7.5 (right), the pair interaction energies represent dispersion energies, which decay with the inverse pair distance to the sixth power. Figure 7.11 gives the pair interaction energies $\Delta E^{\mathrm{o}}_{\mathrm{PQ}}$ (absolute values) as a function of pair distance for the alanine(10) oligomer. Pairs separated by less than 2 Å have been omitted because there is no clear distinction between Coulomb hole effects (Figure 7.5, left) and dispersion effects (Figure 7.5, right) for short pair distances.

As expected the magnitude of the pair interaction energies $\Delta E^{\mathrm{o}}_{\mathrm{PQ}}$ decreases rapidly with pair distance due to the r_{PQ}^{-6} dependence of dispersion interactions. In fact, a power regression fit (red line in Figure 7.11) to the function $f(r_{\mathrm{PQ}}) = a r_{\mathrm{PQ}}^{-b}$ gives $b = 6.016$.

From a practical point of view the rapid decrease of pair interaction energies with pair distance implies that pairs separated by more than a certain distance (denoted the pair distance cutoff) may be omitted from the DEC calculation with a negligible effect on the total correlation energy. Thus, for a large molecule the number of pair interaction energies that needs to be calculated scales linearly with the size of the molecule. In practice, a pair distance cutoff of 10 Å

[3] We were not able to carry out a full molecular standard MP2 calculation for alanine(20). The total correlation energy listed for this molecule was calculated using the DEC scheme.

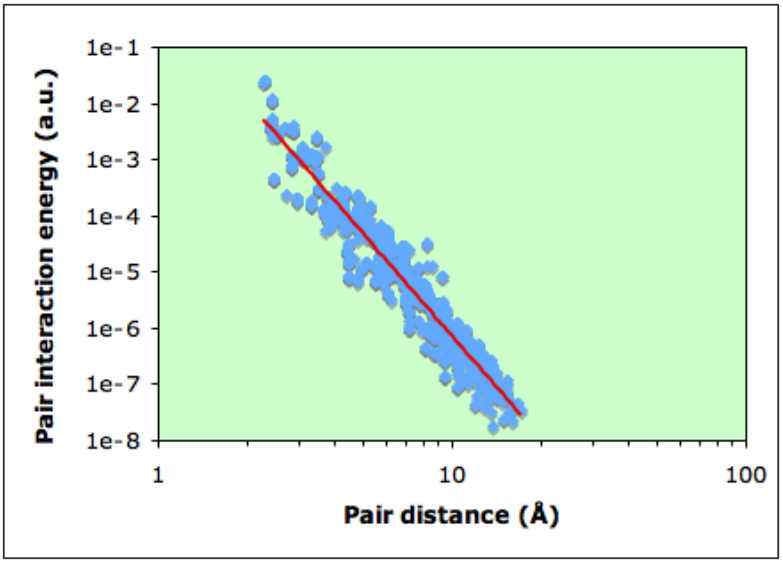

Figure 7.11: Pair interaction energies (absolute values) against pair distance for alanine(10).

is reasonable for a general non-metallic molecular system, whereas 15 Å is a more conservative value. We note that the small contributions from the omitted pair interaction energies can be estimated by extrapolation using a power regression fit (such as the red curve in Figure 7.11) for the calculated pair interaction energies.

7.6 Summary

The DEC CC method for determining the correlation energy is summarized in Figure 7.6. The most important features of the DEC scheme are the following:

- The DEC scheme is *linearly scaling*, because the fragment sizes are roughly independent of system size, and since distant pairs can be neglected.
- The DEC scheme is also *embarrassingly parallelizable*, because the fragment calculations are independent.
- The DEC scheme ensures *error control* in the sense that the error in the correlation energy compared to a standard calculation is defined by the FOT before the calculation is carried out. During the calculation the orbital fragment sizes are determined in a *black box* manner to ensure that the *predefined accuracy* is achieved.
- For the MP2 model the errors in the correlation energy are size extensive, whereas the *relative error is system independent.*

Chapter 8

The DEC method II: Different orbital partitionings and amplitude errors

This chapter describes the work presented in **paper [8]**.

8.1 Introduction

In Chapter 7 the foundation for the DEC CC method was established. In this chapter the DEC scheme is investigated in more detail.

In Section 8.2 a *virtual partitioning* of the correlation energy is introduced, analogous with the occupied partitioning in Section 7.3. In Section 8.3 we perform an error analysis of the CC amplitudes used in a DEC calculation, and in Section 8.4 the DEC model is compared to some existing local CC methods.

8.2 Different partitionings of the correlation energy

8.2.1 Full molecular system

For simplicity we restrict ourselves to the MP2 model in this chapter, and the singles amplitudes are therefore omitted. Note, however, that the following discussion is also valid for the CCSD model where singles are included.

By omitting singles amplitudes the DEC partitioning of the correlation energy in Eqs. (7.14)-(7.16) becomes,

$$E^{\mathrm{o}}_{\mathrm{P}} = \sum_{\substack{ij\in\underline{P}\\ab}} t^{ab}_{ij} L_{iajb} \tag{8.1}$$

$$\Delta E^{\mathrm{o}}_{\mathrm{PQ}} = \sum_{\substack{i\in\underline{P}\\j\in\underline{Q}}} \sum_{ab} t^{ab}_{ij} L_{iajb} + \sum_{\substack{i\in\underline{Q}\\j\in\underline{P}}} \sum_{ab} t^{ab}_{ij} L_{iajb} \tag{8.2}$$

$$E_{\mathrm{corr}} = \sum_{\mathrm{P}} E^{\mathrm{o}}_{\mathrm{P}} + \sum_{P>Q} \Delta E^{\mathrm{o}}_{\mathrm{PQ}} \tag{8.3}$$

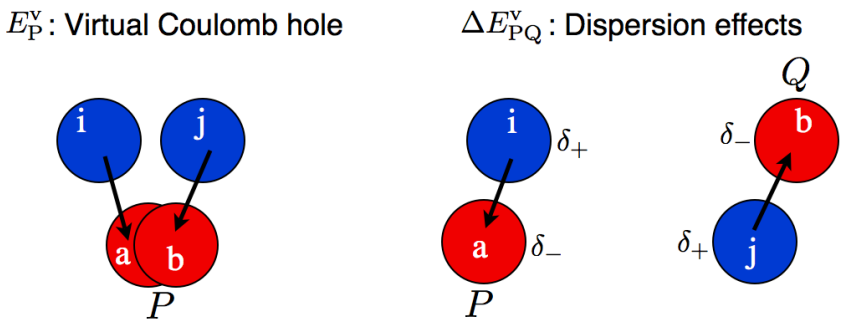

Figure 8.1: Illustrations of excitations from occupied orbitals ϕ_i and ϕ_j (blue) into virtual orbitals ϕ_a and ϕ_b (red). Left: Short-range electron-electron repulsion described by the atomic fragment energies $E_{\mathrm{P}}^{\mathrm{v}}$ (virtual Coulomb hole). Right: Dispersion effects described by virtual pair interaction energies $\Delta E_{\mathrm{PQ}}^{\mathrm{v}}$.

In the atomic fragment energy $E_{\mathrm{P}}^{\mathrm{o}}$ in Eq. (8.1) both occupied indices are assigned to the atomic site P, while the occupied indices in $\Delta E_{\mathrm{PQ}}^{\mathrm{o}}$ in Eq. (8.2) are assigned to the atomic sites P and Q. Equivalently, the partitioning of the correlation energy may be based on the virtual indices. Specifically, by defining virtual atomic fragment and pair interaction energies as

$$E_{\mathrm{P}}^{\mathrm{v}} = \sum_{\substack{ab\in\overline{P}\\ij}} t_{ij}^{ab} L_{iajb} \tag{8.4}$$

$$\Delta E_{\mathrm{PQ}}^{\mathrm{v}} = \sum_{\substack{a\in\overline{P}\\b\in\overline{Q}}} \sum_{ij} t_{ij}^{ab} L_{iajb} + \sum_{\substack{a\in\overline{Q}\\b\in\overline{P}}} \sum_{ij} t_{ij}^{ab} L_{iajb} \tag{8.5}$$

the correlation energy in Eq. (7.10) may be written as

$$E_{\mathrm{corr}} = \sum_{\mathrm{P}} E_{\mathrm{P}}^{\mathrm{v}} + \sum_{P>Q} \Delta E_{\mathrm{PQ}}^{\mathrm{v}} \tag{8.6}$$

For a calculation on the full molecular system the correlation energy expressions in Eq. (8.3) and (8.6) yield the same result, whereas the individual fragment energies differ – for example, $E_{\mathrm{P}}^{\mathrm{o}} \neq E_{\mathrm{P}}^{\mathrm{v}}$ and $\Delta E_{\mathrm{PQ}}^{\mathrm{o}} \neq \Delta E_{\mathrm{PQ}}^{\mathrm{v}}$. Thus, the occupied partitioning in Eqs. (8.1)-(8.3) and the virtual partitioning in Eqs. (8.4)-(8.6) constitute two equivalent – but independent – approaches to calculating the correlation energy, as will be discussed in more detail in Section 8.2.2.

Let us comment on the physical interpretation of the different orbital partitionings assuming local HF orbitals. In connection with Figure 7.5 (left) it was argued that the occupied atomic fragment energy $E_{\mathrm{P}}^{\mathrm{o}}$ describes a coulomb hole in the wave function in terms of excitations from occupied orbitals ϕ_i and ϕ_j centered on atomic site P to the virtual excitation space, while the occupied pair interaction energy $\Delta E_{\mathrm{PQ}}^{\mathrm{o}}$ describes dispersion effects as depicted in Figure 7.5 (right). Similar qualitative interpretations can be made for the fragment energies entering the virtual partitioning scheme. $E_{\mathrm{P}}^{\mathrm{v}}$ describes excitations from the occupied orbital space to virtual orbitals ϕ_a and ϕ_b centered on atom P, which, in a sense, is a virtual Coulomb hole, see Figure 8.1 (left). The virtual pair interaction energy $\Delta E_{\mathrm{PQ}}^{\mathrm{v}}$ describes dispersion effects in terms of excitations from the occupied orbital space to orbitals ϕ_a and ϕ_b centered on atomic sites P and Q, respectively, see Figure 8.1 (right).

To highlight the equivalence between the occupied and virtual partitioning schemes – and at at the same time illustrate the importance of using local orbitals – Figure 8.2 gives a numerical example where pair interaction energies are plotted against pair distance, while atomic fragment energies are plotted at zero distance. Orbitals of different locality have been used for both the occupied (left) and virtual (right) partitioning schemes. Dispersion effects decay with the inverse pair distance to the sixth power r^{-6}. For an efficient description of these effects it is thus important that the pair interaction energies display this behavior. Clearly, the r^{-6} decay of dispersion effects cannot be effectively exploited when delocalized canonical orbitals (top) are used; no distance dependence is observed in this case. For the semi-local orbitals (middle) the r^{-6} decay is starting to become apparent, while the pair interaction energies for the most local orbitals[1] (bottom) display a clear r^{-6} dependence. Thus, the use of local orbitals is crucial for an efficient description of the dispersion interactions. The pair interaction energy plots for the occupied and virtual orbitals are very similar, demonstrating that (i) they both describe the same physical effect (dispersion), and (ii) the occupied and virtual orbitals have similar locality. We also note that the distribution of atomic fragment energies becomes more homogeneous for the local orbitals.

8.2.2 Orbital fragments for occupied and virtual partitioning schemes

It is well-known that the total correlation energy E_{corr} is invariant with respect to a unitary transformation among the occupied orbitals and among the virtual orbitals. Similar conditions hold for the fragment energies. In particular, the occupied fragment energies E_{P}^{o} and $\Delta E_{\text{PQ}}^{\text{o}}$ in Eqs. (8.1) and (8.2) are invariant to orbital rotations among the virtual orbitals [8], while the virtual fragment energies E_{P}^{v} and $\Delta E_{\text{PQ}}^{\text{v}}$ in Eqs. (8.4) and (8.5) are invariant with respect to orbitals rotations among the occupied orbitals. This is a conceptually important result stating that the orbital invariance of the total correlation energy is somewhat preserved for the fragment energies. From a practical point of view the most efficient evaluation of the fragment energies are obtained when both occupied and virtual orbitals are local as discussed in Section 7.3. Specifically, using local orbitals the virtual space summations in Eqs. (8.1) and (8.2) may be restricted as in Eqs. (7.18) and (7.19),

$$E_{\text{P}}^{\text{o}} = \sum_{\substack{ij\in\underline{P} \\ ab\in[\overline{P}]}} t_{ij}^{ab} L_{iajb} \tag{8.7}$$

$$\Delta E_{\text{PQ}}^{\text{o}} = \Big(\sum_{\substack{i\in\underline{P} \\ j\in\underline{Q}}} + \sum_{\substack{i\in\underline{Q} \\ j\in\underline{P}}} \Big) \sum_{ab\in[\overline{P}]\cup[\overline{Q}]} t_{ij}^{ab} L_{iajb} \tag{8.8}$$

Since the occupied and virtual orbitals are equally local (see Chapter 10), we may in a similar fashion approximate the occupied summations in the virtual atomic fragment energies and pair

[1] These orbitals were localized using the localization strategy described in Chapter 10.

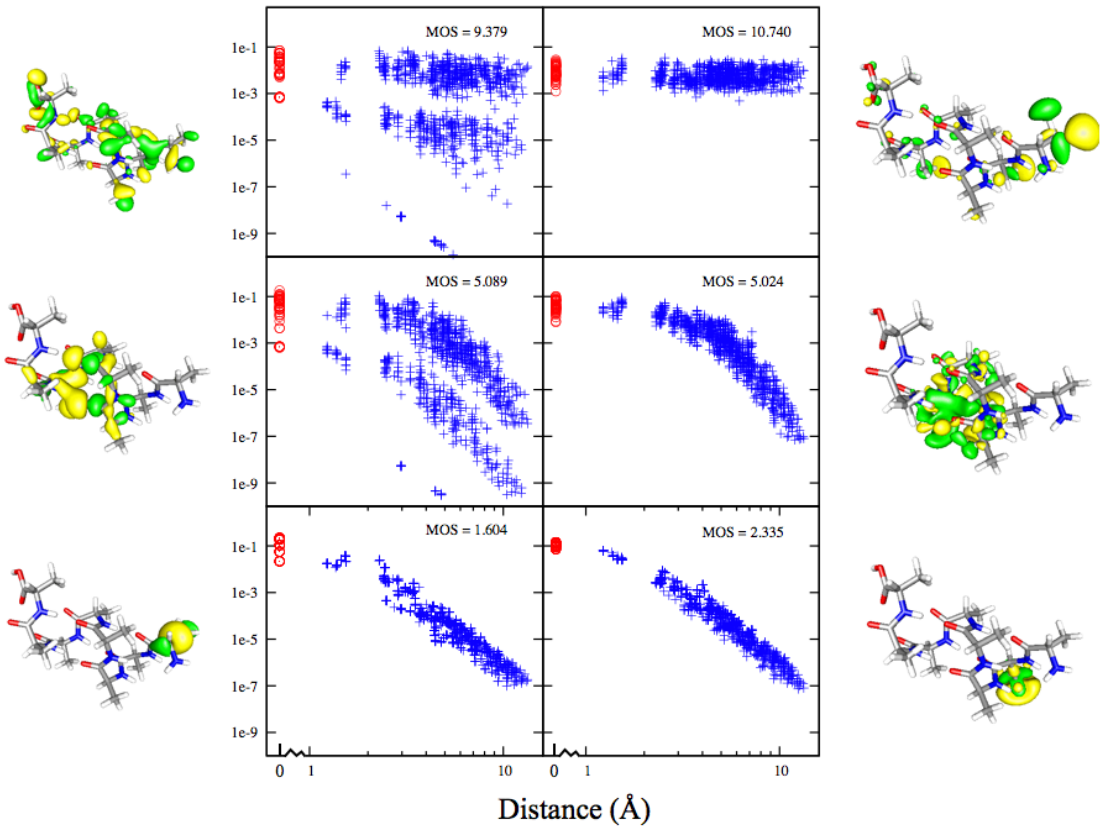

Figure 8.2: Pair interaction energies (blue crosses) against pair distance and atomic fragment energies (red circles at zero distance) for an alanine(8) alpha-helix at the full molecular MP2/cc-pVDZ level of theory. Calculations using occupied (left) and virtual (right) orbital partitionings are shown for delocalized canonical orbitals (top), semi-local orbitals (middle), and localized orbitals (bottom). Also shown are the least local occupied orbital (left), the least local virtual orbital (right), and the corresponding maximum orbital spreads (MOS), which is a measure of orbital locality (see Chapter 10).

interaction energies in Eqs. (8.4) and (8.5),

$$E_{\mathrm{P}}^{\mathrm{v}} = \sum_{\substack{ab\in\overline{P}\\ij\in[\underline{P}]}} t_{ij}^{ab} L_{iajb} \tag{8.9}$$

$$\Delta E_{\mathrm{PQ}}^{\mathrm{v}} = \Big(\sum_{\substack{a\in\overline{P}\\b\in\overline{Q}}} + \sum_{\substack{a\in\overline{Q}\\b\in\overline{P}}}\Big) \sum_{ij\in[\underline{P}]\cup[\underline{Q}]} t_{ij}^{ab} L_{iajb} \tag{8.10}$$

where $[\underline{P}]$ is the set of occupied orbitals spatially close to atomic site P (including $\underline{P}$).

The orbital fragment spaces needed to determine the fragment energies using the virtual partitioning scheme may be determined in exactly the same manner as was done for the occupied partitioning scheme in connection with Figure 7.8 – with the roles of the occupied and virtual orbital spaces reversed. For comparison, an occupied and a virtual atomic fragment are displayed in Figure 8.3.

To demonstrate the equivalence of the occupied and virtual partitionings we have in Table 8.1 given the error in the DEC-MP2 correlation energy compared to a full molecular MP2/cc-pVDZ calculation as a function of the FOT for both partitionings. The test system is the arachidic acid molecule (saturated fatty acid of composition $C_{20}H_{40}O_2$) with a geometry obtained using the Maestro program [79]. Since the fragments have been individually optimized to the given FOTs, the energy errors are proportional to the FOT and of similar size for both partitionings.

Let us summarize some important features for the occupied and virtual orbital partitionings:

- The sizes of the orbital spaces are optimized independently for the occupied and virtual partitioning schemes to ensure that the fragment energies $E_{\mathrm{P}}^{\mathrm{o}}$ and $E_{\mathrm{P}}^{\mathrm{v}}$ are determined to a given accuracy defined by the FOT.

- The correlation energy can be calculated using either the occupied or the virtual partitioning scheme. Thus, for large molecular systems –where it is not possible to carry out a full molecular reference CC calculation – these two independent schemes provides an internal consistency check for the calculated correlation energy.

- The use of both occupied and virtual partitionings turns out to be essential for determining the DEC-MP2 molecular gradient, as will be described in Section 9.

Table 8.1: Energy errors ΔE_{corr} (a.u.) compared to full molecular calculation for occupied and virtual partitionings using different fragment optimization thresholds (FOTs). The calculations were carried out on arachidic acid at the MP2/cc-pVDZ level of theory.

FOT	ΔE_{corr} (occ.)	ΔE_{corr} (virt.)
10^{-3}	0.028254	0.027579
10^{-4}	0.003201	0.001865
10^{-5}	0.000269	0.000261
10^{-6}	0.000033	0.000011

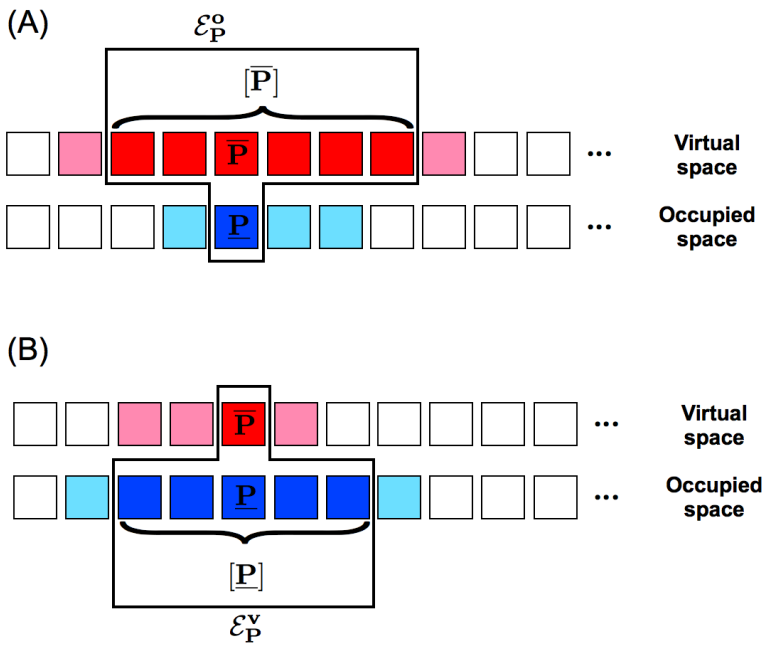

Figure 8.3: Illustration of a single atomic fragment for atomic site P using occupied (A) and virtual (B) partitionings of the orbital space. Each square represents the set of occupied or virtual orbitals assigned to a particular atom. For each partitioning scheme the atomic fragment energy is evaluated using the energy orbital space (EOS) (dark-red and dark-blue), whereas the CC amplitude equations are solved in the amplitude orbital space (AOS) (dark-red, dark-blue, pink, and light-blue).

8.3 Error analysis of DEC amplitudes

We now examine the errors that occur in the DEC fragment calculations, where the fragment energies are determined to an accuracy defined by the FOT. For simplicity only an atomic fragment energy using the occupied partitioning is considered. A similar analysis can be performed for pair fragments as well as for fragments entering the virtual partitioning scheme.

The atomic fragment energy is determined to a given FOT, i.e.,

$$E^{\mathrm{o}}_{\mathrm{P,full}} = E^{\mathrm{o}}_{\mathrm{P,dec}} + \delta^{\mathrm{o}}_{\mathrm{P}}, \qquad \delta^{\mathrm{o}}_{\mathrm{P}} \propto \mathrm{FOT} \tag{8.11}$$

where $E^{\mathrm{o}}_{\mathrm{P,full}}$ is determined from a full CC calculation, as in Eq. (8.1), and the approximate DEC energy $E^{\mathrm{o}}_{\mathrm{P,dec}}$ is determined using Eq. (8.7). The amplitudes of a full molecular calculation $t^{ab}_{ij,\mathrm{full}}$ may in the DEC EOS space be expressed as:

$$t^{ab}_{ij,\mathrm{full}} = t^{ab}_{ij,\mathrm{dec}} + \delta t^{ab}_{ij}; \qquad (ij \in \underline{P}, ab \in [\overline{P}]) \tag{8.12}$$

where $t^{ab}_{ij,\mathrm{dec}}$ is an amplitude from the DEC calculation [Figure 8.3(A)] and δt^{ab}_{ij} is a correction term. Inserting Eq. (8.12) into Eq. (8.1) and using Eq. (8.7), we may divide the energy errors into two different types:

$$\delta^{\mathrm{o}}_{\mathrm{P}} = \delta^{\mathrm{o}}_{\mathrm{1P}} + \delta^{\mathrm{o}}_{\mathrm{2P}} \tag{8.13}$$

where

$$\delta^{\mathrm{o}}_{1\mathrm{P}} = \sum_{\substack{i,j\in \mathrm{P} \\ a,b\in[\overline{P}]}} \delta t^{ab}_{ij}(2g_{iajb} - g_{ibja}) \tag{8.14}$$

and

$$\delta^{\mathrm{o}}_{2\mathrm{P}} = \sum_{ij\in \mathrm{P}} \sum_{ab\setminus a\wedge b\in[\overline{P}]} t^{ab}_{ij,\mathrm{full}}(2g_{iajb} - g_{ibja}) \tag{8.15}$$

The $\delta^{\mathrm{o}}_{1\mathrm{P}}$ errors arise because the amplitudes $t^{ab}_{ij,\mathrm{dec}}$ of the EOS have been determined in a restricted orbital space [Figure 8.3(A)]. The EOS amplitudes thus interact with each other and with the amplitudes of the buffer space, but the weak interactions with amplitudes outside this buffer space have been neglected. The errors in the EOS amplitudes δt^{ab}_{ij} resulting from neglecting this weak interaction are proportional to $\delta^{\mathrm{o}}_{1\mathrm{P}}$.

The $\delta^{\mathrm{o}}_{2\mathrm{P}}$ errors arise because amplitudes referencing virtual orbitals outside the $[\overline{P}]$ space are neglected. To gain more insight into the δ_2 errors we note that, for a set of local orbitals, the Fock matrix is diagonally dominant and, for analysis purposes, the $t^{ab}_{ij,\mathrm{full}}$ amplitudes determined from Eq. (7.13) may therefore be approximated with their diagonal component

$$t^{ab}_{ij,\mathrm{full}} \approx -(\Delta F^{ab}_{ij})^{-1} g_{iajb} \tag{8.16}$$

where we have used that $g_{iajb} = g_{aibj}$ since we assume real orbitals, and where ΔF^{ab}_{ij} is given by

$$\Delta F^{ab}_{ij} = F_{aa} + F_{bb} - F_{ii} - F_{jj} \tag{8.17}$$

Applying Eq (8.16) in Eq. (8.15) gives

$$\delta^{\mathrm{o}}_{2\mathrm{P}} = -\sum_{ij\in \mathrm{P}} \sum_{ab\setminus a\wedge b\in[\overline{P}]} t^{ab}_{ij,\mathrm{full}}(2t^{ab}_{ij,\mathrm{full}} - t^{ba}_{ij,\mathrm{full}})\Delta F^{ab}_{ij} \tag{8.18}$$

Roughly speaking, the δ_2 errors are thus proportional to the square of the amplitudes which are neglected in the DEC calculation.

In an actual calculation one will in general observe a mixture of these two error types. However, it is instructive to consider the two limiting cases, where either $\delta^{\mathrm{o}}_{1\mathrm{P}}$ or $\delta^{\mathrm{o}}_{2\mathrm{P}}$ is the dominant contribution to the total energy error $\delta^{\mathrm{o}}_{\mathrm{P}}$:

1. $\delta^{\mathrm{o}}_{1\mathrm{P}} \gg \delta^{\mathrm{o}}_{2\mathrm{P}}$: In this case the errors in the amplitudes δt^{ab}_{ij} are linear in the energy error $\delta^{\mathrm{o}}_{\mathrm{P}} \approx \delta^{\mathrm{o}}_{1\mathrm{P}}$, which is proportional to the FOT, i.e.,

$$\delta t^{ab}_{ij} \propto \mathrm{FOT} \qquad (ij \in \underline{P}, ab \in [\overline{P}]) \tag{8.19}$$

2. $\delta^{\mathrm{o}}_{2\mathrm{P}} \gg \delta^{\mathrm{o}}_{1\mathrm{P}}$: The error in the energy $\delta^{\mathrm{o}}_{\mathrm{P}} \approx \delta^{\mathrm{o}}_{2\mathrm{P}}$ (which is still proportional to the FOT) depends quadratically on the amplitudes outside the EOS $[\overline{P}]$. Roughly speaking, the amplitudes outside the EOS are therefore proportional to the square root of the FOT:

$$t^{ab}_{ij,\mathrm{full}} \propto \mathrm{FOT}^{1/2} \qquad (ij \in \underline{P}, ab \setminus a \wedge b \in [\overline{P}]) \tag{8.20}$$

Let us conclude this section by presenting some calculated amplitude errors for MP2/cc-pVDZ calculations on the arachidic acid molecule (same calculations as in Table 8.1) for atomic fragment calculations using the occupied partitioning scheme. (Similar results are obtained for pair fragments and for fragments entering the virtual partitioning scheme). We let Δ_{ij}^{ab} denote the difference between the (i,j,a,b)th component of the DEC amplitudes $t_{ij,\mathrm{dec}}^{ab}$ and the full molecular amplitudes $t_{ij,\mathrm{dec}}^{ab}$:

$$\Delta_{ij}^{ab} = t_{ij,\mathrm{dec}}^{ab} - t_{ij,\mathrm{full}}^{ab} \tag{8.21}$$

For a given atomic fragment the *mean error* $\bar{\Delta}$, the *standard deviation* Δ_{std}, the *mean absolute error* $\bar{\Delta}_{\mathrm{abs}}$, and the *maximum absolute error* Δ_{max} are given by:

$$\bar{\Delta} = \frac{1}{N_{\mathrm{amp}}} \sum_{ijab} \Delta_{ij}^{ab} \tag{8.22a}$$

$$\Delta_{\mathrm{std}} = \left(\frac{\sum_{ijab} (\Delta_{ij}^{ab} - \bar{\Delta})^2}{N_{\mathrm{amp}} - 1} \right)^{1/2} \tag{8.22b}$$

$$\bar{\Delta}_{\mathrm{abs}} = \frac{1}{N_{\mathrm{amp}}} \sum_{ijab} |\Delta_{ij}^{ab}| \tag{8.22c}$$

$$\Delta_{\mathrm{max}} = \max_{ijab} |\Delta_{ij}^{ab}| \tag{8.22d}$$

When considering amplitude errors of type 1 for an atomic fragment P, the summation indices $ijab$ in Eq. (8.22) run over the orbitals inside the EOS ($ij \in \underline{P}$ and $ab \in [\overline{P}]$), and N_{amp} is the number of EOS amplitudes. For errors of type 2, the virtual indices run over orbitals outside the EOS ($ij \in \underline{P}$, while ϕ_a, ϕ_b, or both are assigned to atoms outside the EOS), and N_{amp} is the number of such amplitudes. For errors of type 2 we have $t_{ij,\mathrm{dec}}^{ab} = 0$, since, by definition, no CC amplitudes outside the EOS are used to when calculating the atomic fragment energy $E_{\mathrm{P}}^{\mathrm{o}}$.

In Table 8.2 the average values of the error measures in Eq. (8.22) for all atomic fragments are given. When the FOT is lowered all error measures decrease because the amplitudes inside the EOS become increasingly accurate (error type 1), and because fewer (small) amplitudes outside the EOS are neglected (error type 2). The errors of type 1 and 2 are of similar magnitude, and as a consequence we do not observe any of the limiting cases listed above.

In conclusion, the important message from Table 8.2 is that the amplitudes (and not just the correlation energy itself) become increasingly accurate when the FOT in decreased. Therefore, molecular properties calculated using these amplitudes will also become increasingly accurate when tightening the FOT.

8.4 Comparing DEC to existing local coupled-cluster methods

Having discussed the DEC model in this and the previous chapter, let us now compare the DEC model to existing local CC methods.

The local correlation wave function method development was pioneered by Pulay [138] and Saebø and Pulay [139], and the local coupled-cluster method of Hampel and Werner [140] and

Table 8.2: Amplitude errors for atomic fragments using the occupied partitioning scheme. Standard deviation Δ_{std}, mean absolute error $\bar{\Delta}_{\mathrm{abs}}$, and maximum absolute errors Δ_{max} (all in a.u.) for amplitudes referencing atomic fragments inside and outside the EOS.

1. Inside EOS

FOT	Δ_{std}	$\bar{\Delta}_{\mathrm{abs}}$	Δ_{max}
10^{-3}	$1.1 \cdot 10^{-5}$	$4.3 \cdot 10^{-6}$	$4.2 \cdot 10^{-4}$
10^{-4}	$1.4 \cdot 10^{-6}$	$5.6 \cdot 10^{-7}$	$5.2 \cdot 10^{-5}$
10^{-5}	$2.6 \cdot 10^{-7}$	$7.6 \cdot 10^{-8}$	$1.5 \cdot 10^{-5}$
10^{-6}	$6.2 \cdot 10^{-8}$	$1.3 \cdot 10^{-8}$	$5.6 \cdot 10^{-6}$

2. Outside EOS

FOT	Δ_{std}	$\bar{\Delta}_{\mathrm{abs}}$	Δ_{max}
10^{-3}	$5.9 \cdot 10^{-6}$	$6.2 \cdot 10^{-7}$	$9.0 \cdot 10^{-4}$
10^{-4}	$1.9 \cdot 10^{-6}$	$2.3 \cdot 10^{-7}$	$2.0 \cdot 10^{-4}$
10^{-5}	$4.7 \cdot 10^{-7}$	$6.1 \cdot 10^{-8}$	$5.2 \cdot 10^{-5}$
10^{-6}	$1.2 \cdot 10^{-7}$	$1.7 \cdot 10^{-8}$	$1.1 \cdot 10^{-5}$

Schütz and Werner [141–144] constitutes a prominent early contribution. Many other local coupled-cluster methods have been proposed, including atomic orbital-based CC [145–147], the natural linear scaling approach [148], the cluster-in-molecule approach [149–151], the divide-and-conquer approach [152], the fragment molecular orbital approach [153], the incremental scheme [154, 155], and Laplace-MP2 [156–161].

For local CC methods the standard CC correlation energy is, in general, an asymptotic limit, which is obtained when all local thresholds are removed. In practice, *ad hoc* approximations to the standard CC method are introduced in the local CC methods. The approximations include *a priori* assignments of local orbital spaces, and, for some models, bond cuts of the molecular system. At the end of a local CC calculation that relies on *ad hoc* approximations, the precision of the calculation compared to a full CC calculation is in general not known.

One may argue that compared to the large errors in CC calculations due to the basis set incompleteness and the approximate CC wave function model, the approximations that are introduced in local CC methods are acceptable. However, in chemistry one is typically interested in the energy differences of molecular conformers – for example reaction enthalpies and interaction energies of van der Waals complexes – which are small compared to total energies. To obtain a reliable and accurate description of these small differences, it is important to know the errors introduced by the local approximations compared to conventional calculations. We note that in some cases the "errors" introduced by the local approximations can be advantageous. For example, the approximations in the local CC method of Werner and coworkers may eliminate

basis set superposition errors (BSSEs) [162].

The most important feature of the DEC method compared to existing local CC methods is the control of the error in the correlation energy compared to a conventional calculation. This control is achieved by expanding the local orbital fragment spaces in a black box manner during the calculation, rather than determining these spaces according to some preset thresholds. An additional source of error control in the DEC method – which is not present in other local CC methods – is the internal consistency check of the final correlation energy obtained by invoking the occupied and virtual partitioning schemes discussed in Section 8.2. Furthermore, the DEC method employs (nonredundant) local virtual orbitals, rather than (redundant) projected atomic orbitals (PAOs), which are usually used in existing local CC methods. The biggest problem with the current version of the DEC program is that the individual orbital fragments can become quite large if a high accuracy (low FOT) is requested. At the same there are fairly many fragments to be handled for a large molecule[2] even though the number of fragments scales only linearly with system size. Possible improvements to reduce the computational cost are discussed in connection with future perspectives for the DEC method in Section 11.2.

Finally, let us describe other local CC methods in more detail and compare to the DEC scheme. We shall limit ourselves to some of the methods which, as the DEC scheme, use a full HF reference state.

- **Local coupled-cluster method**

  In the local coupled-cluster (LCC) method of Werner and coworkers [140–144] a set of local occupied orbitals $|\phi_i\rangle$,

  $$|\phi_i\rangle = \sum_{\mu} |\chi_\mu\rangle C_{\mu i} \tag{8.23}$$

  is used to span the occupied orbital space, while PAOs $|\tilde{\chi}\rangle$ are used to span the virtual orbital space

  $$|\tilde{\chi}_\mu\rangle = \Big(1 - \sum_i |\phi_i\rangle\langle\phi_i|\Big)|\chi_\mu\rangle \tag{8.24}$$

  To each localized orbital $|\phi_i\rangle$ a local orbital domain of PAOs $[i]$ is selected, typically using the completeness criterion of Boughton and Pulay [163]. Electron pairs ij are assigned the union of orbital domains $[ij]$ for orbitals $|\phi_i\rangle$ and $|\phi_j\rangle$. Using these approximations the CC singles and doubles operators in Eqs. (7.3) and (7.4) are written as

  $$T_1 = \sum_i \sum_{\mu\in[i]} t_i^\mu E_{\mu i} \tag{8.25}$$

  $$T_2 = \frac{1}{2} \sum_{ij} \sum_{\mu\nu\in[ij]} t_{ij}^{\mu\nu} E_{\mu i} E_{\nu j} \tag{8.26}$$

  where the PAO summation indices $\mu\nu$ are restricted to the local domains. In the LCC method the CC amplitude equations are thus solved for the full molecular system, such

[2] We only have a relatively limited number of processors available at the supercomputer facilities in Aarhus, and therefore we cannot fully exploit the fact that the fragment calculations are embarrassingly parallelizable.

that only amplitudes inside the predefined orbital domains are nonzero. In contrast, the DEC method consists of a series of independent fragment calculations, where the CC amplitude equations are solved in a restricted orbital space for each fragment. Further approximations can be introduced in the LCC method, such as approximate treatments of weak and distant pairs, leading to linear scaling with system size [144].

- **Cluster-in-a-molecule**

  The cluster-in-a-molecule (CIM) method introduced by Li *et al.* [149] employs a similar partitioning of the correlation energy as the DEC method, but the summations run over the individual orbitals, rather than over atomic sites:

$$E_{\text{corr}} = \sum_{I} \Delta E_{[I]} + \sum_{I \neq J} \Delta E_{[IJ]} \tag{8.27}$$

  where

$$\Delta E_{[I]} = \sum_{ab \in \{I\}} t_{ii}^{ab} L_{iajb} \tag{8.28}$$

$$\Delta E_{[IJ]} = \sum_{ab \in \{IJ\}} t_{ij}^{ab} L_{iajb} \tag{8.29}$$

  The orbital domain $[I]$ is a "cluster" containing the occupied orbital ϕ_i, a set of neighbouring virtual orbitals or PAOs $\{I\}$, and some local environment orbitals (similar to the buffer spaces in the DEC scheme). The pair cluster $[IJ]$ is constructed from the union of orbital domains for clusters $[I]$ and $[J]$. Computational savings in the CIM method have been made by neglecting all amplitudes t_{ij}^{ab} where the value of a screening function $\Omega(i,j)$ is below some predefined threshold [149]:

$$\Omega(i,j) = \left(\sum_{\mu\nu} C_{\mu i}^2 S_{\mu\nu}^2 C_{\nu j}^2 \right)^{1/2} \tag{8.30}$$

  Many pair interactions (ϕ_i, ϕ_j) presenting dispersion effects will be neglected based on this criteria. Recently, an alternative energy partitioning scheme (less reminiscent of the DEC scheme) and modified selection criteria for the orbital fragment spaces (e.g., by correlating two MOs ϕ_i and ϕ_j if the absolute value of the corresponding Fock matrix element F_{ij} is above a preset threshold ζ) have been proposed for the CIM method [150, 151].

- **The incremental scheme**

  In the incremental scheme of Stoll [154] the energy E of a system in partitioned as

$$E = \sum_{I} \Delta\epsilon_I + \frac{1}{2!} \sum_{IJ} \Delta\epsilon_{IJ} + \frac{1}{3!} \sum_{IJK} \Delta\epsilon_{IJK} + \dots \tag{8.31}$$

$$\Delta\epsilon_I = \epsilon_I; \qquad \Delta\epsilon_{IJ} = \epsilon_{IJ} - \Delta\epsilon_I - \Delta\epsilon_J; \qquad \dots \tag{8.32}$$

  where ϵ_I is the energy of a subsystem I, ϵ_{IJ} is the energy of subsystems I and J together, etc. By using local occupied orbitals and defining local excitation spaces in terms of

PAOs (similar to the LCC method), Friedrich and coworkers [155] applied the incremental scheme to obtain the CC correlation energy. Eq. (8.31) is typically truncated after third or fourth order. As demonstrated in the CIM and DEC methods the correlation energy can be expressed in terms of only single and pair "subsystems". In a sense, triple- and higher-order subsystems are included in the incremental scheme to compensate for the fact that the virtual excitation spaces employed in the single and pair calculations are too small. Thus, the incremental scheme typically uses many more subsystems than the DEC method, but these subsystems are smaller.

- **Laplace-MP2**

  In the canonical basis the MP2 correlation energy is given by,

$$E_{\text{corr}} = -\sum_{ijab} \frac{g_{iajb}(2g_{iajb} - g_{ibja})}{\varepsilon_a + \varepsilon_b - \varepsilon_i - \varepsilon_j} \tag{8.33}$$

  where ε_i and ε_j (ε_a and ε_a) are occupied (virtual) orbital energies. The Laplace transformation suggested by Almlöf [156],

$$\frac{1}{x_q} = \int_0^\infty \exp(-x_q t)dt \approx \sum_{\alpha=1}^{\tau} w^{(\alpha)} \exp(-x_q t^{(\alpha)}) \tag{8.34}$$

  may be applied to the energy denominator in Eq. (8.33) by substituting $x_q{=}\varepsilon_a{+}\varepsilon_b{-}\varepsilon_i{-}\varepsilon_j$. The integrals in Eq. (8.34) can be approximated by a few (typically 5-8) grid points τ giving sufficient accuracy. Häser [157] and Ayala and Scuseria [158] have used the Laplace approach to formulate *atomic orbital based MP2* (AO-MP2). Recently, Ochsenfeld and coworkers have used efficient integral screening techniques and presented state-of-the-art implementations of the AO-MP2 scheme [159–161]. The Lagrange AO-MP2 approach is quite different from the DEC approach, but it is, to some extent, possible to control the error compared to a conventional MP2 calculation by increasing the number of grid points τ – similar to the error control in terms of the FOT in the DEC scheme. However, the AO-MP2 strategy cannot be generalized to more advanced CC methods.

Chapter 9

MP2 molecular gradient using the DEC scheme

This chapter describes the work presented in **paper [9]**.

9.1 Introduction

The determination of molecular equilibrium structures – i.e., local minima on the potential energy surface – is one of the most important tasks of electronic structure theory. An efficient geometry optimization requires that molecular gradients are evaluated analytically.

The analytical evaluation of molecular gradients was initiated by the seminal work of Pulay in 1969 [62] on the HF molecular gradient. Following this work, the MP2 molecular gradient was formulated by Pople and coworkers [164]. The MP2 molecular gradient has traditionally been formulated in the canonical MO basis [164–167]. Such formulations are prone to high-order computational scaling with system size and can therefore not be used for calculations on large molecular systems.

Different approaches have been attempted for reducing the high-order scaling of traditional MP2 formulations. Using the MP2 resolution of the identity (MP2-RI) approach [168, 169] reduced scaling for the MP2 molecular gradient has been obtained [170–173]. A different strategy proposed by Schweizer, Doser, and Ochsenfeld [174] is to abandon the MO basis and reformulate the MP2 gradient equations in the AO basis using Laplace transformations of the energy denominator [156]. In a local CC context Werner and coworkers have presented molecular gradients for the local MP2 energy [175] and also extended this approach to employ density-fitting techniques [176].

In this chapter we describe how the MP2 molecular gradient may be evaluated within the DEC framework. The formulation is linear-scaling and embarrassingly parallelizable and thus suitable for calculations on large molecular systems. The errors in the DEC-MP2 molecular gradient compared to the standard MP2 gradient may be controlled by the same FOT used to control the error in the correlation energy in Chapters 7 and 8.

9.2 Full molecular calculation

9.2.1 The Lagrangian

We consider a closed-shell molecular system at some general geometry $\mathbf{x}$ described at the MP2 level of theory. At this geometry the MP2 amplitude equation in Eq. (7.13) is given by,

$$\begin{aligned} {}^t\Omega_{aibj}(\mathbf{x}) = g_{aibj}(\mathbf{x}) &+ \sum_c t_{ij}^{cb}(\mathbf{x})F_{ac}(\mathbf{x}) + \sum_c t_{ij}^{ac}(\mathbf{x})F_{bc}(\mathbf{x}) \\ &- \sum_k t_{kj}^{ab}(\mathbf{x})F_{ki}(\mathbf{x}) - \sum_k t_{ik}^{ab}(\mathbf{x})F_{kj}(\mathbf{x}) = 0 \end{aligned} \tag{9.1}$$

Furthermore, the HF optimization condition (the Brillouin theorem) is satisfied [63]

$${}^\kappa\Omega_{ai}(\mathbf{x}) = \langle \mathrm{HF}(\mathbf{x})|[E_{ai}(\mathbf{x}), H(\mathbf{x})]|\mathrm{HF}(\mathbf{x})\rangle = 0 \tag{9.2}$$

where $H(\mathbf{x})$ and $E_{ai}(\mathbf{x})$ are given by Eqs. (1.3) and (7.5), respectively, evaluated at a general geometry $\mathbf{x}$.

At $\mathbf{x}$ the MP2 energy $E_{\mathrm{MP2}}(\mathbf{x})$ (including the HF contribution) may be expressed as,

$$E_{\mathrm{MP2}}(\mathbf{x}) = E_{\mathrm{HF}}(\mathbf{x}) + E_{\mathrm{corr}}(\mathbf{x}) = E_{\mathrm{HF}}(\mathbf{x}) + \sum_{ijab} t_{ij}^{ab}(\mathbf{x})L_{iajb}(\mathbf{x}) \tag{9.3}$$

where we have used Eq. (7.10).

The MP2 energy in Eq. (9.3) is not determined variationally, and consequently its derivatives are not subject to the $2n$+1 rule (Section 1.7). To avoid solving for first-order amplitude parameters when evaluating the molecular gradient it is advantageous to construct a variational MP2 Lagrangian [31] by adding to the MP2 energy the constraints in Eqs. (9.1) and (9.2) associated with the two sets of Lagrange multipliers $\bar{t}$ and $\bar{\kappa}$,

$$L(\mathbf{x}, \bar{t}, \bar{\kappa}) = E_{\mathrm{MP2}}(\mathbf{x}) + \frac{1}{2}\sum_{aibj} \bar{t}_{ij}^{ab}(\mathbf{x}){}^t\Omega_{ijab}(\mathbf{x}) + \sum_{ai} \bar{\kappa}_{ai}(\mathbf{x}){}^\kappa\Omega_{ai}(\mathbf{x}) \tag{9.4}$$

The variational conditions for the MP2 Lagrangian yield the following equations:

$$\frac{\partial L(\mathbf{x}, \bar{t}, \bar{\kappa})}{\partial \bar{t}_{ij}^{ab}(\mathbf{x})} = {}^t\Omega_{ijab}(\mathbf{x}) = 0 \tag{9.5a}$$

$$\frac{\partial L(\mathbf{x}, \bar{t}, \bar{\kappa})}{\partial \bar{\kappa}_{ai}(\mathbf{x})} = {}^\kappa\Omega_{ai}(\mathbf{x}) = 0 \tag{9.5b}$$

$$\frac{\partial L(\mathbf{x}, \bar{t}, \bar{\kappa})}{\partial t_{ij}^{ab}(\mathbf{x})} = 0 \tag{9.5c}$$

$$\frac{\partial L(\mathbf{x}, \bar{t}, \bar{\kappa})}{\partial \kappa_{ai}(\mathbf{x})} = 0 \tag{9.5d}$$

Eqs. (9.5a) and (9.5b) trivially yields the equations for the t- and κ-parameters in Eqs. (9.1) and (9.2), respectively, whereas Eqs. (9.5c) and (9.5d) determine the multipliers.

9.2.2 The molecular gradient

By construction $L(\mathbf{x}, \bar{t}, \bar{\kappa})$ satisfies the $2n$+1 rule for the response parameters and the $2n$+2 rule for the multipliers. Therefore, the molecular gradient evaluated at some reference geometry $\mathbf{x}_0$ may be obtained as the partial derivative of the Lagrangian in Eq. (9.4), i.e.,

$$\begin{aligned}\left.\frac{dE}{dx}\right|_{\mathbf{x}=\mathbf{x}_0} &= \left.\frac{\partial L}{\partial x}\right|_{\mathbf{x}=\mathbf{x}_0} \equiv L^{(x)} \\ &= E^{(x)}_{\mathrm{MP2}} + \frac{1}{2}\sum_{abij} \bar{t}^{ab(0)}_{ij}\ {}^{t}\Omega^{(x)}_{ijab} + \sum_{ai} \bar{\kappa}^{(0)}_{ai}\ {}^{\kappa}\Omega^{(x)}_{ai}\end{aligned} \tag{9.6}$$

where a superscript (x) denotes partial differentiation with respect to a nuclear coordinate x. Since only zeroth order multipliers are considered in this work we shall henceforth omit the '(0)' superscript and write the zeroth order multipliers simply as $\bar{t}^{ab}_{ij}$ and $\bar{\kappa}_{ai}$.

The MP2 gradient in Eq. (9.6) may be expressed in the following form [9]:

$$L^{(x)} = L^{(x)}_{\text{1-el}} + L^{(x)}_{\text{reort}} + L^{(x)}_{\text{coulomb}} + L^{(x)}_{\text{exchange}} + L^{(x)}_{\Theta} + h^{(x)}_{\text{nuc}} \tag{9.7}$$

The nuclear-nuclear repulsion contribution $h^{(x)}_{\text{nuc}}$ can be identified by differentiation of Eq. (1.4d), while the one-electron, reorthonormalization, Coulomb, exchange, and $L^{(x)}_{\Theta}$ contributions are given by,

$$L^{(x)}_{\text{1-el}} = \sum_{\mu\nu} h^{(x)}_{\mu\nu}(2D+\rho)_{\mu\nu} \tag{9.8a}$$

$$L^{(x)}_{\text{reort}} = -\frac{1}{2}\sum_{\mu\nu} S^{(x)}_{\mu\nu} W_{\mu\nu} \tag{9.8b}$$

$$L^{(x)}_{\text{coulomb}} = 2\sum_{\mu\nu} J^{(x)}_{\mu\nu}(\mathbf{D})(2D+\rho)_{\mu\nu} \tag{9.8c}$$

$$L^{(x)}_{\text{exchange}} = -\sum_{\mu\nu} K^{(x)}_{\mu\nu}(\mathbf{D})(2D+\rho)_{\mu\nu} \tag{9.8d}$$

$$L^{(x)}_{\Theta} = \frac{1}{2}\sum_{ijab} \Theta^{ab}_{ij} g^{(x)}_{aibj} \tag{9.8e}$$

where all contributions (except $L^{(x)}_{\Theta}$) are written in the AO basis. $D_{\mu\nu}$ is the HF density matrix in the AO basis, and $S^{(x)}_{\mu\nu}$ is the differentiated overlap matrix in the AO basis. The effective "MP2 density matrix" $\boldsymbol{\rho}$ matrix is most easily written in the MO basis,

$$\boldsymbol{\rho} = \begin{pmatrix} -X_{ij} & -\bar{\kappa}^{T}_{ia} \\ -\bar{\kappa}_{ai} & Y_{ab} \end{pmatrix} \tag{9.9}$$

where $\mathbf{X}$ and $\mathbf{Y}$ are calculated from amplitudes and multipliers,

$$X_{ij} = \sum_{abk} t^{ba}_{ki}\bar{t}^{ba}_{kj}; \qquad Y_{ab} = \sum_{cij} t^{ca}_{ji}\bar{t}^{cb}_{ji}; \tag{9.10}$$

and the $\boldsymbol{\rho}$ matrix transforms to the AO basis according to

$$\rho_{\mu\nu} = \sum_{pq} C_{\mu p}\rho_{pq}C_{\nu q} \tag{9.11}$$

The coulomb and exchange transformations on a general matrix $\mathbf{A}$ (in the AO basis) are given by:

$$J_{\mu\nu}(\mathbf{A}) = \sum_{\tau\epsilon} g_{\mu\nu\tau\epsilon} A_{\tau\epsilon} \tag{9.12a}$$

$$K_{\mu\nu}(\mathbf{A}) = \sum_{\tau\epsilon} g_{\mu\tau\epsilon\nu} A_{\tau\epsilon} \tag{9.12b}$$

The reorthonormalization matrix $\mathbf{W}$ can be written in the following form (all quantities are given in the AO basis),

$$\mathbf{W} = 4\mathbf{DFD} + \mathbf{\Phi} + \boldsymbol{\rho}^s \mathbf{F}\bar{\mathbf{D}} + \mathbf{DG}(\boldsymbol{\rho}^s)\bar{\mathbf{D}} \tag{9.13}$$

where (in the AO basis)

$$\boldsymbol{\rho}^s = \boldsymbol{\rho} + \boldsymbol{\rho}^T \tag{9.14a}$$

$$\bar{D}_{\mu\nu} = \sum_{p} C_{\mu p} C_{\nu p} \tag{9.14b}$$

$$\mathbf{G}(\boldsymbol{\rho}^s) = 2\mathbf{J}(\boldsymbol{\rho}^s) - \mathbf{K}(\boldsymbol{\rho}^s) \tag{9.14c}$$

and the p summation in Eq. (9.14b) runs over both occupied and virtual orbital indices. The $\mathbf{\Phi}$ matrix in the MO basis is given by,

$$\Phi_{ij}^{\mathrm{oo}} = \sum_{abk} \Theta_{ki}^{ba} g_{bkaj} \tag{9.15a}$$

$$\Phi_{ic}^{\mathrm{ov}} = \sum_{abk} \Theta_{ki}^{ba} g_{bkac} \tag{9.15b}$$

$$\Phi_{ab}^{\mathrm{vv}} = \sum_{cij} \Theta_{ji}^{ca} g_{cjbi} \tag{9.15c}$$

$$\Phi_{ak}^{\mathrm{vo}} = \sum_{cij} \Theta_{ji}^{ca} g_{cjki} \tag{9.15d}$$

and it transforms to the AO basis in the same way as $\boldsymbol{\rho}$ in Eq. (9.11). The o and v superscripts indicate whether the indices refer to the **occupied** or to the **virtual** orbital spaces. The four-dimensional array Θ entering Eq. (9.15) and the $L_{\Theta}^{(x)}$ contribution is calculated from a linear combination of t amplitudes and $\bar{t}$ multipliers,

$$\Theta_{iajb} = 4t_{ij}^{ab} - 2t_{ij}^{ba} + \bar{t}_{ij}^{ab} \tag{9.16}$$

Finally, the coulomb and exchange transformations in $L_{\mathrm{coulomb}}^{(x)}$ and $L_{\mathrm{exchange}}^{(x)}$ are evaluated as in Eq. (9.12a) and (9.12b) but with differentiated integrals.

9.2.3 Multiplier equations

The multiplier equations are determined from Eqs. (9.5c) and (9.5d). The equation for the $\bar{t}$ multipliers may be written as,

$$2L_{aibj} + \sum_{c} \left(\bar{t}_{ij}^{cb} F_{ac} + \bar{t}_{ij}^{ac} F_{bc}\right) - \sum_{k} \left(\bar{t}_{kj}^{ab} F_{ki} + \bar{t}_{ik}^{ab} F_{kj}\right) = 0 \tag{9.17}$$

Note that Eq. (9.17) for the $\bar{t}$ multipliers is equivalent to the equation for the t amplitudes in Eq. (7.13) – except from the fact that $2L_{aibj}$ occurs in Eq. (9.17), whereas g_{aibj} occurs in (7.13). Consequently, when a local HF basis is used, the multipliers are local in much the same way as the amplitudes (Section 7.4.1).

The equation for the $\bar{\kappa}$ multipliers becomes,

$$\mathbf{E}^{[2]}\bar{\boldsymbol{\kappa}} = \mathbf{R}(\mathbf{X}, \mathbf{Y}, \boldsymbol{\Phi}) \tag{9.18}$$

The right-hand side matrix is given by

$$R_{ai}(\mathbf{X}, \mathbf{Y}, \boldsymbol{\Phi}) = \Phi_{ia} - \Phi_{ai} + G_{ai}(\mathbf{M}) \tag{9.19}$$

where $G_{ai}(\mathbf{M})$ is a two-electron Fock transformation [as in Eq. (9.14c)] transformed to the MO basis with one virtual and one occupied index,

$$G_{ai}(\mathbf{M}) = \sum_{\mu\nu} C_{\mu a} C_{\nu i} G_{\mu\nu}(\mathbf{M}) \tag{9.20a}$$

$$\mathbf{M} = \mathbf{Y}_{\mathrm{AO}} + \mathbf{Y}_{\mathrm{AO}}^T - \mathbf{X}_{\mathrm{AO}} - \mathbf{X}_{\mathrm{AO}}^T \tag{9.20b}$$

In Eq. (9.20b) $\mathbf{X}_{\mathrm{AO}}$ and $\mathbf{Y}_{\mathrm{AO}}$ are the $\mathbf{X}$ and $\mathbf{Y}$ matrices in the AO basis, which transform according to Eq. (9.11).

The electronic Hessian transformation $\mathbf{E}^{[2]}\bar{\boldsymbol{\kappa}}$ is given by

$$(\mathbf{E}^{[2]}\bar{\boldsymbol{\kappa}})_{ai} = 2\sum_b \bar{\kappa}_{bi} F_{ab} - 2\sum_j \bar{\kappa}_{aj} F_{ij} + 2G_{ai}(\bar{\boldsymbol{\kappa}}^s_{\mathrm{AO}}) \tag{9.21}$$

where $\bar{\boldsymbol{\kappa}}^s_{\mathrm{AO}}$=$\bar{\boldsymbol{\kappa}}_{\mathrm{AO}}$+$\bar{\boldsymbol{\kappa}}^T_{\mathrm{AO}}$ is a symmetrized $\bar{\boldsymbol{\kappa}}$ matrix in the AO basis.

9.3 DEC scheme

The equations defining the molecular gradient in Section 9.2 are valid for any choice of HF basis. If a local HF basis is employed it is possible to simplify the computational effort by applying the DEC scheme to evaluate the MP2 gradient. Specifically, it is possible to perform all manipulations of four-index quantities (two-electron integrals g, t amplitudes, and $\bar{t}$ multipliers) at the *orbital fragment level*, while two-index quantities (including Coulomb and exchange contributions) are treated for the *full molecular system*. Inspection of the MP2 gradient contributions in Eq. (9.8) reveals that the determination of $\mathbf{X}$, $\mathbf{Y}$, $\boldsymbol{\Phi}$, and $L^{(x)}_{\Theta}$ involves four-index quantities, and the main task when formulating the DEC-MP2 gradient scheme is thus to exploit the locality of the HF orbitals to evaluate these quantities in small orbital fragment spaces. The details are given in Section 3.4 of paper [9]. In this work we just note that it is important to invoke both the occupied and the virtual orbital partitioning schemes discussed in Section 8.2.

The DEC scheme for evaluating the MP2 molecular gradient is summarized in Figure 9.1:

- A full molecular HF calculation is carried out and a set of local HF orbitals is determined.

- Atomic fragment calculations and pair fragment calculations are carried out using both the occupied and virtual orbital partitionings (independently) to determine $\mathbf{X}$, $\mathbf{Y}$, $\mathbf{\Phi}$, and $L_\Theta^{(x)}$. It turns out that $\mathbf{Y}$, $\mathbf{\Phi}^{\mathrm{vv}}$, $\mathbf{\Phi}^{\mathrm{vo}}$, and $L_\Theta^{(x)}$ are most easily evaluated using the occupied partitioning scheme, whereas the determination of the $\mathbf{X}$, $\mathbf{\Phi}^{\mathrm{oo}}$, and $\mathbf{\Phi}^{\mathrm{ov}}$ requires the virtual partitioning scheme.

- The right-hand side matrix $\mathbf{R}(\mathbf{X}, \mathbf{Y}, \mathbf{\Phi})$ for the $\bar{\kappa}$ equation is constructed from $\mathbf{X}$, $\mathbf{Y}$, and $\mathbf{\Phi}$, and the $\bar{\kappa}$ equation is solved for the full molecular system.

- The "effective MP2 densities" $\boldsymbol{\rho}$ and $\mathbf{W}$ for the full molecular system are constructed from $\mathbf{X}$, $\mathbf{Y}$, $\mathbf{\Phi}$, and $\bar{\kappa}$.

- Finally, the MP2 molecular gradient is evaluated using $\boldsymbol{\rho}$, $\mathbf{W}$, and $L_\Theta^{(x)}$ (and the HF density).

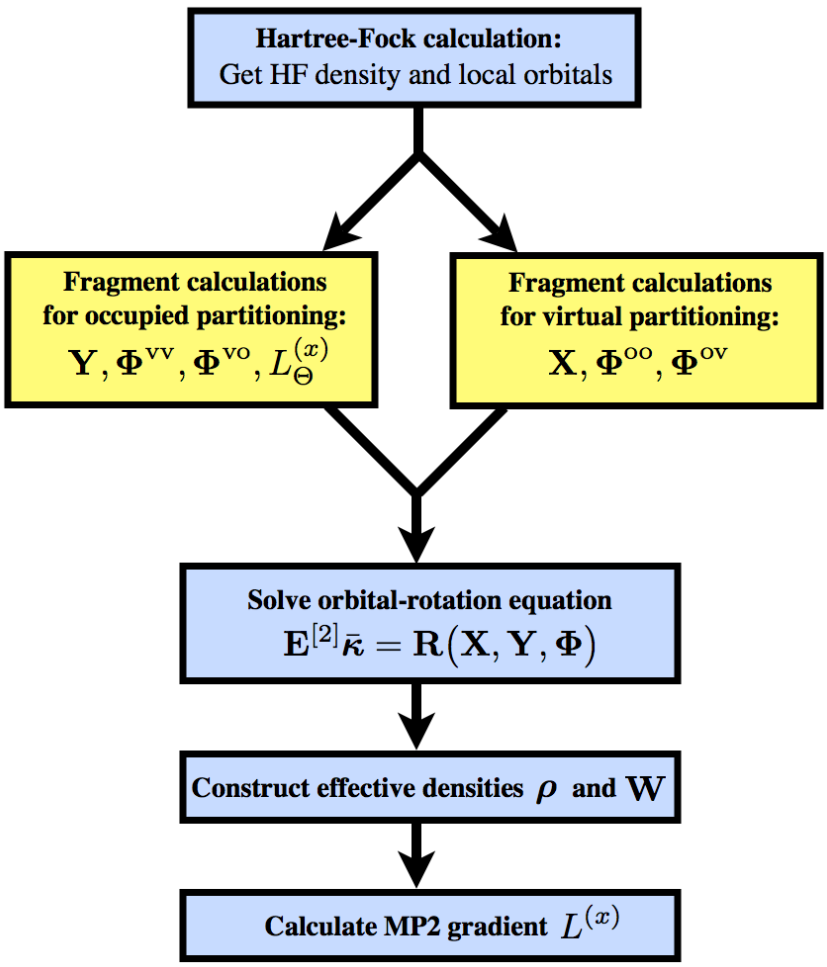

Figure 9.1: Overview of the main steps in the DEC-MP2 gradient scheme, where yellow boxes denote fragment calculations, whereas light-blue boxes denote full molecular calculations. Note that all manipulations of four-index quantities are carried out at the orbital fragment level. In this way four-index quantities are never constructed for the full molecular system.

Let us conclude this section by commenting on the scaling of the computational time with system size for the DEC-MP2 gradient scheme. By construction, the number of fragments to consider scales quadratically with system size. As demonstrated in Section 7.5.2, distant atomic pairs representing dispersion energies (decaying rapidly with the inverse pair distance to the sixth power) may be omitted from a DEC energy calculation with negligible effects on the total correlation energy. This leads to a linear-scaling number of pair fragments for a large molecule. Similarly, in a DEC-MP2 molecular gradient calculation, distant atomic pairs describing dispersion forces (derivatives of dispersion energies with respect to nuclear displacements) may be omitted from the DEC calculation because their effects on the MP2 gradient is negligible. (This statement is supported by numerical results in Section 9.4.2.) The evaluation of the DEC-MP2 gradient is thus linear-scaling. Furthermore, the fragment calculations (yellow boxes of Figure 9.1) are independent, making the evaluation of $\mathbf{X}$, $\mathbf{Y}$, $\mathbf{\Phi}$, and $L_\Theta^{(x)}$ linear-scaling and embarrassingly parallel. With respect to the manipulations of two-index quantities (including coulomb and exchange transformations), the MP2 gradient equations may be viewed as generalized HF gradient expressions with the effective MP2 density matrix $\boldsymbol{\rho}$ and the MP2 reorthonormalization matrix $\mathbf{W}$ replacing the HF density matrix $\mathbf{D}$ and the HF reorthonormalization matrix $\mathbf{DFD}$. Thus, manipulations of two-index quantities in the DEC-MP2 gradient scheme (light-blue boxes of Figure 9.1) may be carried out in a linear-scaling manner using similar techniques as for the HF gradient [177–179]. In summary, all steps in the evaluation of the DEC-MP2 molecular gradient can be made linear-scaling, and the fragment calculations are furthermore embarrassingly parallelizable.

9.4 Results

In this section we compare DEC-MP2 molecular gradients to standard MP2 gradients by considering the arachidic acid molecule (same molecular structure and basis set as in Section 8.2.2).

Before describing the results let us comment on the relation between the FOT and the accuracy of the DEC-MP2 molecular gradient compared to the conventional MP2 gradient. The accuracy of the DEC-MP2 molecular gradient is ultimately determined by the accuracy of the t amplitudes and $\bar{t}$ multipliers, which enter linearly in the MP2 gradient expression. As discussed in Section 8.3 the amplitudes are subject to two types of errors. The amplitude errors of type 1 scales linearly with the FOT, whereas the errors of type 2 scales with $\mathrm{FOT}^{1/2}$. (A similar analysis can be performed for the $\bar{t}$ multipliers). Thus, if the FOT is decreased by a factor 10, we expect the errors of the DEC-MP2 molecular gradient to diminish by a factor between $10^{1/2}$ (type 2 errors are dominating) and 10 (type 1 errors are dominating).

Table 9.1: Standard deviation Δ_{std}, absolute error $\bar{\Delta}_{\text{abs}}$, and maximum absolute errors Δ_{max} (all in mHartree/bohr) for DEC-MP2 gradients compared to standard MP2 gradients for various fragment optimization thresholds (FOTs). The calculations were carried out on arachidic acid using the cc-pVDZ basis set.

FOT	Δ_{std}	$\bar{\Delta}_{\text{abs}}$	Δ_{max}
10^{-3}	0.99	0.43	7.1
10^{-4}	0.29	0.13	1.5
10^{-5}	0.028	0.012	0.13
10^{-6}	0.0040	0.0018	0.022

9.4.1 Gradient error measures

We let Δ_i denote the difference between the ith component of the DEC-MP2 gradient x_i^{dec} and the full molecular MP2 gradient x_i^{full}:

$$\Delta_i = x_i^{\text{dec}} - x_i^{\text{full}} \tag{9.22}$$

and consider the mean error $\bar{\Delta}$, the standard deviation Δ_{std}, the mean absolute error $\bar{\Delta}_{\text{abs}}$, and the maximum absolute error Δ_{max}:

$$\bar{\Delta} = \frac{1}{3N}\sum_{i=1}^{3N}\Delta_i \tag{9.23a}$$

$$\Delta_{\text{std}} = \sqrt{\frac{\sum_{i=1}^{3N}(\Delta_i - \bar{\Delta})^2}{3N-1}} \tag{9.23b}$$

$$\bar{\Delta}_{\text{abs}} = \frac{1}{3N}\sum_{i=1}^{3N}|\Delta_i| \tag{9.23c}$$

$$\Delta_{\text{max}} = \max_i |\Delta_i| \tag{9.23d}$$

where the summations run over all gradient components, i.e., N is the number of atoms.

Table 9.1 gives Δ_{std}, $\bar{\Delta}_{\text{abs}}$, and Δ_{max} for DEC-MP2 gradient calculations on arachidic acid using different FOTs. In general, the errors decrease when the FOT is decreased. In particular, in accordance with the error analysis in Section 8.3 and the discussion above, the error measures in Table 9.1 decrease by a factor between $10^{1/2}\approx 3.2$ and 10 when the FOT is lowered by an order of magnitude. For example, Δ_{std} decreases by roughly 3.4 when the FOT is lowered from 10^{-3} to 10^{-4}, whereas Δ_{std} decreases by ca. 10 when the FOT is lowered from 10^{-4} to 10^{-5}.

9.4.2 The use of pair distance cutoffs

In Section 9.3 it was stated that distant pairs may be omitted from the DEC-MP2 gradient calculation without affecting the accuracy of the gradient, since these pairs describe dispersion effects which decay rapidly with pair distance. In this section we present numerical results supporting this statement.

Table 9.2: Standard deviation Δ_{std}, absolute error $\bar{\Delta}_{\mathrm{abs}}$, and maximum absolute errors Δ_{max} (all in mHartree/bohr) for DEC-MP2 gradient calculations using different pair-cutoffs compared to a full molecular calculation on arachidic acid (cc-pVDZ basis) for FOT = 10^{-6}.

Pair-cutoff (Å)	Δ_{std}	$\bar{\Delta}_{\mathrm{abs}}$	Δ_{max}
all pairs	0.0040	0.0018	0.022
20	0.0040	0.0018	0.022
15	0.0040	0.0018	0.022
10	0.0040	0.0019	0.022
8	0.0041	0.0021	0.022
6	0.0063	0.0047	0.033
4	0.037	0.024	0.232
2	0.91	0.63	6.3
0	2.5	1.6	17

Table 9.2 gives Δ_{std}, $\bar{\Delta}_{\mathrm{abs}}$, and Δ_{max} for FOT=10^{-6}, where pairs separated by more than a given pair distance cutoff have been omitted. The pair distances cutoff values range from one extreme, where all pairs are included, to the other extreme where all pairs are omitted. The row with all pairs included corresponds to the values presented in Table 9.1. For a pair-cutoff of roughly 10 Å or above, the errors are the same as when all pairs are included. In other words, pairs separated by more than 10 Å do not contribute to the MP2 molecular gradient and may be omitted from the gradient calculation. Thus, for large molecules, the number of pair fragments to consider scales only *linearly* (rather than quadratically) with the molecular system size.

9.5 Summary and perspectives

We have demonstrated that the MP2 molecular gradient can be evaluated using the DEC scheme as summarized in Figure 9.1. The scheme is linear-scaling and embarrassingly parallel. All manipulations of four-index quantities are carried out using small local orbital fragment spaces (yellow steps in Figure 9.1), whereas the HF-like two-index manipulations involving effective MP2 densities are carried out for the full molecular system (light-blue steps in Figure 9.1). Roughly speaking, the short-range electron correlation effects (four-index quantities) are treated locally using orbital fragments, whereas a proper treatment of the long-range electronic interactions (two-index quantities) requires that the full molecular system is considered.

The errors of the DEC-MP2 molecular gradient compared to a standard MP2 molecular gradient may be controlled (and made arbitrarily small) by tightening the FOT parameter. An obvious next step is to apply the DEC-MP2 molecular gradient in the context of performing a geometry optimization for a large molecular system. This is a subject for future investigations. At this stage we note that – since the FOT parameter controls the error in the MP2 gradient –

it will be advantageous to tighten the FOT parameter during the geometry optimization, such that a more accurate MP2 gradient is obtained when the molecular geometry is close to the equilibrium structure.

Considering future perspectives, we believe that the development of the DEC-MP2 molecular gradient is an initial step towards performing geometry optimizations and towards calculating higher order energy derivatives for large molecular systems within the DEC framework – both at the MP2 level of theory and for more accurate CC methods, such as the CCSD model.

Chapter 10

Local orbitals

This chapter describes the work presented in **paper [10]**.

10.1 Introduction

When describing the DEC method in Chapters 7-9 a central assumption is the existence of a set of local orbitals for both the occupied and the virtual orbital spaces. In this chapter it is demonstrated how such orbitals can be obtained.

The CC energy is invariant under rotation among the occupied and among the virtual MOs. This freedom can be used to transform the conventional canonical orbitals to a local HF basis [138]. A large variety of different localization procedures have been proposed [180–193]. Three localization functions are commonly used. The scheme attributed to Boys [180–182] minimizes the spatial extent of the MOs by maximizing the distance between the orbital centroids. This is equivalent to maximizing the function

$$\xi_{Boys} = \sum_p \sum_x \langle \phi_p | x | \phi_p \rangle^2 \tag{10.1}$$

where $|\phi_p\rangle$ refers to a set of occupied (or virtual) MOs and x is a component of the position operator. The scheme by Edmiston–Ruedenberg (ER) [183–185] maximizes the self-repulsion energy

$$\xi_{ER} = \sum_p (\phi_p \phi_p | \phi_p \phi_p) \tag{10.2}$$

The scheme by Pipek–Mezey (PM) [189, 190] minimizes the number of atomic centers over which each MO extends by maximizing the sum of squares of the gross atomic Mulliken population of the MOs

$$\xi_{PM} = \sum_p \sum_A |\langle \phi_p | P_A | \phi_p \rangle|^2 \tag{10.3}$$

where P_A is the projection operator onto the space of atomic orbitals centered on atom A. Ref. [190] gives a brief introduction to the different localization functions and the Jacobi sweep that is usually used to obtain the localized MOs.

For the occupied molecular orbitals, the above localization functions usually have strong and isolated minima, and the localization functions have been successfully optimized using a Jacobi sweep of iterations to give a set of local occupied HF orbitals. However, for the virtual space it is extremely difficult to obtain a set of localized orthonormal orbitals using a Jacobi sweep of iterations [194]. In the absence of localized virtual HF orbitals, redundant PAOs, where the occupied orbital space is projected out of the AO basis, have been used to span the virtual orbital space [139–144, 146, 147, 150, 151, 154, 155, 195–197]. Besides being redundant, a more severe drawback of the PAOs is that they are much less local than localized occupied HF orbitals.

In Section 10.2 it is described how local orthonormal orbitals for both the occupied and virtual orbital spaces can be obtained. Section 10.3 contains some illustrative results, and in Section 10.4 we give some concluding remarks.

10.2 Local orbitals using powers of the orbital variance

10.2.1 Preceding developments

The orbital localization procedure described in paper [10] relies to some extent – historically as well as the practical implementation — on preceding developments carried out in the Aarhus quantum chemistry group. Let us therefore put the work presented in paper [10] into the appropriate perspective by summarizing these developments.

In Ref. [198] local orbitals for both the occupied and virtual orbital spaces are obtained by applying the least-change approach [198, 199] in combination with the three-level optimization algorithm [200, 201] for the HF energy. The least-change algorithm utilizes the fact that the solution to the Fock eigenvalue equation can be divided into three parts: (1) a transformation from the AO basis to an orthonormal basis, (2) a HF optimization condition in this orthonormal basis, which ensures that the Fock matrix is block-diagonal with vanishing elements between the occupied and virtual HF orbitals, and (3) a canonical condition, which ensures that the Fock matrix is diagonal with orbital energies on the diagonal.

The canonical condition severely delocalizes the HF orbitals and it is therefore removed from the solution of the Fock eigenvalue equation in the least-change approach, where the smallest possible transformation matrices are determined from the AO basis to its orthogonalized counterpart and from this orthogonalized basis to an optimized HF basis. The least-change approach gives a set of local occupied and local virtual HF orbitals [198], because small transformations are carried out on the local AO basis. The major problem with the least-change algorithm is that in part 2, the identification of the smallest transformation matrix depends on the ordering of the orthonormal orbitals, i.e., whether an orthonormal basis function is associated with the occupied or the virtual orbital space. The optimal ordering can be identified by examining the orbital spread for all different orderings, which is an $\mathcal{O}(n^5)$ process [198] (n being the number of orthonormal orbitals). The ordering that leads to the smallest maximum orbital spread gives the local least-change molecular (LCM) orbitals.

When determining the LCM orbitals for larger molecular systems, the number of orderings becomes prohibitively large. To avoid the expensive reordering procedure one may instead use a simple and cheap version of the LCM orbitals, where the ordering of the orthonormal orbitals is simply based on their orbital occupancies (projections against the occupied space). These simplified LCM orbitals are not local enough for efficient use in a subsequent correlated calculation. However, they provide a better starting guess than the completely delocalized canonical orbitals for generating a set of truly local orbitals for both the occupied and virtual orbital spaces.

10.2.2 Orbital variance as a localization measure

The *orbital variance* Ω_p for an orbital $|\phi_p\rangle$ is defined as its average deviation from its average position squared

$$\Omega_p = \sum_x \left(\langle \phi_p | \left(x - \langle \phi_p | x | \phi_p \rangle \right)^2 | \phi_p \rangle \right) = \sum_x \left(\langle \phi_p | x^2 | \phi_p \rangle - \langle \phi_p | x | \phi_p \rangle^2 \right) \tag{10.4}$$

and the corresponding *orbital spread* σ_p is the square root of this number

$$\sigma_p = \Omega_p^{1/2} \tag{10.5}$$

The orbital variance (or spread) of an orbital $|\phi_p\rangle$ is a measure of the spatial extent of that orbital and thus of the locality of the orbital.

Consider a set of orthonormal orbitals $\mathcal{S}$, which refers either to the set of occupied orbitals or to the set of virtual orbitals. The sum of the variances for the orbitals in the set $\mathcal{S}$ is a measure of the locality for this set

$$\xi = \sum_{p \in \mathcal{S}} \Omega_p \tag{10.6}$$

Minimizing ξ while keeping the orbitals orthonormal gives the set of orbitals that on average are most local.

In local correlation methods it is important that the *average* orbital variance is small. However, it is equally important that the *maximum* orbital variance is small, because a single delocalized orbital will destroy the locality of the set of orbitals as a whole. For example, in the context of the DEC method, a single delocalized virtual orbital would have to be included in all atomic fragments $P, Q, R, \ldots$ of the form in Figure 7.7, thereby destroying the locality of the DEC atomic fragment calculations.

A small maximum orbital variance can be obtained by introducing a penalty on the orbitals with large orbital variances. This may be accomplished by using powers of the variance

$$\xi_m = \sum_{p \in \mathcal{S}} \Omega_p^m \tag{10.7}$$

as a measure of locality, where m is a positive integer. Increasing m increases the penalty for having orbitals with a large orbital variance (outlier orbitals) and thus makes the distribution of

orbital spreads for the orbitals in $\mathcal{S}$ more uniform. We note that the minimization of ξ_1 (m=1) is equivalent to the Boys minimization procedure [180–182].

In a HF calculation, the molecular core orbitals are in general almost identical to the atomic core orbitals. If the molecular core orbitals are included in the summation in Eq. (10.7), the molecular valence orbitals will get small undesirable tail coefficients referencing the core orbitals. We therefore exclude the molecular core orbitals from the summation in Eq. (10.7) to maintain the division of electrons into core and valence spaces.

The trust-region method of Fletcher [202] can be used to minimize ξ_m for both the occupied and the virtual HF orbitals. The minimization is most difficult for the virtual set of HF orbitals, where many very large negative Hessian eigenvalues are encountered in the initial iterations. For the occupied HF orbitals only small negative Hessian eigenvalues are encountered in the initial iterations and these disappear fast during the optimization. This is probably the reason why a Jacobi sweep of iterations, in general, is able to optimize the Boys function for the occupied orbitals but not for the virtual orbitals. For more details regarding the minimization of ξ_m the reader is referred to paper [10]. We note that the computational cost of the localization procedure is negligible compared to the total HF calculation.

10.3 Illustrative results

We now give examples of local occupied and virtual HF orbitals obtained by minimizing the localization function ξ_m in Eq. (10.7) using the set of simplified LCM orbitals described in Section 10.2.1 as a starting guess. Localized orbitals for the following molecules will be considered: Superbenzene ($C_{24}H_{12}$) with a B3LYP/cc-pVTZ optimized geometry; Buckminsterfullerene (C_{60}) with a B3LYP/6-31G(d,p) optimized geometry; and the $I27_{SS}$ domain of the titin protein (392 atoms) with a BP86/6-31G optimized geometry (but with 6-31G* basis functions on the three sulfur atoms and on two carbon atoms as described in Ref. [203]). The effects of increasing m in Eq. (10.7) will be investigated. Calculations using different cardinal numbers X of Dunning's correlation-consistent basis sets [137] cc-pVXZ are presented. In particular, we consider $X = D, T, Q$ for superbenzene, $X = D, T$ for C_{60}, and only $X = D$ for the titin fragment.

10.3.1 Maximum orbital spread

The maximum orbital spread (MOS) for a set of orbitals $\mathcal{S}$ is given by

$$\mathrm{MOS} = \max_{p \in \mathcal{S}} \sigma_p \tag{10.8}$$

where σ_p is given in Eq. (10.5). We use the MOS as a measure of the locality of the set $\mathcal{S}$.

The MOSs are presented for superbenzene (Table 10.1), C_{60} (Table 10.2), and the titin fragment (Table 10.3) for the occupied (Occ) and virtual (Virt) HF orbitals when ξ_m is optimized for m=1, 2, ..., 10. For the titin fragment only m=1, 2, ..., 5 results are reported.

Table 10.1: Maximum orbital spreads (a.u.) for localized superbenzene orbitals using different penalty exponents m. Also shown are maximum orbital spreads (a.u.) for least-change molecular (LCM) orbitals, projected atomic orbitals (PAO), and canonical molecular orbitals (CMO).

	cc-pVDZ		cc-pVTZ		cc-pVQZ	
	Occ	Virt	Occ	Virt	Occ	Virt
1	2.288	3.004	2.292	3.261	3.012	7.614
2	2.253	2.717	2.256	2.447	2.258	2.560
3	2.226	2.263	2.228	2.317	2.239	2.337
4	2.192	2.245	2.193	2.113	2.208	2.241
5	2.170	2.234	2.171	2.064	2.192	2.177
6	2.156	2.224	2.157	2.050	2.180	2.122
7	2.146	2.213	2.146	2.040	2.171	2.079
8	2.138	2.202	2.138	2.032	2.163	2.041
9	2.131	2.194	2.132	2.025	2.157	2.021
10	2.126	2.189	2.127	2.020	2.151	2.007
LCM	3.300	4.152	3.300	4.553	3.444	5.747
PAO	—	3.550	—	3.551	—	3.844
CMO	7.458	10.737	7.452	11.551	7.452	12.160

Table 10.2: Maximum orbital spreads (a.u.) for localized C_{60} orbitals using different penalty exponents m. Also shown are maximum orbital spreads (a.u.) for projected atomic orbitals (PAO), and canonical molecular orbitals (CMO).

	cc-pVDZ		cc-pVTZ	
	Occ	Virt	Occ	Virt
1	2.281	2.868	2.285	3.212
2	2.156	2.426	2.159	2.469
3	2.128	2.349	2.131	2.310
4	2.114	2.311	2.118	2.235
5	2.100	2.288	2.101	2.189
6	2.088	2.274	2.089	2.160
7	2.080	2.263	2.081	2.140
8	2.073	2.255	2.074	2.124
9	2.068	2.249	2.069	2.112
10	2.064	2.244	2.065	2.103
PAO	—	3.469	—	3.497
CMO	7.211	9.257	7.222	10.225

Table 10.3: Maximum orbital spreads (a.u.) for localized orbitals for the $I27_{SS}$ domain of the titin protein using different penalty exponents m. Also shown are maximum orbital spreads (a.u.) for projected atomic orbitals (PAO), and canonical molecular orbitals (CMO).

	cc-pVDZ	
	Occ	Virt
1	2.245	3.483
2	2.188	2.644
3	2.163	2.519
4	2.153	2.467
5	2.133	2.415
PAO	—	4.710
CMO	24.754	26.334

In Figure 10.1 we present graphical illustrations of the least local occupied orbital and the least local virtual orbital for superbenzene, C_{60}, and the titin fragment for m=2. Furthermore, on the front page of this thesis the least local virtual orbital for the insulin molecule (cc-pVDZ basis) using m=2 is displayed (hydrogen atoms are omitted for clarity).

Different molecules and different cardinal numbers

Considering the occupied HF orbitals for the cc-pVXZ bases, the MOS with m=1 is similar for X=D and X=T, while for X=Q there is a significant increase. For example, for superbenzene with m=1 the MOS is 2.29 (cc-pVDZ), 2.29 (cc-pVTZ), and 3.01 (cc-pVQZ). When m increases the MOS of the occupied orbitals decreases and becomes similar for all cardinal numbers. For superbenzene with m=10 we thus obtain 2.13 (cc-pVDZ), 2.13 (cc-pVTZ), and 2.15 (cc-pVQZ) for the MOS for the occupied orbitals. The similarity between the MOSs for the occupied orbitals reflects that the occupied orbitals are described well at the cc-pVDZ level and that only small changes are introduced in the occupied orbitals when the cardinal number is increased. For larger m values the MOSs become similar, even for molecules with rather different electronic structures. For example for m=5 the MOSs for the occupied orbitals in the cc-pVDZ calculations are 2.17, 2.10, and 2.13 for superbenzene, C_{60}, and the titin fragment, respectively.

For the virtual HF orbitals, the MOS varies somewhat with the cardinal number. For m=1 the MOS increases with the cardinal number, and outliers may be encountered. For example, for superbenzene the MOS for the virtual HF orbitals is 3.00 (cc-pVDZ), 3.26 (cc-pVTZ) and 7.61 (cc-pVQZ), where the latter is an extreme outlier (to be detailed in Section 10.3.2). For larger m values the MOS decreases and the outliers disappear. It is also seen that for larger m values the MOS may become smaller for the virtual orbitals when the cardinal number is increased. For example, for C_{60} and m=10 the MOS is 2.24 (cc-pVDZ) and 2.10 (cc-pVTZ). To understand this somewhat counter-intuitive result, recall that when the cardinal number is increased from

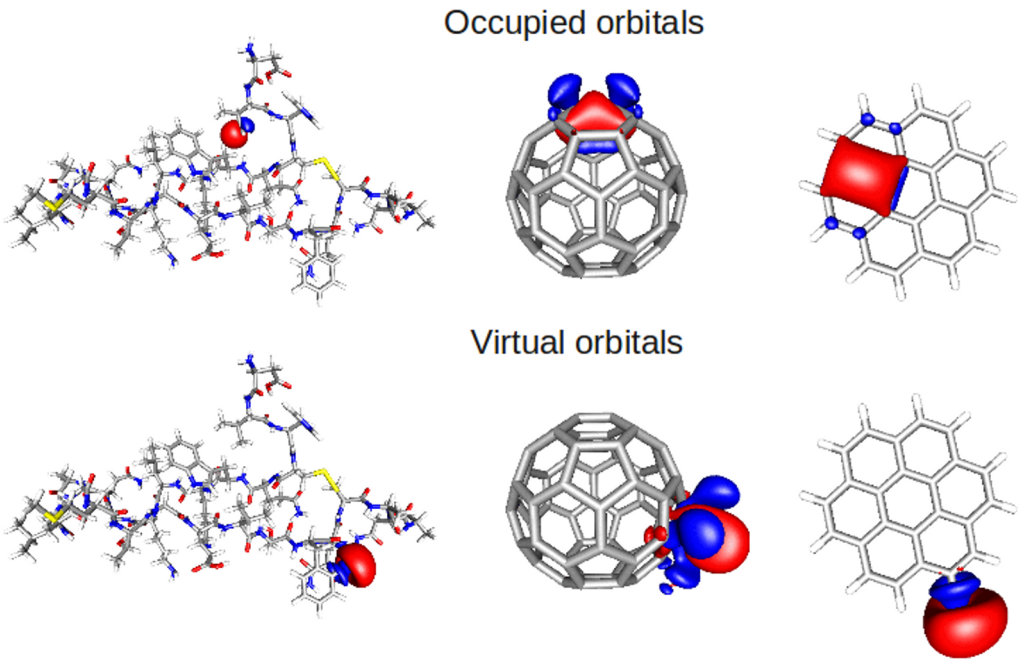

Figure 10.1: Least local orbitals for the occupied and virtual orbital spaces for the $I27_{SS}$ domain of the titin protein (left), C_{60} (middle), and superbenzene (right) plotted with orbital amplitude values of 0.03 (a.u.). The calculations were carried out using the cc-pVDZ basis and a power exponent m=2.

X to X+1, we add atomic basis functions which are more local than the localized molecular HF orbitals for cardinal number X. The added atomic basis functions therefore have the flexibility to make the MOS smaller for cardinal number X+1 than for X.

Similar to the occupied orbitals, the locality of the virtual HF orbitals is nearly system independent for larger m values and for a given basis set. For example, for the cc-pVDZ basis and m=5 the MOS for the virtual orbitals is 2.23, 2.29, and 2.42 for superbenzene, C_{60}, and the titin fragment, respectively.

It is also worth mentioning that for larger m values the difference between the MOSs for the occupied and virtual orbitals decreases. In fact, for larger cardinal numbers the virtual orbitals may have a smaller MOS than the occupied orbitals. For example, for the cc-pVQZ superbenzene calculation with m=10, the MOS is 2.15 for the occupied orbitals and 2.01 for the virtual orbitals.

Comparing local virtual orbitals with PAOs

In Tables 10.1, 10.2, and 10.3 we have also reported the MOSs for the PAOs [Eq. (8.24)] spanning the virtual HF orbital space and (only Table 10.1) for the occupied and virtual LCM orbitals.

The MOS for the LCM orbitals is significantly larger than for the localized orbitals, while the PAO values are in between the values for the virtual LCM orbitals and our localized virtual orbitals. In general, the PAOs seem to become less local when the size of the molecular system is increased. For example, using the cc-pVDZ basis, the MOS for the PAOs of C_{60} is 3.47, while

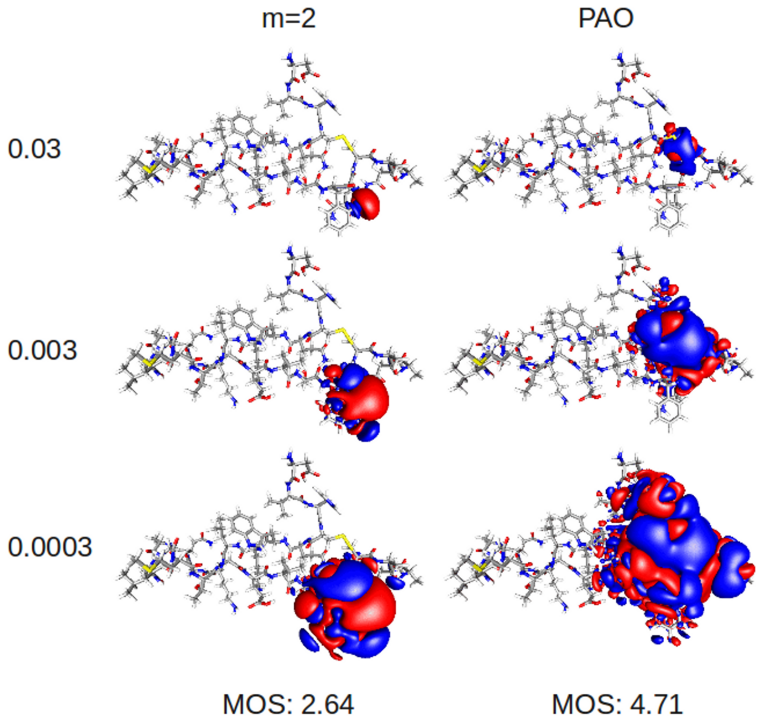

Figure 10.2: Least local virtual orbital for power exponent m=2 (left), and least local PAO (right) plotted for different orbital amplitude values 0.03, 0.003, and 0.0003 (a.u.). The calculations were carried out on the $I27_{SS}$ domain of the titin protein using the cc-pVDZ basis.

it is 4.71 for the larger titin fragment. The latter value is significantly larger than the MOS for our least local virtual orbital in the m=2 case (2.64). The fact that the MOS is a meaningful measure of locality is supported by Figure 10.2, where these two orbitals are displayed for orbital amplitude values of 0.03, 0.003, and 0.0003. The displayed orbitals substantiate that the least local PAO is significantly less local than our least local virtual orbital for m=2.

10.3.2 Detailed analysis of the virtual local orbitals for superbenzene

To understand what is happening when the penalty for delocalized orbitals is increased we have in Figure 10.3 displayed the orbital spreads for the individual virtual orbitals in a cc-pVQZ calculation on superbenzene for m=1 and m=2 along with illustrations of the least and most local virtual orbitals.

It is seen that outliers occur for m=1. In particular, Figure 10.3 reveals the presence of one extreme outlier orbital with an orbital spread of 7.61, which is basically spread out over the full molecular system. By increasing the penalty to m=2 the outliers disappear, and the orbital spread distribution becomes very uniform, such that all virtual orbitals have orbital spreads of about 2. The removal of virtual outlier orbitals when m is increased happens at the expense that the most local virtual orbitals are delocalized. For example, when the maximum orbital spread is decreased from 7.61 to 2.56 by increasing m, the minimum orbital spread is increased from 0.97 to 1.63.

In Figure 10.3 we have also displayed the orbital spreads for all PAOs and plotted the PAOs

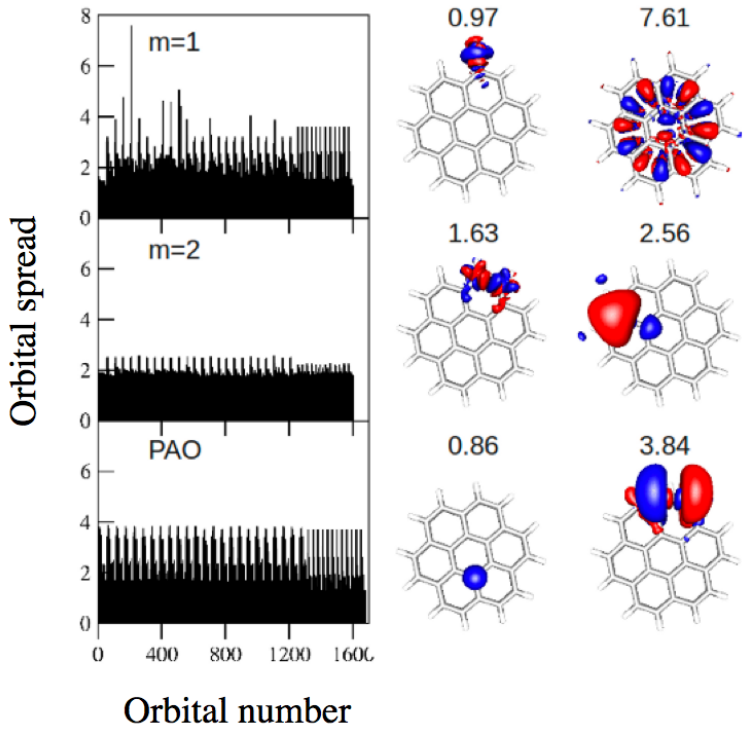

Figure 10.3: Virtual orbitals obtained with power exponents m=1 (top) and m=2 (middle) and PAOs (bottom) in a cc-pVQZ calculation on the superbenzene molecule. The orbitals were plotted using orbital amplitude values of 0.03 a.u. **Left column**: Orbital spreads (a.u.) against orbital number for all virtual orbitals. **Middle column:** Most local virtual orbital or PAO and associated orbital spread. **Right column:** Least local virtual orbital or PAO and associated orbital spread.

with the smallest (0.86) and largest (3.84) orbital spreads. The orbital spreads for the PAOs are in general larger than the orbital spreads for the virtual orbitals with m=2. It is also seen that the distribution of orbital spreads is more homogeneous for the virtual orbitals with m=2 than for the PAOs.

10.4 Conclusion

We have demonstrated that a set of local orthonormal HF orbitals can be obtained for both the occupied and virtual orbital spaces. The local HF orbitals are obtained by setting up localization functions where not only the occupied (or virtual) HF orbitals on average are most local, but where a penalty is also imposed for delocalized orbitals. Increasing this penalty leads to a more uniform distribution of orbital spreads – i.e., all orbitals become equally local. We have also shown that orbitals for molecules with rather different electronic structures are equally local.

Our local virtual HF orbitals (for m>1) are more local than the PAOs which are often used to span the virtual orbital space in local correlation calculations. Furthermore, the local virtual orbitals are non-redundant and orthonormal, in contrast to the PAOs. The local orbitals have already been applied for the DEC method, but also for other local correlation methods these orbitals appear to be a superior alternative to the commonly used PAOs.

Chapter 11

Summary and outlook

The overall goal of the work presented in this PhD thesis is to develop methods that enable electronic structure calculations on large molecular systems. The work falls into two subcategories, which are summarized individually below.

11.1 Part A

Part A is devoted to response theory formulations at the self-consistent field level of theory. A few key contributions are:

- An atomic orbital-based density matrix formulation of self-consistent field response theory is described, where the use of time- and perturbation-dependent basis functions is an integrated part of the formulation. This very general formulation allows for the straightforward determination of computationally tractable expressions for any molecular property which can be described in terms of response functions. Since the response functions are expressed in the atomic orbital basis, linear scaling with system size can be obtained for large molecular systems, where sparse matrix algebra can be exploited.

- In damped response theory finite excited state lifetimes are introduced in terms of complex frequencies. Damped response theory is an efficient tool for determining absorption spectra for large molecular systems in any frequency range without detailed knowledge about the individual excited states.

The developments described above are publically available in the LSDalton (Linear-Scaling Dalton) program [12].

So far, the response theory formulations presented here have mainly been used in test calculations. Future perspectives include applications of these developments to "real life" systems. To mention just one possible application, it is well-known that large conjugated molecules in general have large two-photon absorption cross sections. The damped response theory formulation of two-photon absorption in Chapter 6 is an efficient tool for studying the two-photon properties of these systems computationally. Such studies may aid experimentalists in designing

new compounds with increased two-photon absorption cross sections with potential use in, for example, 3D microscopy and pharmaceutical applications.

11.2 Part B

In part B the Divide-Expand-Consolidate (DEC) coupled-cluster (CC) method is described. Here we summarize the main ideas:

- In the DEC scheme the local nature of the dynamical electron correlation is exploited to partition a full CC calculation into a set of small orbital fragment calculations. The scheme is linearly scaling and embarrassingly parallelizable. Importantly, the error in the correlation energy introduced by the orbital fragmentations can be controlled (and made arbitrarily small) by tightening the so-called fragment optimization threshold parameter. This flexibility is achieved by optimizing the orbital fragment sizes in a black box manner during the calculation. At this stage the DEC scheme has been developed for the MP2 and CCSD correlation energies, and for the MP2 molecular gradient.

- A basic assumption for the applicability of the DEC model is the existence of a set of local HF orbitals. In Chapter 10 it is shown that local orbitals for both the occupied and virtual orbital spaces can be obtained by minimizing powers of the orbital variance.

The DEC scheme is very promising for calculating the CC correlation energy for large molecular systems. Experience gained by the development of the MP2 molecular gradient also allows one to be optimistic with respect to developing second- and higher-order energy derivatives – both for the MP2 model and for higher order CC models.

The DEC project is still at an initial stage, and several new developments are currently being investigated to improve the performance. Most calculations presented here have been carried out using the MP2 model, since the DEC-CCSD code is still at a testing stage. Furthermore, the relatively small cc-pVDZ basis set has been used in most calculations. Clearly, the goal is to improve the DEC code such that calculations using more accurate CC models, such as CCSD or maybe even CCSD(T), and larger basis sets can be routinely applied. The main bottleneck for achieving this goal is that the orbital fragments for a general three-dimensional molecule can become too large to be handled efficiently by the current DEC code if a high accuracy (accurate CC model, large basis set, and low fragment optimization threshold) is requested. We are currently investigating different strategies for improving the performance of the DEC program:

- The current implementation of the CC amplitude equations in the DEC program is not yet optimal, and the implementation could be significantly improved such that larger orbital fragments can be handled. However, it may be more advantageous to use the DEC program in combination with another quantum chemistry program, where an efficient parallel CC implementation already exists, such that the solution of the individual fragment amplitude

equations can be easily parallelized, or at least run with an optimal operation count. In this way the DEC program will constitute the main driver and the only task of the external quantum chemistry program will be to provide CC amplitudes for the fragments based on input from the DEC program. We expect that this can be done without much effort, since a DEC CC fragment calculation is simply a standard CC calculation carried out in a reduced orbital space.

- The largest (and therefore computationally most expensive) pair fragments are those referencing distant atomic sites, where the orbital spaces of the corresponding atomic fragments do not overlap. However, the contributions to the correlation energy (or the molecular gradient) from such pairs are very small, since they describe dispersion effects. Therefore, it is a waste of computational resources to calculate these small contributions very accurately, and a more economical approach is to use smaller orbital spaces for distant pairs.

- The number of fragments can be reduced by combining atomic fragments – for example, two atomic fragments P and Q can be combined into a superfragment $\mathcal{P} = P \cup Q$. If the orbital spaces for the original atomic fragments P and Q overlap significantly, the construction of a superfragment will lead to savings in the total computational time by reducing the number of pair fragments. One possible strategy is to (i) construct the atomic fragments as described in Chapter 7, (ii) investigate the overlap of the orbital spaces for these atomic fragments to construct superfragments whenever feasible, and (iii) carry out single and pair fragment calculations for these superfragments.

- It is advantageous to develop more local molecular orbitals as this will lead to smaller orbital fragments in DEC calculations. This can possibly be achieved by using other localization functions than the one described in Chapter 10.

In conclusion, the DEC approach provides an efficient scheme for carrying out large scale CC calculations with control of the error relative to a standard CC calculation. There are still technical obstacles to be addressed before calculations on large molecules can be routinely carried out. However, we are confident that these issues will be solved and that DEC will become a fully fledged computational tool for studying large molecular systems.

11.3 Dansk resume

I teoretisk kemi bruges kvantekemiske modeller til at beregne information om molekylære systemer. De kvantekemiske beregninger udføres ofte på supercomputere og kan anvendes i kombination med eksperimenter til at fortolke disse samt til at forudsige nye eksperimenter. Til en vis grad kan kvantemekaniske beregninger også erstatte eksperimentelle undersøgelser, og således kan dyre og potentielt farlige eksperiementer udføres billigt og risikofrit på en computer. Eksempelvis kan mange molekyler "fremstilles" og undersøges på computeren (i stedet for i laboratoriet) for derved at identificere nogle få molekyler, der besidder en given egenskab. Den største udfordring for eksisterende kvantemekaniske modeller er at beregningstiden vokser dramatisk for store molekyler – især for de mest nøjagtige modeller. Eksempelvis vokser beregningstiden for den såkaldte CCSD metode med systemets størrelse i sjette potens – dvs. hvis en beregning på et lille molekyle tager 1 time, så vil en beregning på et molekyle af ti-dobbelt størrelse tage 10^6 timer, altså 114 år! Vi er ofte interesserede i at studere store molekyler – f.eks. vil man gerne kunne undersøge kvantemekanisk hvordan et medikament binder til et protein – men dette er ofte ikke muligt med de traditionelle implementationer af kvantemekaniske modeller pga. den eksplosive vækst i beregningstid.

I løbet af mit PhD studie har jeg undersøgt, hvordan man kan reformulere eksisterende kvantemekaniske modeller, således at disse bliver anvendelige for store molekyler – ideelt set skal beregningstiden kun vokse lineært med molekylets størrelse. Dette er blevet gjort for responsteori (bestemmelse af molekylære egenskaber) indenfor den såkaldte selv-konsistente felt-model, samt for energi- og energigradient-beregninger med den mere nøjagtige coupled-cluster model. Sidstnævnte formulering er ikke blot lineært skalerende, men også triviel at parallelisere, således at en beregning på et stort molekyle kan splittes op i små separate beregninger, som kan køres uafhængigt af hinanden på en supercomputer med mange processorer. Herved nedsættes den totale beregningstid drastisk. Der er stadig tekniske detaljer, der skal forbedres før vi rutinemæssigt kan udføre beregninger på store systemer, men de grundlæggende formuleringer er blevet udviklet, implementeret og testet.

Bibliography

[1] K. Kristensen, P. Jørgensen, A. J. Thorvaldsen, and T. Helgaker, *J. Chem. Phys.* **129**, 214103 (2008).

[2] A. J. Thorvaldsen, K. Ruud, K. Kristensen, P. Jørgensen, and S. Coriani, *J. Chem. Phys.* **129**, 214108 (2008).

[3] S. Coriani, A. J. Thorvaldsen, K. Kristensen, and P. Jørgensen, *J. Chem. Phys.* **13**, 4224 (2011).

[4] K. Kristensen, J. Kauczor, T. Kjærgaard, and P. Jørgensen, *J. Chem. Phys.* **131**, 044112 (2009).

[5] T. Kjærgaard, K. Kristensen, J. Kauczor, P. Jørgensen, S. Coriani, and A. J. Thorvaldsen, *J. Chem. Phys.* **135**, 024112 (2011).

[6] K. Kristensen, J. Kauczor, A. J. Thorvaldsen, P. Jørgensen, T. Kjærgaard, and A. Rizzo, *J. Chem. Phys.* **134**, 214104 (2011).

[7] K. Kristensen, M. Ziółkowski, B. Jansík, T. Kjærgaard, and P. Jørgensen, *J. Chem. Theory Comput.* **7**, 1677 (2011).

[8] I.-M. Høyvik, K. Kristensen, B. Jansík, and P. Jørgensen, *"On the theoretical foundation of the divide-expand-consolidate (DEC) coupled cluster method. Numerical illustrations using second order Møller-Plesset perturbation theory"* (in preparation).

[9] K. Kristensen, S. Reine, T. Kjærgaard, B. Jansík, I.-M. Høyvik, and P. Jørgensen, *"MP2 molecular gradient using the Divide-Expand-Consolidate approach"* (submitted).

[10] B. Jansík, S. Høst, K. Kristensen, and P. Jørgensen, *J. Chem. Phys.* **134**, 194104 (2011).

[11] T. Helgaker, S. Coriani, P. Jørgensen, K. Kristensen, J. Olsen, and K. Ruud, *"Recent advances in wave-function-based methods of molecular-property calculations"* (submitted).

[12] LSDALTON*, a linear scaling molecular electronic structure program, Release Dalton2011*, 2011, See http://daltonprogram.org.

[13] J. Olsen and P. Jørgensen, *J. Chem. Phys.* **82**, 3235 (1985).

[14] C. Puzzarini, J. F. Stanton, and J. Gauss, *Int Rev Phys Chem* **29**, 273 (2010).

[15] G. R. Fleming, *Chemical Applications of Ultrafast Spectroscopy*, Oxford University Press, New York, 1986.

[16] J. Laane, H. Takahashi, and A. D. Bandrauk, *Structure and Dynamics of Electronic Excited States*, Springer, Heidelberg, 1998.

[17] T. Helgaker, M. Jaszuński, and K. Ruud, *Chem Rev* **99**, 293 (1999).

[18] F. Neese, *Coordin Chem Rev* **253**, 526 (2009).

[19] A. Pedone, M. Biczysko, and V. Barone, *Chemphyschem* **11**, 1812 (2010).

[20] R. W. Boyd, *Nonlinear Optics*, Academic Press, San Diego, 1992.

[21] S. Mukamel, *Principles of Nonlinear Optics and Spectroscopy*, Oxford University Press, New York, 1995.

[22] M. G. Papadopoulos, J. Leszczynski, and A. Sadlej, editors, volume I of *Challenges and Advances in Computational Chemistry and Physics*, Springer, 2006.

[23] L. Barron, *Molecular Light Scattering and Optical Activity, Second Edition*, Cambridge, 2004.

[24] K. Sasagane, F. Aiga, and R. Itoh, *J. Chem. Phys.* **99**, 3738 (1993).

[25] O. Christiansen, P. Jørgensen, and C. Hättig, *Int. J. Quantum Chem.* **68**, 1 (1998).

[26] P. W. Langhoff, S. Epstein, and M. Karplus, *Rev. Mod. Phys* **44**, 602 (1972).

[27] H. Hellmann, *Einführung in die Quantenchemie*, Deuticke, Leipzig, 1937.

[28] R. P. Feynman, *Phys Rev* **56**, 340 (1939).

[29] E. Wigner, *Math. Naturw. Anz. Ung. Akad. Wiss.* **53**, 477 (1935).

[30] N. C. Handy and H. F. S. III, *J. Chem. Phys.* **81**, 5031 (1984).

[31] P. Jørgensen and T. Helgaker, *J. Chem. Phys.* **89**, 1560 (1988).

[32] T. Helgaker and P. Jørgensen, in *Methods in Computational Molecular Physics*, S. Wilson and G. H. F. Diercksen, Eds., Plenum Press, New York (1992).

[33] P. Hohenberg and W. Kohn, *Phys. Rev.* **136**, B864 (1964).

[34] W. Kohn and L. J. Sham, *Phys. Rev.* **140**, A1133 (1965).

[35] E. Runge and E. K. U. Gross, *Phys. Rev. Letters* **52**, 997 (1984).

[36] C. A. Ullrich and E. K. U. Gross, *Phys. Rev. Letters* **74**, 872 (1995).

[37] M. E. Casida, in *Recent Advances in Density Functional Methods*, Vol. 1, D. P. Chong, editor, World Scientific (1995).

[38] M. A. L. Marques and E. K. U. Gross, *Annu. Rev. Phys. Chem.* **55**, 427 (2004).

[39] M. Häser and R. Ahlrichs, *J. Comput. Chem.* **10**, 104 (1989).

[40] C. A. White, B. G. Johnson, P. M. W. Gill, and M. Head-Gordon, *Chem. Phys. Letters* **230**, 8 (1994).

[41] G. R. Ahmadi and J. Almlöf, *Chem. Phys. Letters* **246**, 364 (1995).

[42] C. A. White and M. Head-Gordon, *J. Chem. Phys.* **104**, 2620 (1996).

[43] C. Ochsenfeld, C. A. White, and M. Head-Gordon, *J. Chem. Phys.* **109**, 1663 (1998).

[44] S. Goedecker, *Rev. Mod. Phys.* **71**, 1085 (1999).

[45] S. Goedecker and G. E. Scuseria, *Comp. Sci. Eng.* **5**, 14 (2003).

[46] J. M. Perez-Jorda and W. Yang, *Chem. Phys. Letters* **241**, 469 (1995).

[47] R. E. Stratmann and G. E. Scuseria, *Chem. Phys. Letters* **257**, 213 (1996).

[48] T. Helgaker, H. Larsen, J. Olsen, and P. Jørgensen, *Chem. Phys. Letters* **327**, 397 (2000).

[49] H. Larsen, P. Jørgensen, J. Olsen, and T. Helgaker, *J. Chem. Phys.* **113**, 8908 (2000).

[50] H. Larsen, T. Helgaker, and J. P. Jørgensen, *J. Chem. Phys.* **115**, 10344 (2001).

[51] A. M. Niklasson and M. Challacombe, *Phys. Rev. Letters* **92**, 193001 (2004).

[52] V. Weber, A. M. Niklasson, and M. Challacombe, *Phys. Rev. Letters* **92**, 193002 (2004).

[53] S. Coriani, S. Høst, B. Jansík, L. Thøgersen, J. Olsen, P. Jørgensen, S. Reine, F. Pawłowski, T. Helgaker, and P. Sałek, *J. Chem. Phys.* **126**, 154108 (2007).

[54] J. Kussmann and C. Ochsenfeld, *J. Chem. Phys.* **127**, 204103 (2007).

[55] T. Kjærgaard, P. Jørgensen, J. Olsen, S. Coriani, and T. Helgaker, *J. Chem. Phys.* **129**, 054106 (2008).

[56] F. London, *J. Phys. Radium* **8**, 397 (1937).

[57] T. Helgaker and P. Jørgensen, *J. Chem. Phys.* **95**, 2595 (1991).

[58] T. Helgaker, P. J. Wilson, R. D. Amos, and N. C. Handy, *J. Chem. Phys.* **113**, 2983 (2000).

[59] M. Krykunov and J. Autschbach, *J. Chem. Phys.* **125**, 034102 (2006).

[60] M. Krykunov and J. Autschbach, *J. Chem. Phys.* **126**, 024101 (2007).

[61] A. J. Thorvaldsen, K. Ruud, A. Rizzo, and S. Coriani, *J. Chem. Phys.* **129**, 164110 (2008).

[62] P. Pulay, *Mol. Phys.* **17**, 197 (1969).

[63] T. Helgaker, P. Jørgensen, and J. Olsen, *Molecular Electronic Structure Theory, First Edition*, Wiley, 2000.

[64] L. D. Barron and A. D. Buckingham, *Chem. Phys. Letters* **492**, 199 (2010).

[65] P. L. Polavarapu, *Int. J. Quantum Chem.* **106**, 1809 (2006).

[66] P. J. Stephens, *J. Phys. Chem.* **89**, 748 (1985).

[67] P. J. Stephens and M. A. Lowe, *Annu. Rev. Phys. Chem.* **36**, 213 (1985).

[68] P. J. Stephens, *J. Phys. Chem.* **91**, 1712 (1987).

[69] P. A. Galwas, PhD thesis, Cambridge University, Cambridge, UK, 1983.

[70] A. D. Buckingham, P. W. Fowler, and P. A. Galwas, *Chem. Phys.* **112**, 1 (1987).

[71] P. Lazzeretti, R. Zanasi, and P. J. Stephens, *J. Phys. Chem.* **91**, 6761 (1986).

[72] M. Reiher and J. Neugebauer, *J. Chem. Phys.* **118**, 1634 (2003).

[73] K. L. Bak, P. Jørgensen, T. Helgaker, K. Ruud, and H. J. A. Jensen, *J. Chem. Phys.* **98**, 8873 (1993).

[74] K. L. Bak, P. Jørgensen, T. Helgaker, and K. Ruud, *Faraday Discuss.* **99**, 121 (1994).

[75] B. J. Orr and J. F. Ward, *Mol. Phys.* **20**, 513 (1971).

[76] P. Norman, D. M. Bishop, H. J. A. Jensen, and J. Oddershede, *J. Chem. Phys.* **123**, 194103 (2005).

[77] P. Norman, D. M. Bishop, H. J. A. Jensen, and J. Oddershede, *J. Chem. Phys.* **115**, 10323 (2001).

[78] J. Kauczor, P. Jørgernsen, and P. Norman, *J. Chem. Theory Comput.* **7**, 1610 (2011).

[79] Maestro v. 8.5; Schrödinger, LLC: Cambridge, MA (2008); http://www.schrodinger.com.

[80] E. R. Davidson, *J. Comput. Phys.* **17**, 87 (1975).

[81] W. Butscher and W. E. Kammer, *J. Comput. Phys.* **20**, 313 (1976).

[82] S. Coriani, P. Jørgensen, A. Rizzo, K. Ruud, and J. Olsen, *Chem. Phys. Letters* **300**, 61 (1999).

[83] H. Solheim, L. Frediani, K. Ruud, and S. Coriani, *Theor. Chem. Accounts* **119**, 231 (2008).

[84] M. Krykunov, M. Seth, T. Ziegler, and J. Autschbach, *J. Chem. Phys.* **127**, 244102 (2007).

[85] S. Coriani, C. Hattig, P. Jørgensen, and T. Helgaker, *J. Chem. Phys.* **113**, 3561 (2000).

[86] Y. Honda, M. Hada, M. Ehara, H. Nakatsuji, J. Downing, and J. Michl, *Chemical Physics Letters* **355**, 219 (2002).

[87] M. Seth and T. Ziegler, *J. Chem. Theory Comput.* **3**, 434 (2007).

[88] D. Ganyushin and F. Neese, *J. Chem. Phys.* **128**, 114117 (2008).

[89] M. Seth, T. Ziegler, and J. Autschbach, *J. Chem. Phys.* **129**, 104105 (2008).

[90] M. Seth, M. Krykunov, T. Ziegler, and J. Autschbach, *J. Chem. Phys.* **128**, 234102 (2008).

[91] M. Seth, M. Krykunov, T. Ziegler, J. Autschbach, and A. Banerjee, *J. Chem. Phys.* **128**, 144105 (2008).

[92] M. Seth and T. Ziegler, *J. Chem. Phys.* **124**, 144105 (2006).

[93] M. Seth, T. Ziegler, A. Banerjee, J. Autschbach, S. J. A. van Gisbergen, and E. J. Baerends, *J. Chem. Phys.* **120**, 10942 (2004).

[94] Y. Honda, M. Hada, M. Ehara, H. Nakatsuji, and J. Michl, *J. Chem. Phys.* **123**, 164113 (2005).

[95] H. Solheim, K. Ruud, S. Coriani, and P. Norman, *J. Phys. Chem. A* **112**, 9615 (2008).

[96] H. Solheim, K. Ruud, S. Coriani, and P. Norman, *J. Chem. Phys.* **128**, 094103 (2008).

[97] T. Kjaergaard, P. Jørgensen, A. J. Thorvaldsen, P. Sałek, and S. Coriani, *J. Chem. Theory Comput.* **5**, 1997 (2009).

[98] T. Kjaergaard, B. Jansík, P. Jørgensen, S. Coriani, and J. Michl, *J. Phys. Chem. A* **111**, 11278 (2007).

[99] M. Faraday, *Philos. Mag.* **28**, 294 (1846).

[100] M. Faraday, *Philos. Trans. R. Soc. London* **136**, 1 (1846).

[101] D. J. Caldwell and H. Eyring, *The Theory of Optical Activity*, Wiley-Interscience, New York, 1971.

[102] A. D. Buckingham and P. J. Stephens, *Adv. Res. Chem. Phys.* **17**, 399 (1966).

[103] P. N. Schatz and A. McCaffery, *Q. Rev. Chem. Soc.* **23**, 552 (1969).

[104] R. Serber, *Phys. Rev.* **41**, 489 (1932).

[105] P. J. Stephens, *Chem. Phys. Letters* **2**, 241 (1968).

[106] P. J. Stephens, *J. Chem. Phys.* **52**, 3489 (1970).

[107] P. J. Stephens, **25**, 201 (1974).

[108] P. J. Stephens, *Adv. Chem. Phys.* **35**, 197 (1976).

[109] J. E. Marsden and M. J. Hoffman, *Basic Complex Analysis*, W. H. Freeman, New York, 1998.

[110] M. Göeppert-Mayer, *Ann. Phys.* **9**, 273 (1931).

[111] W. Kaiser and C. G. B. Garrett, *Phys. Rev. Lett.* **7**, 229 (1961).

[112] I. D. Abella, *Phys. TRev. Lett.* **9**, 453 (1962).

[113] J. H. Strickler and W. W. Webb, *Proc. SPIE* **1398**, 107 (1990).

[114] W. Denk, J. H. Strickler, and W. W. Webb, *Science* **248**, 73 (1990).

[115] J. D. Bhawalkar, G. S. He, and P. N. Prasad, *Rep. Prog. Phys.* **59**, 1041 (1996).

[116] P. Sperber and A. Penzkofer, *Opt. Quantum Electron.* **18**, 381 (1986).

[117] D. A. Parthenopoulos and P. M. Rentzepis, *Science* **245**, 843 (1989).

[118] J. H. Strickler and W. W. Webb, *Opt. Lett.* **16**, 1780 (1991).

[119] F. Terenziani, C. Katan, E. Badaeva, S. Tretiak, and M. Blanchard-Desce, *Adv. Mat.* **20**, 4641 (2008).

[120] G. S. He, L.-S. Tan, Q. Zheng, and P. N. Prasad, *Chem. Rev.* **108**, 1245 (2008).

[121] M. Rumi and J. W. Perry, *Adv. in Optics and Photonics* **2**, 451 (2010).

[122] P. R. Monson and W. M. McClain, *J. Chem. Phys.* **53**, 29 (1970).

[123] K. P. Huber and G. Herzberg, *Molecular Spectra and Molecular Structure IV. Constants of Diatomic Molecules*, Van Nostrand: Reinhold, New York, 1. edition, 1979.

[124] C. Toro, L. De Boni, N. Lin, F. Santoro, A. Rizzo, and F. E. Hernández, *Chem. Eur. J.* **16**, 3504 (2010).

[125] C. Toro, L. De Boni, N. Lin, F. Santoro, A. Rizzo, and F. E. Hernández, *Chirality* **22**, E202 (2010).

[126] N. Lin, F. Santoro, X. Zhao, C. Toro, L. D. Boni, F. E. Hernández, and A. Rizzo, *J. Phys. Chem. B* **115**, 811 (2011).

[127] R. Sahnoun, S. Koseki, and Y. Fujimura, *J. Mol. Struct.* **735-736**, 315 (2005).

[128] D. P. Craig and T. Thirunamachandran, *Molecular Quantum Electrodynamics. An Introduction to Radiation Molecule Interaction*, Dover Publications, Inc., Mineaol, New York, 1984.

[129] S. Grimme, *WIREs Comput Mol Sci* **1**, 211 (2011).

[130] I. Shavitt and R. J. Bartlett, *Many-Body Methods in Chemistry and Physics. MBPT and Coupled-Cluster Theory*, Cambridge Uni. Press, Cambridge, 2009.

[131] C. Møller and M. S. Plesset, *Phys. Rev.* **46**, 618 (1934).

[132] G. Purvis and R. J. Bartlett, *J Chem Phys* **76**, 1910 (1982).

[133] K. Raghavachari, G. W. Trucks, J. A. Pople, and M. Head-Gordon, *Chem Phys Lett* **157**, 479 (1989).

[134] J. Noga and R. J. Bartlett, *J Chem Phys* **86**, 7041 (1987), Erratum: Ibid. **89**, 3401 (1988).

[135] G. E. Scuseria and H. F. Schaefer, *Chem Phys Lett* **152**, 382 (1988).

[136] I.-M. Høyvik, K. Kristensen, B. Jansík, P. Jørgensen, T. Kjærgaard, S. Reine, and J. Jakowski, "Orbital spaces for the divide-expand-consolidate coupled cluster scheme" (in preparation).

[137] T. H. Dunning, Jr., *J. Chem. Phys.* **90**, 1007 (1989).

[138] P. Pulay, *Chem. Phys. Letters* **100**, 151 (1983).

[139] S. Saebø and P. Pulay, *Ann. Rev. Phys. Chem.* **44**, 213 (1993).

[140] C. Hampel and H.-J. Werner, *J. Chem. Phys.* **104**, 6286 (1996).

[141] M. Schütz, G. Hetzer, and H.-J. Werner, *J. Chem. Phys.* **111**, 5691 (1999).

[142] G. Hetzer, M. Schütz, H. Stoll, and H.-J. Werner, *J. Chem. Phys.* **113**, 9443 (2000).

[143] M. Schütz, *J. Chem. Phys.* **113**, 9986 (2000).

[144] M. Schütz and H.-J. Werner, *J. Chem. Phys.* **114**, 661 (2001).

[145] G. E. Scuseria and P. Y. Ayala, *J. Chem. Phys.* **111**, 8330 (1999).

[146] O. Christiansen, P. Manninen, P. Jørgensen, and J. Olsen, *J. Chem. Phys.* **124**, 084103 (2006).

[147] V. Weijo, P. Manninen, P. Jørgensen, O. Christiansen, and J. Olsen, *J. Chem. Phys.* **127**, 074106 (2007).

[148] N. Flocke and R. J. Bartlett, *J. Chem. Phys.* **121**, 10935 (2004).

[149] S. Li, J. Ma, and Y. Jiang, *J. Comput. Chem.* **23**, 237 (2002).

[150] W. Li, P. Piecuch, J. R. Gour, and S. Li, *J. Chem. Phys.* **131**, 114109 (2009).

[151] W. Li and P. Piecuch, *J. Phys. Chem. A* **114**, 8644 (2010).

[152] M. Kobayashi and H. Nakai, *J. Chem. Phys.* **129**, 044103 (2008).

[153] D. G. Fedorov and K. Kitaura, *J. Chem. Phys.* **123**, 134103 (2005).

[154] H. Stoll, *Chem. Phys. Letters* **191**, 548 (1992).

[155] J. Friedrich, M. Hanrath, and M. Dolg, *J. Chem. Phys.* **126**, 154110 (2007).

[156] J. Almlöf, *Chem. Phys. Letters* **181**, 319 (1991).

[157] M. Häser, *Theor Chim Acta* **87**, 147 (1993).

[158] P. Y. Ayala and G. E. Scuseria, *J. Chem. Phys.* **110**, 3660 (1999).

[159] D. S. Lambrecht, B. Doser, and C. Ochsenfeld, *J. Chem. Phys.* **123**, 184102 (2005).

[160] C. Ochsenfeld, J. Kussmann, and D. S. Lambrecht, *Reviews in computational chemistry, Volume 23*, p. 1, VCH Publishers, Inc., New York, 2007.

[161] B. Doser, D. S. Lambrech, and C. Ochsenfeld, *Chem. Phys. Phys. Chem* **10**, 3335 (2008).

[162] M. Schütz, G. Rauhut, and H.-J. Werner, *J. Phys. Chem. A* **102**, 5997 (1998).

[163] J. W. Boughton and P. Pulay, *J. Comput. Chem.* **14**, 736 (1993).

[164] J. A. Pople, R. Krishnan, H. B. Schlegel, and J. S. Binkley, *Int. J. Quantum. Chem. Symp.* **13**, 225 (1979).

[165] N. C. Handy, R. D. Amos, J. F. Gaw, J. E. Rice, and E. D. Simandiras, *Chem. Phys. Lett.* **120**, 151 (1985).

[166] E. D. Simandiras, R. D. Amos, and N. C. Handy, *Chem. Phys.* **114**, 9 (1987).

[167] T. Helgaker, P. Jørgensen, and N. C. Handy, *Theor Chim Acta* **76**, 227 (1989).

[168] M. Feyereisen, G. Fitzgerald, and A. Komornicki, *Chem. Phys. Letters* **208**, 359 (1993).

[169] O. Vahtras, J. Almlöf, and M. Feyereisen, *Chem. Phys. Letters* **213**, 514 (1993).

[170] F. Weigend and M. Häser, *Theor. Chim. Acta* **97**, 331 (1997).

[171] Y. M. Rhee, R. A. DiStasio, R. C. Lochan, and M. Head-Gordon, *Chem. Phys. Letters* **426**, 197 (2006).

[172] R. A. DiStasio, R. P. Steele, Y. M. Rhee, Y. Shao, and M. Head-Gordon, *J. Comput. Chem.* **28**, 839 (2007).

[173] S. Kossmann and F. Neese, *J. Chem. Theory Comput.* **6**, 2325 (2010).

[174] S. Schweizer, B. Doser, and C. Ochsenfeld, *J. Chem. Phys.* **128**, 154101 (2008).

[175] A. E. Azhary, G. Rauhut, P. Pulay, and H.-J. Werner, *J. Chem. Phys.* **108**, 5185 (1998).

[176] M. Schütz, H.-J. Werner, R. Lindh, and F. R. Manby, *J. Chem. Phys.* **121**, 737 (2004).

[177] C. Ochsenfeld, *Chem. Phys. Letters* **327**, 216 (2000).

[178] Y. Shao, C. A. White, and M. Head-Gordon, *J. Chem. Phys.* **114**, 6572 (2001).

[179] S. Reine, A. Krapp, M. F. Iozzi, V. Bakken, T. Helgaker, F. Pawłowski, and P. Sałek, *J. Chem. Phys.* **133**, 044102 (2010).

[180] S. F. Boys, *Rev. Mod. Phys.* **32**, 296 (1960).

[181] J. M. Foster and S. F. Boys, *Rev. Mod. Phys.* **32**, 300 (1960).

[182] S. F. Boys, *Quantum Theory of Atoms, Molecules and Solid State*, p. 253, Academic, New York, 1966.

[183] C. Edmiston and K. Ruedenberg, *Rev. Mod. Phys.* **35**, 457 (1963).

[184] C. Edmiston and K. Ruedenberg, *J. Chem. Phys.* **43**, S97 (1965).

[185] C. Edmiston and K. Ruedenberg, Localized Atomic and Molecular Orbitals. III, in *Quantum Theory of Atoms, Molecules and Solid State*, edited by P.-O. Löwdin, p. 263, Academic, New York, 1966.

[186] D. A. Kleier, T. A. Halgren, J. John H. Hall, and W. N. Lipscomb, *J. Chem. Phys.* **61**, 3905 (1974).

[187] W. von Niessen, *J. Chem. Phys.* **56**, 4290 (1972).

[188] V. Magnasco and A. Perico, *J. Chem. Phys.* **47**, 971 (1967).

[189] J. Pipek, *Int. J. Quantum Chem.* **36**, 487 (1989).

[190] J. Pipek and P. G. Mezey, *J. Chem. Phys.* **90**, 4916 (1989).

[191] D. Maynau, S. Evangelisti, N. Guihéry, C. J. Calzado, and J.-P. Malrieu, *J. Chem. Phys.* **116**, 10060 (2002).

[192] C. Angeli, C. J. Calzado, R. Cimiraglia, S. Evangelisti, N. Guihéry, T. Leininger, J.-P. Malrieu, D. Maynau, J. V. P. Ruiz, and M. Sparta, **101**, 1389 (2003).

[193] F. Aquilante, T. B. Pedersen, A. S. de Merás, and H. Koch, *J. Chem. Phys.* **125**, 174101 (2006).

[194] J. E. Subotnik, A. D. Dutoi, and M. Head-Gordon, *J. Chem. Phys.* **123**, 114108 (2005).

[195] S. Saebø and P. Pulay, *J. Chem. Phys.* **86**, 914 (1987).

[196] S. Saebø and P. Pulay, *J. Chem. Phys.* **88**, 1884 (1988).

[197] P. E. Maslen, M. S. Lee, and M. Head-Gordon, *Chem. Phys. Letters* **319**, 205 (2000).

[198] M. Ziółkowski, B. Jansík, P. Jørgensen, and J. Olsen, *J. Chem. Phys.* **131**, 124112 (2009).

[199] L. Cederbaum, J. Schirmer, and H.-D. Meyer, *J. Phys. A* **22**, 2427 (1989).

[200] B. Jansík, S. Høst, M.P.Johansson, P.Jørgensen, J. Olsen, and T. Helgaker, *J. Chem. Theory Comput.* **5**, 1027 (2009).

[201] B. Jansík, S. Høst, M.P.Johansson, J.Olsen, P.Jørgensen, and T. Helgaker, *Chem. Phys. Phys. Chem* **11**, 5805 (2009).

[202] R. Fletcher, *Practical Methods of Optimization*, Wiley, Chichester, 1990.

[203] S. Reine, A. Krapp, M. F. Iozzi, V. Bakken, T. Helgaker, F. Pawłowski, and P. Sałek, *J. Chem. Phys.* **133**, 044102 (2010).

Papers